Theory of Josephson effect in junctions with complex ferromagnetic/normal metal weak link region

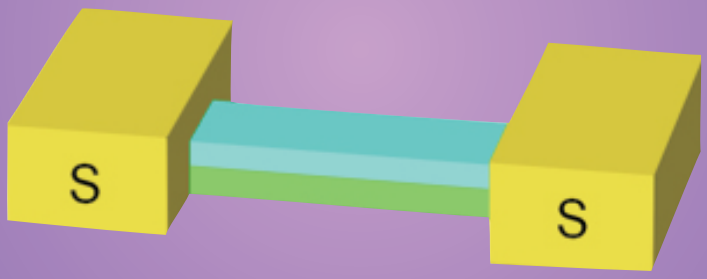

Tatiana Karminskaya

THEORY OF JOSEPHSON EFFECT IN JUNCTIONS WITH COMPLEX FERROMAGNETIC/NORMAL METAL WEAK LINK REGION

Ph.D. thesis of Tatiana Karminskaya

Graduation committee:

Chairman:	prof. dr. G. van der Steenhoven	University of Twente
Secretary:	prof. dr. G. van der Steenhoven	University of Twente
Promotor:	prof. dr. H. Rogalla	University of Twente
Asst. promotor:	dr. A.A. Golubov	University of Twente
Members:	prof. dr. H. Hilgenkamp	University of Twente
	prof. dr. P. Kelly	University of Twente
	dr. A. Brinkman	University of Twente
	prof. dr. M. Yu. Kupriyanov	Moscow State University
	prof. dr. J. Aarts	Leiden University

The research described in this thesis was performed in the Faculty of Science and Technology and the MESA$^+$ Institute of Nanotechnology at the University of Twente (Enschede, The Netherlands), in collaboration with Moscow State University (Moscow, Russia). This research was financially supported by the Dutch NanoNed program under project TCS 7029.

Printed by Ipskamp Drukkers, Enschede, The Netherlands.

ISBN: 978-90-365-3160-3

THEORY OF JOSEPHSON EFFECT IN JUNCTIONS WITH COMPLEX FERROMAGNETIC/NORMAL METAL WEAK LINK REGION

DISSERTATION

to obtain
the degree of doctor at the University of Twente,
on the authority of the rector magnificus,
prof.dr. H. Brinksma,
on account of the decision of the graduation committee,
to be publicly defended
on Wednesday, 16th of February 2011 at 12:45

by

Tatiana Karminskaya

born on 23th of July 1982
in Neustrelitz , Germany

This dissertation is approved by:
prof.dr. H.Rogalla, promotor
dr. A.A. Golubov, assistant promotor

Contents

Chapter 1

Introduction

1.1 Superconductivity and proximity effect

Superconductivity is a physical phenomenon that occurs in many chemical elements, compounds and alloys. Electrical and magnetic properties of materials in the superconducting state differ significantly from the same properties in a normal state. The phenomenon of superconductivity was discovered in 1911 by H. Kammerling-Onnes in his study of the resistance of mercury. He found that when cooled below 4.2 K, mercury's resistance vanishes abruptly. Normal state can be restored by applying a sufficiently strong current (greater than the critical current) across the material or putting it in a sufficiently strong external magnetic field (greater than the critical magnetic field).

The first theory, that successfully described phenomenology of the electrodynamics of superconductors, was the London theory (1935). The Ginzburg-Landau theory (GL theory), is also a phenomenological theory, but it takes into account the quantum effects to describe the superconductivity by introducing the effective wave function (the order parameter) . Since the GL theory was based on the theory of phase transitions, it is valid only near the critical temperature of superconductor. In 1956, L. Cooper suggested the idea of bound electrons, Cooper pairs, which can arise for arbitrarily small attraction between electrons which are near the Fermi surface. Based on this idea, Bardeen, Cooper and Schrieffer formulated microscopic theory of superconductivity (the BCS thery). Since Cooper pairs are bose particles, at a temperature below T_C they can accumulate in the ground state described by a single wave function. Consequently, such condensate can flow without dissipation. L.P. Gor'kov developed the microscopic theory of superconductivity further (1958) via application of the method of Green's functions.

In the last few years investigation of superconductivity was directed on study of superconductors with unconventional pairing mechanisms and Cooper pair symmetry and on study of hybrid structures with superconductors. There exist many interesting phenomena in hybrid SN (superconductor-normal metal) structures. Cooper pairs can penetrate into

normal metal at some distance which in the diffusive case (i.e. when electron scattering mean free path is small) is proportional to $(\frac{D_N}{T})^{1/2}$, where D_N is the electronic diffusion coefficient. So, superconducting properties can be induced near the interface on this length scale. This effect is called the proximity effect. In hybrid structures which consist of two superconductors that are connected via a weak link region (dielectric material, normal metal, constriction) there is, a so called, Josephson effect: the current flows through the junction without dissipation if the current is smaller than the critical value, I_C. This superconducting current, I_S, is 2π-periodic function of the phase difference φ of wave functions of superconducting electrodes and for the simplest case is given by $I_S = I_C \sin(\varphi)$.

There is a considerable interest in Josephson structures containing ferromagnetic materials in their weak link region [1]- [4]. The proximity effect in SF structures leads to the penetration of superconducting correlations into ferromagnetic metal to a length of the order $(\frac{D_F}{H})^{1/2}$ in the diffusive case, where H is exchange energy of ferromagnetic material.

Unlike SN structures, in SF structures these correlations are not only attenuated on the coherence length, but also oscillate as a function of the thickness of the ferromagnetic layer. Such behavior of the wave function can be qualitatively explained as follows. Cooper pair, consisting of electrons with opposite momenta and spins penetrates through the SF interface into the ferromagnet. In the presence of exchange field H in a ferromagnetic material, electrons with spins oriented along the field decrease their energy by H, and electrons with spins directed against the field, increase their energy by H. Therefore, in the presence of an exchange field the Cooper pairs have a non-zero momentum, which leads to oscillation of the wave function in ferromagnet (see Fig.1) [5]. This phenomenon is similar to the Fulde-Ferrel-Larkin-Ovchinnikov oscillations in magnetic superconductors [6], [7].

Due to the oscillating character of the wave function, the critical temperature of a structures containing a ferromagnetic layers behaves nonmonotonicaly [8] - [11]. For the same reason the critical current I_C in SFS junctions oscillates as a function of the thickness of ferromagnetic layer. The junction changes the states with positive values of the I_C to the states with negative values of critical current ($0-\pi$-transition). This phenomenon was predicted theoretically in [12] for Josephson junctions with magnetic impurities within the dielectric layer and in [13] - [14] for SFS junctions in the clean and dirty limits. The first experimental evidences were found in [15] - [18] .

To study the proximity effect in SF structures, one can use the methods of quantum field theory [19] - [24]. The structure can be described in terms of Green's functions that

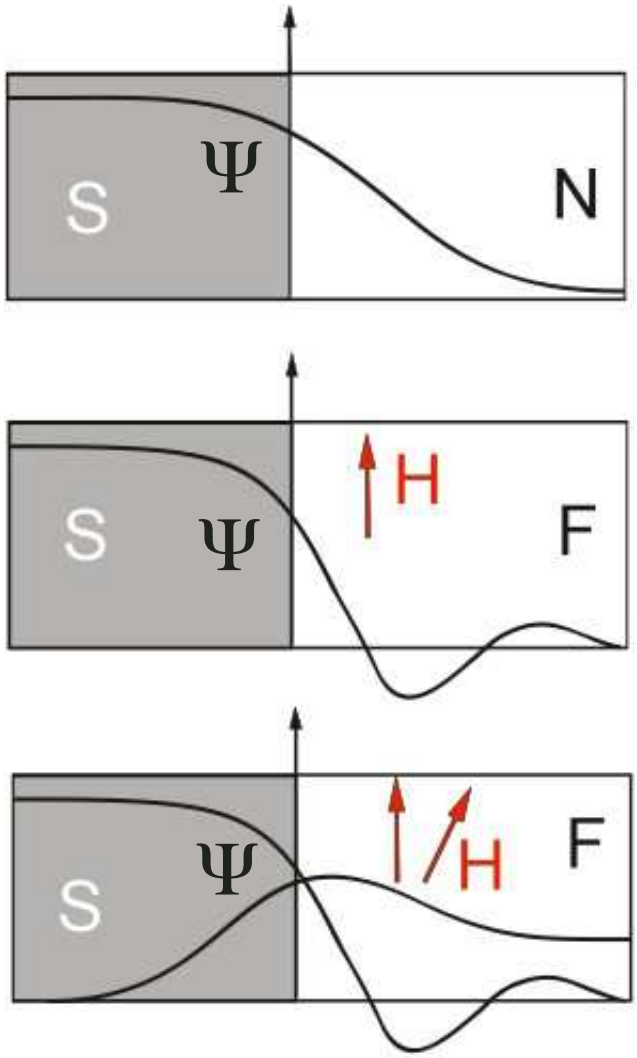

Figure 1.1. Proximity effect in SN structure, SF structure with uniform magnetization and SF structure with nonuniform magnetization.

satisfy the Gor'kov equation. In metals with high concentration of impurities, mean free path is small compared with all other lengt scales (dirty limit). In this case, the Green's functions in the first approximation are isotropic, allowing us to use the Usadel equation [25] for Green's functions averaged over the Fermi surface. In the stationary and equilibrium case these equations have the following form

$$D\partial_r(g\partial_r g) - \omega_n[\hat{k}_0\hat{\tau}_3\hat{\sigma}_0, g] - i[\hat{k}_0\overline{h}, g] - i[\Delta\hat{k}_0\hat{\tau}_2\hat{\sigma}_3, g] = 0,$$

where g is an 8×8 matrix in Keldysh×Nambu×Spin space, $\hat{k}_i, \hat{\tau}_i, \hat{\sigma}_i$ are Pauli matrixes ($i = 0, 1, 2, 3$), $D = vl/3$ - is the diffusion coefficient (v is the velocity at the Fermi surface and l is the mean free path), $\omega_n = \pi T(2n+1)$ is the Matsubara frequencies ($n = 0, \pm 1, \pm 2...$), Δ is the pair potential (it is nonzero for superconductors and is zero for other materials). Matrix $\overline{h}$ describes ferromagnetic properties in Usadel equation. For example, if the ferromagnet

has monodomain structure and its magnetization vector lies in the (y, z) plane then

$$\overline{h} = H(\hat{\tau}_3\hat{\sigma}_3 \cos\alpha + \hat{\tau}_0\hat{\sigma}_2 \sin\alpha),$$

where H is exchange energy of ferromagnetic material.

Matrix g in the Keldysh space can be represented as

$$g = \begin{pmatrix} G^R & G^K \\ 0 & G^A \end{pmatrix},$$

where $G^R, G^A, G^K$are retarded, advanced and Keldysh parts correspondingly. There is also a normalization condition

$$g^2 = 1,$$

from which one can obtain that retarded, advanced and Keldysh Green's functions are connected via the expression

$$G^K = G^R\hat{f} - \hat{f}G^A,$$

where $\hat{f}$ is the matrix distribution function, therefore one can content oneself with only the retarded part of matrix g.

In the Nambu space, the retarded part can be represented as follows:

$$G^R = G + F = \hat{\tau}_3 g^R + \hat{\tau}_0 g^{Rt} + i\hat{\tau}_2 f^R + i\hat{\tau}_1 f^{Rt}, G^R = \begin{pmatrix} g^R + g^{Rt} & f^R + if^{Rt} \\ -f^R + if^{Rt} & -g^R + g^{Rt} \end{pmatrix}.$$

In the spin space we have

$$f^R = \sigma_3 f_3 + \sigma_0 f_0, f^R = \begin{pmatrix} f_0 + f_3 & 0 \\ 0 & f_0 - f_3 \end{pmatrix}, f^{Rt} = \sigma_1 f_1,$$

$$g^R = \sigma_0 g_0 + \sigma_3 g_3, g^R = \begin{pmatrix} g_0 + g_3 & 0 \\ 0 & g_0 - g_3 \end{pmatrix}, g^{Rt} = \sigma_2 g_2,$$

where $f_{3,}g_0$ are singlet Green's functions, $f_{0,}g_3$ are triplet Green's functions with zero projection of spin, and f_1, g_2 are triplet functions for correlations with nonzero spin projection.

Usadel equations must be supplemented by boundary conditions obtained in [26]

$$\gamma\xi_1 g_1 \frac{\partial g_1}{\partial r} = \xi_2 g_2 \frac{\partial g_2}{\partial r},$$

$$\gamma_B \xi_1 g_1 \frac{\partial g_1}{\partial r} = [g_1, g_2],$$

interconnecting functions on atomically sharp interfaces of materials. Parameters $\gamma = \frac{\rho_2 \xi_2}{\rho_1 \xi_1}, \gamma_B = \frac{R_B A_B}{\rho_1 \xi_1}$ are the suppression parameters at the SF interface. Here $\xi_{1,2}, \rho_{1,2}$ are the coherence lengths and resistivities of the first and second metals respectively, R_B, A_B are the resistance and the area of interface. Applicability of these equations and boundary conditions is justified, if the value of the exchange energy is much smaller than the Fermi energy.

For several cases, the so-called, Φ parametrization is useful. In this parametrization, Green's functions G and F can be represented as follows

$$G = \frac{\tilde{\omega_n}}{\sqrt{\tilde{\omega_n}^2 + \Phi\Phi^*_{-\omega_n}}}, \; F = \frac{\Phi}{\sqrt{\tilde{\omega_n}^2 + \Phi\Phi^*_{-\omega_n}}},$$

where $\widetilde{\omega} = \omega + iH$. In this parametrization $\Phi = \Delta$ in a bulk superconductor and the normalization condition is automatically fulfiled thus decreasing the number of equations.

1.2 Motivation

The existence of the oscillatory dependence of the critical current on the distance between superconducting electrodes has been reliably confirmed in a number of experiments using a variety of ferromagnetic materials and types of Josephson junctions [27] - [42]. Use of π transitions, for which the critical current has a negative value, has been discussed in [43] - [47] for the implementation of qubits and for superconducting electronics. However, these structures have some significant drawbacks, limiting their application.

The first of them is the small magnetude of the characteristic scale penetration of superconductivity in a ferromagnet. Indeed, analysis of existing experimental data [27] - [42] shows that the value of the exchange energy, H, in ferromagnetic materials scales between $850\ K \div 2300\ K$. Such large values of H lead to effective decay length, $\xi_{F1} \approx 1.2 \div 4.6\ nm$, and period of oscillations, $\xi_{F2} \approx 0.3 \div 2\ nm$, of thickness dependence of a SFS junction critical current, I_C. These values turned out to be much smaller compared to the decay length, $\xi_N \approx 10 \div 100\ nm$, in similar SNS structures. This fact makes it difficult to fabricate SFS junctions with reproducible parameters. It also leads to suppression of the $I_C R_N$ product thus limiting the cutoff frequency of the junctions. Since a search of exotic ferromagnetic materials with smaller value of H is a challenging problem [42], one has to seek for another solutions.

One possible way to increase the decay length in a ferromagnetic barrier is the use of the long-range proximity effect due to induced spin-triplet superconductivity [2], [77], [58]-[60] in structures with nonuniform magnetization. If magnetization of a ferromagnetic barrier is homogeneous, then only the singlet component and triplet component, with projection $S_z = 0$, of the total Cooper-pair spin are induced in the F region. These superconducting correlations are short-ranged, i.e. they extend into the F layer over a short distance of the order of $\xi_{F1} = \sqrt{D_F/H}$ in the diffusive case. However, in the case of inhomogeneous magnetization, e.g. in the presence of magnetic domain walls or a SF multilayer with noncollinear directions of magnetization of different F layers, a long-range triplet component (LRTC) with $S_z = \pm 1$ may appear (see Fig.1). It decays into F region over distance $\xi_F = \sqrt{D_F/2\pi T_C}$ (here T_C is the critical temperature of the S layer), which is a factor $\sqrt{H/2\pi T_c}$ larger than ξ_{F1}. The latter property might lead to the long-range effects observed in some experiments [62], [63], [64]- [68].

The transformation of decay length from ξ_{F1} to ξ_F might also take place in the vicinity of a domain wall even without generation of an odd triplet component [79] - [87]. This enhancement depends on an effective exchange field which is determined by the thicknesses and exchange fields of the neighboring domains. If a sharp domain wall is parallel [83], [86] or perpendicular to the SF interface [87] and the thickness of ferromagnetic layers, $d_f \lesssim \xi_{F1}$, then for the antiparallel direction of magnetization the exchange field effectively averages out, and the decay length of superconducting correlations becomes close to that of a single nonmagnetic N metal $\xi_F = \sqrt{D_F/2\pi T_C}$. It should be mentioned that for typical ferromagnetic materials ξ_F is still small compared to the decay length ($\xi_N \gtrsim 100\ nm$) of high conductivity metals such as Au, Cu or Ag. This difference can be understood if one takes into account at least two factors. First, typical values of Fermi velocities in ferromagnetic materials (see e.g. the analysis of experimental data done in [39], [40]) are of the order of 2×10^5 m/s, about an order of magnitude smaller than in high conductivity metals. The second factor is the rather small electron mean free path in ferromagnets, especially alloys like CuNi, PtNi, etc.

The second disadvantage of the existing SFS structures lies in the difficulty in organizing the control of the magnitude of the critical current. Control of the critical current of SFS junctions can be achieved by changing the direction of the magnetization vectors of the ferromagnetic layers. Such management has much in common with the giant magnetoresistance effect [48] - [49]. The possibility of such a control in SFS junctions having

different complexities of weal link region has been intensively discussed earlier. The first group of suggestions was concentrated on tunnel SFIFS Josephson junctions which consist of SF sandwiches separated by dielectric (I) layer [59], [50]- [54]. It was shown that switching from parallel to antiparallel direction of F layer magnetization vectors may result in enhancement of critical current of these devices as well as in transition from zero to π states. However, practical realization of this switching is complex task, which is difficult to implement. The next class of SFS junctions exploits the idea of interplay between singlet and odd triplet superconducting components inside a Josephson structure [58], [60], [55]- [57]. In SFSF devices [60], where one of the F films is screened from the external magnetic field by a superconducting electrode a change of direction of the upper F layer magnetization can be more easily realized than in junctions having two or more F layers between superconducting banks. Unfortunately, to implement the effective I_C modulation it is necessary to fit two alternative conditions. On one hand, thickness of the S layer in the FSF part of the structure must be large enough in order to have a reasonable critical temperature [88]. On the other hand, to provide the connectedness of the magnetization directions of the F films, which is a necessary condition for generation of the odd triplet component, this thickness must be small. Similar problems occur in realization of FSF spin valve devices (see e.g. [89]). Recently, the possibility of experimental realization of deflection of the magnetization direction of one of F layers from the initial antiferromagnetic configuration of F films has been demonstrated in spin valve structure designed to control the critical temperature of superconducting film [89].

In this work, research focused on finding solutions to eliminate the above-stated deficiencies in SFS Josephson junctions with traditional geometry. To this end, new types of SFS Josephson junctions were suggested in which the weak links are composed from NF, or FNF multilayer structure. This work aimed at carrying out theoretical studies of processes in these structures and proof of the fundamental features, such as extending the period of oscillation and the scale of the decay of the critical current to values of about ξ_N, and organization of effective control of the magnitude I_c

1.3 Contents of Chapters

In Chapter 2, S-FN-S Josephson junctions are discussed. These junctions are made of two massive superconducting electrodes, connected by an NF bilayer. It is assumed that

supercurrent flows in the direction parallel to the FN-boundaries of composite weak-link region.

In section 2.1, S-FN-S structures are described in the framework of the quasiclassical Usadel equations in the limit of thin ferromagnetic and normal layers. The assumption of small layer thickness significantly simplifies the problem and gives possibility to find analytical expressions for the Green's functions. From these expressions an expression for the critical current of the structure is obtained. The critical current is expressed as the sum of two terms, which correspond to one of its wave vectors.

In section 2.2, the analysis of the wave vectors and the critical current obtained in section 2.1 is performed for a number of limiting cases. It is shown that in the limit of large resistance of the FN boundary the films are practically independent and the critical current flows through two independent channels. In the ferromagnetic film there is a slight increase in the scale of the damping and period of oscillations of the critical current, and in the normal film oscillations appear, but with a much greater period ξ_N. In the limit of small resistance of the FN boundary two cases are considered: highly conducting ferromagnet and highly conducting normal metal. In the first case, the structure is similar to an SFS junction, where critical current decays very sharply, while in the latter case one of the wave vectors can produce oscillations of the critical current with period and scale of decay of the order of ξ_N. Thus, in Chapter 2 it is proved that in S-FN-S structure the scale of the damping and the oscillation period of the critical current can be significantly increased compared with the same parameters for the SFS junction, since the use of a FN structure as a material of weak region reduces the effective exchange energy of the ferromagnetic film.

In Chapter 3, the S-FNF-S Josephson junction is considered. Such junction consists of two massive superconducting electrodes, connected by an FNF trilayer. In this chapter the possibility of controlling the critical current in the Josephson junctions is discussed. The direction of magnetization of one of the F-layers can be fixed using an antiferromagnetic substrate. It is assumed that the magnetization vector of the other F layer can vary both in magnitude and in sign, being collinear with the first.

In section 3.1, the approach is described to study S-FNF-S junctios in the framework of the quasiclassical Usadel equations in the limit of thin ferromagnetic and normal films. Under the assumption of thin layers, the analytical expressions for the Green's functions are obtained, through which an expression for the critical current of the structure can be found. The critical current can be expressed as the sum of three terms with corresponding

wave vectors.

Section 3.2 presents analysis of the wave vectors and critical current for a number of limiting cases. It is shown that for equal values of magnetizations, both the sign and the absolute value of the critical current of the structure are analogous to that considered in Chapter 1. In the limit of large resistance of the FN interface the films are practically independent. In the limit of high conducting film the two wave vectors are equal to the partial wave vectors of ferromagnetic films, while the third wave vector describes the oscillations of the critical current with period and the scale of the decay on the order of ξ_N. Furthermore, it is shown that for a strictly antiparallel orientation of magnetizations the average exchange energy is zero, so the critical current does not oscillate. Also, there are no oscillations of critical current at the some value of the exchange energy of one of the ferromagnetic layers. The critical current is always positive at equal in magnitude and opposite in direction magnetizations. Therefore, when switching the magnetization from parallel to antiparallel configuration, the critical current can remain zero state or change the sign. The critical current can also significantly change its value. The maximum absolute value of the critical current is achieved for unequal magnetizations in the 0 state and the π state. Thus, in Chapter 3 it is proven that the S-FNF-S junction is useful for the control of both the value and sign of the critical current, while maintaining advantages of S-FN-S structures.

In Chapter 4, the S-FNF-S Josephson junction is considered in the general case when the magnetization vectors of the F layers are noncollinear. The possibility of the critical current control by rotation of magnetization vectors is discussed. At angle $\alpha \neq 0, \pi$ in addition to the singlet $\langle\psi_\uparrow\psi_\downarrow\rangle + \langle\psi_\downarrow\psi_\uparrow\rangle$ and triplet $\langle\psi_\uparrow\psi_\downarrow\rangle - \langle\psi_\downarrow\psi_\uparrow\rangle$ components also the equal spin triplet components $\langle\psi_\uparrow\psi_\uparrow\rangle$ and $\langle\psi_\downarrow\psi_\downarrow\rangle$ arise, which also contribute to the critical current. Chapter 4 shows how these triplet correlations affect the critical current of the structure.

In section 4.1, an approach to the description of the S-FNF-S junctions is developed in the framework of the quasiclassical Usadel equations in the matrix form. The regime of thin ferromagnetic and normal layers is discussed. It is then shown how components of the matrix condensate functions can be obtained in the presence of triplet superconducting correlations.

In section 4.2, it is shown that the expression for the Green's functions obtained in Section 4.1 can be significantly simplified in limit of high conducting normal film. In this case, the analytical expressions for the critical transition current and wave vectors structure

is obtained.

In section 4.3, we analyse the wave vectors for the limiting case corresponding to the high conducting normal film. It is shown that taking into account the triplet component with nonzero projection leads to a noticeable change in behavior of the wave vectors depending on the misorientation angle of the magnetization vectors. Also, the period of oscillations tends to infinity at not strictly antiparallel orientation of the magnetization vector, but at some misorientation angle.

In Section 4.4, the critical current of the structure is analyzed for the same limiting case . It is shown that taking into account the triplet component with nonzero spin projection leads to the transition from 0 to π state at some misorientation angle rather than at strictly parallel orientation of the magnetizations. It is proven that when the misorientation angle is larger then some critical one, a new type of π state is possible in the structure. This state is due to superposition of nonoscillatory contributions. The distance between superconducting electrodes at which the $0-\pi$ transition can be realized, depends on the misorienation angle α, and this distance tends to infinity at antiparallel magnetizations. Thus, in Chapter 4 it is proven that the control of critical current is possible in S-FNF-S junction at small angles, and the existence of a new π state is demonstrated.

In Chapter 5, properties of S-FN-S Josephson junctions with arbitrary thickness of the F and N films in the weak link region are theoretically investigated.

In Section 5.1, an approach to study of S-FN-S junction is developed in the framework of the quasiclassical Usadel equations for an arbitrary thickness of the ferromagnetic and normal films.

In Section 5.2, it is shown that taking into account the finite thickness of the films leads to an infinite number of wave vectors. Therefore, the critical current is the sum of an infinite number of terms. It is shown that the expression for the critical current is simplified in the case for which the main contribution to the current is yielded by terms corresponding to the minimum wave vectors. The limitations on the thickness of normal film for such assumption are defined. It is shown that the expression for the critical current has the same structure as previously obtained in Chapter 1 and differs from it only by wave vector.

In Section 5.3, the analysis of the wave vectors is performed. It is shown that since the structure of the expression for the critical current remains the same, the results obtained in the previous chapters are qualitatively correct not just for the approximation of small film

thicknesses, but in the general case. It is shown that for thicknesses of the ferromagnetic film larger than ξ_F, wave vectors become almost independent of this thickness.

In Section 5.4, the behavior of the critical current is analyzed. For thickness of a ferromagnet much larger than its coherence length, one can define critical distances L_n when I_C changes sign. It is shown that for thickness of a ferromagnet comparable to the coherence length, strong variations of I_C occur as a function of the F film thickness, if the distance between superconducting electrodes L is close to L_n. Beyond these narrow critical areas the sign and the period of the critical current do not depend on the thickness of the F film if the thickness is large than ξ_F.

In Chapter 6, Josephson effect in S-FN-S Josephson junctions with different types of weak link reagion is investigated:

- SN-NF-NS structure, which consists of two SN electrodes connected by an NF weak region.

- SNF-N-FNS structure, in which a N film connects SNF multilayer electrodes.

- SNF-NF-FNS structure, in which the S electrodes are located on top of the FN structure.

In Section 6.1, an approach to the description of these three types of junctions is developed in the framework of the quasiclassical Usadel equations with different boundary conditions.

In Section 6.2, there is analytical argumentations of advantage of ramp type geometry for simple SNS structure in the case of small transparency of SN interface.

In Section 6.3, critical current for these three ramp type geometries is calculated. The phase diagrams in (L, d) plane are analyzed where 0 and π states are saparated by the lines with zero I_C.

Bibliography

[1] A. A. Golubov, M. Yu. Kupriyanov, and E. Il'ichev, Rev. Mod. Phys. **76**, 411 (2004).

[2] F. S. Bergeret, A. F. Volkov, K. B. Efetov, Rev. Mod. Phys. **77**, 1321 (2005).

[3] K. B. Efetov, I. A. Garifullin, A. F. Volkov and K. Westerhilt, cond-mat/0610708 (2006).

[4] A. I. Buzdin, Rev. Mod. Phys. **77**, 935 (2005).

[5] E. A. Demler, G.B. Arnold and M.R. Beasley, Phys. Rev. B v. **55**, n. 22, p. 15174 (1997).

[6] P. Fulde, R.A. Ferrell. Phys. Rev. v. **135**, A550 (1964).

[7] A.I. Larkin, Yn.N. Ovchinnikov. Zh. Exp. Teor. Fiz v. **47**, 1136 (1964)[Sov. Phys. JETP **20**, 762 (1965)].

[8] A.I. Buzdin, M.Yu. Kupriyanov, Pis'ma Zh. Exp. Teor. Fiz,**52**, 1089 (1990)[JETP Lett. **52**, 487 (1990)].

[9] Z. Radovic, M. Ledvij, Lj. Dobroslaljevic-Grujic, A.I. Buzdin, J.R. Clem, Phys. Rev. B v. **44**, 759 (1991).

[10] L.R. Tagirov, Physica C v. **307**, 145 (1998).

[11] M.G. Khusainov and Yu.N. Proshin, Phys. Rev. B v. **56**, R14283 (1997).

[12] L.N. Bulaevskii, V.V. Kuzii, A.A. Sobyanin, Pis'ma Zh. Exp. Teor. Fiz. **25**, 314 (1977)[JETP Lett. **25**, 290 (1977)].

[13] A.I. Buzdin, L.N. Bulaevskii, S.V. Panyukov, Pis'ma Zh. Exp. Teor. Fiz. **35**, 147 (1982) [JETP Lett. **35**, 178 (1982)].

[14] A.I. Buzdin, M.Yu. Kupriyanov, Pis'ma Zh. Exp. Teor. Fiz. **53**, 308 (1991).

[15] V. V. Ryazanov, V. A. Oboznov, A. Yu. Rusanov, A. V. Veretennikov, A. A. Golubov, and J. Aarts, Phys. Rev. Lett. v. **86**,n. 11, p. 2427 (2001).

[16] V. V. Ryazanov, V. A. Oboznov, A. V. Veretennikov, A. Yu. Rusanov, Phys. Rev. B v. **65**, 02051(R) (2001).

[17] T. Kontos, M. Aprili, J. Lesueur, F. Genet, B. Stephanidis, and R. Boursier, Phys. Rev. Lett. v. **89**, n. 13, p. 137007-1 (2002).

[18] T. Kontos, M. Aprili, J. Lesueur, X. Grison. Phys. Rev. Lett., **86**, n. 2, p. 304, (2001).

[19] A.I. Larkin Yu.N. Ovchinnikov, Zh. Exp. Teor. Fiz. **55**, 2262 (1968)[Sov. Phys. JETP **28**, 1200 (1969)].

[20] A.A. Abrikosov, L.P Gor'kov, I.E. Dzyaloshinski Methods of Quantum field theory in statistical physics (1962).

[21] A.V. Svidzinskii, Spatially inhomogeneous problems in the theory of superconductivity. Methods of quantum field theory in statistical physics. Nauka (1982).

[22] Alexander Atland, B. D. Simons and D. Taras-Semchuk, Advances in physics, v. 49, n. 3, 321 (2000)

[23] J. Rammer, H. Smith, Rev. Mod. Phys. **58**, n. 2, 323 (1986).

[24] W. Belzig, F. K. Wilhelm, C. Bruder, G. Schon, A. D. Zaikin, v. 25, n. 5/6 (1999).

[25] L. Usadel. Generalized differential equation for supercinducting alloys. Phys. Rev. Lett. **25**, 507 (1970).

[26] M. Yu. Kuprianov and V. F. Lukichev, Zh. Eksp. Teor. Fiz. **94**, 139 (1988) [Sov. Phys. JETP **67**, 1163 (1988)].

[27] S. M. Frolov, D. J. Van Harlingen, V. A. Oboznov, V. V. Bolginov, and V. V. Ryazanov, Phys. Rev. B **70**, 144505 (2004).

[28] S. M. Frolov, D. J. Van Harlingen, V. V. Bolginov, V. A. Oboznov, and V. V. Ryazanov, Phys. Rev. B **74**, 020503 (R) (2006).

[29] H. Sellier, C. Baraduc, F. Lefloch, and R. Calemczuck, Phys. Rev. B **68**, 054531 (2003).

[30] Y. Blum, A. Tsukernik, M. Karpovski, A. Palevski, Phys. Rev. B **70**, 214501 (2004).

[31] C. Surgers, T. Hoss, C. Schonenberger, et al, J. Magn. Magn. Mater. **240**, 598 (2002).

[32] C. Bell, R. Loloee, G. Burnell, and M. G. Blamire, Phys. Rev. B **71**, 180501 (R) (2005).

[33] V. Shelukhin, A. Tsukernik, M. Karpovski, Y. Blum, K. B. Efetov, A. F. Volkov, T. Champel, M. Eschrig, T. Lofwander, G. Schon, and A. Palevski, Phys. Rev. B 73 174506 (2006).

[34] V. A. Oboznov, V. V. Bol'ginov, A. K. Feofanov, V. V. Ryazanov, and A. Buzdin, Phys. Rev. Lett. **96**, 197003 (2006).

[35] M. Weides, K. Tillmann, and H. Kohlstedt, Physica C 437-438, 349-352 (2006).

[36] M. Weides, M. Kemmler, H. Kohlstedt, A. Buzdin, E. Goldobin, D. Koelle, R. Kleiner, Appl. Phys. Lett. **89**, 122511 (2006).

[37] M. Weides, M. Kemmler, E. Goldobin, H. Kohlstedt, R. Waser, D. Koelle, R. Kleiner, Phys. Rev. Lett. v. **97**, 247001 (2006).

[38] H. Sellier, C. Baraduc, F. Lefloch, and R. Calemczuck, Phys. Rev. Lett. v. **92**, n. 25, 257005 (2004).

[39] F. Born, M. Siegel, E. K. Hollmann, H. Braak, A. A. Golubov, D. Yu. Gusakova, and M. Yu. Kupriyanov, Phys. Rev. B. **74**, 140501 (2006).

[40] J. W. A. Robinson, S. Piano, G. Burnell, C. Bell, and M. G. Blamire, Phys. Rev. Lett. **97**, 177003 (2006)

[41] J. W. A. Robinson, S. Piano, G. Burnell, C. Bell, and M. G. Blamire, Phys. Rev. B. **76**, 094522 (2007)

[42] M. Yu. Kupriyanov, A. A. Golubov, M. Siegel, Proc. SPIE **6260** p. 227-238 (2006).

[43] L. B. Ioffe, V. B. Geshkenbein, M. V. Feigelman, A. L. Fauchere, G. Blatter, Nature (London) **398** p. 679 (1999).

[44] A. V. Ustinov, V. K. Kaplunenko, J. Appl. Phys. **94** p. 5405 (2003).

[45] G. Blatter, V. B. Geshkenbein, L.B. Ioffe, Phys. Rev. B. **63**, 174511 (2001)

[46] E. Terzioglu, M.R. Beasley. IEEE Trans. Appl. Superc. Phys. Rev. B. **8**, 48 (1998)

[47] Hans Hilgenkamp, M.R. Supercond. Sci. Technol. **21**, 034011 (5pp) (2008)

[48] G. Binasch, P. Grunberg, F. Saurenbach and W. Zinn, Phys. Rev. B v. **39**, 4828 (1989).

[49] M. N. Baibich, J. M. Broto, A. Fert, F. Nguyen Van Dau, F. Petroff, P. Eitenne, G. Creuzet, A. Friederich and J. Chazelas, Phys. Rev. Lett. v. **61**, 2472 (1988).

[50] F. S. Bergeret, A. F. Volkov, and K. B. Efetov, Phys. Rev. Lett. v. **86**, n. 14, 3140 (2001).

[51] Ya. M. Blanter and F. W. J. Hekking, Phys. Rev. B **69**, 024525 (2004).

[52] E. A. Koshina, V. N. Krivoruchko, Phys. Rev. B **63**, 224515 (2001).

[53] V. N. Krivoruchko and E. A. Koshina, Phys. Rev. B **64**, 172511 (2001).

[54] A. A. Golubov, M. Yu. Kupriyanov, and Ya. V. Fominov, Pis'ma Zh. Eksp. Teor. Fiz., **75**, 223 (2002) [JETP Letters, **75**, 190 (2002)].

[55] Z. Pajovic, M. Bozovic, Z. Radovic, J. Cayssol, A. Buzdin, Phys. Rev. B v. **74**, 184509 (2006).

[56] B. Crouzy, S. Tollis, D. A. Ivanov, Phys. Rev. B **75**, 054503 (2007).

[57] Iver B. Sperstad, Jacob Linder and Asle Sodbo, Phys. Rev. B **78**, 104509 (2008).

[58] A. F. Volkov, F. S. Bergeret, and K. B. Efetov, Phys. Rev. Lett. v. **90**, n. 11, 117006 (2003).

[59] F. S. Bergeret, A. F. Volkov, and K. B. Efetov, Phys. Rev. B **64**, 134506 (2001).

[60] F. S. Bergeret, A. F. Volkov, and K. B. Efetov, Phys. Rev. B **68**, 064513 (2003).

[61] T. Lofwander, T. Champel and M. Eschrig, Phys. Rev. B **75**, 014512 (2007).

[62] R. S. Keizer, S. T. B. Goennenwein, T. M. Klapwijk, G. Miao, G. Xiao, A. Gupta, Nature **439**, 825 (2006).

[63] I. Sosnin, H. Cho, V. T. Petrashov, and A. F. Volkov, Phys. Rev. Lett. **96**, 157002 (2006).

[64] J. W. A. Robinson, J. D. S. Witt, M. G. Blamire, Science 329, 59 (2010)

[65] D. Sprungmann, K. Westerholt, H. Zabel, M. Weides, and H. Kohlstedt, Phys. Rev. B **82**, 060505 (2010)

[66] Teun Klapwijk, Nature Physics **6**, 329 (2010)

[67] M. S. Anwar, F. Czeschka, M. Hesselberth, M. Porcu, and J. Aarts, Phys. Rev. B **82**, 100501 (2010)

[68] Trupti S. Khaire, Mazin A. Khasawneh, W. P. Pratt, Jr., and Norman O. Birge, Phys. Rev. Lett. **104**, 137002 (2010)

[69] Y. Asano, Y. Tanaka, and A. A. Golubov, Phys. Rev. Lett. **98**, 037003 (2007).

[70] Y. Asano, Y. Sawa, Y. Tanaka, and A. A. Golubov, Phys. Rev. B **76**, 224525 (2007).

[71] J. Kopu, M. Eschrig, J. C. Cuevas, and M. Fogelstrom, Phys. Rev. B **69**, 094501 (2004).

[72] M. Eschrig, J. Kopu, J. C. Cuevas, and G. Schon, Phys. Rev. Lett. **90**, 137003 (2003).

[73] M. Eschrig and T. Lofwander, Nature Physics **4**, 138 (2008).

[74] V. Braude and Yu. V. Nazarov, Phys. Rev. Lett. **98**, 077003 (2007).

[75] T. Champel, T. Lofwander, and M. Eschrig, Phys. Rev. Lett. **100**, 077003 (2008).

[76] A. V. Galaktionov, M. S. Kalenkov, and A. D. Zaikin, Phys. Rev. B **77**, 094520 (2008).

[77] A. Kadigrobov, R.I. Shekhter and M. Jonson, Eurorhys. Lett., v. **54**, n. 3, 394 (2001).

[78] M. Houzet and A.I. Buzdin, Phys. Rev. B, v. **76**, 060504(R) (2007).

[79] N. M. Chtchelkatchev and I. S. Burmistrov, Phys. Rev. B **68**, 140501(R) (2003).

[80] I. S. Burmistrov and N. M. Chtchelkatchev, Phys. Rev. B **72**, 144520 (2005).

[81] T. Champel and M. Eschrig, PRB **72**, 054523 (2005).

[82] M. Houzet and A. I. Buzdin, Phys. Rev. B **74**, 214507 (2006).

[83] M. A. Maleki and M. Zareyan Physical Review B **74**, 144512 (2006).

[84] Y. V. Fominov, A. F. Volkov, and K. B. Efetov, Phys. Rev. B **75**, 104509 (2007).

[85] A. F. Volkov and A. Anishchanka, Phys. Rev. B **71**, 024501 (2005).

[86] A.F. Volkov, K.B. Efetov Phys Rev B **78**, 024519 (2008).

[87] B. Crouzy, S. Tollis, D. A. Ivanov, Phys. Rev. B **76** , 134502 (2007).

[88] Ya. V. Fominov, A. A. Golubov, and M. Yu. Kupriyanov, Pis'ma Zh. Eksp. Teor. Fiz. **77**, 609 (2003) [JETP Lett. **77**, 510 (2003)].

[89] G. Nowak, H. Zabel et al, Phys. Rev. B **78**, 134520 (2008).

Chapter 2

Effective Decrease in the Exchange Energy in S–(FN)–S Josephson Structures

Introduction

Experimental corroboration [1] of the existence of π contacts in SFS Josephson junctions (S is a superconductor and F is a ferromagnet) stimulated experimental and theoretical investigations of the processes in the SF structures [2–4]. At present, significant efforts are focused on seeking ferromagnetic materials that would allow the manufacture of SFS junctions applicable in various low-power devices. Analysis of the existing experimental data [5–20] shows that the exchange energy H in available ferromagnetic materials lies in a range from 850 to 2300 K. Owing to such high H values, the typical penetration length of superconducting correlations,$\xi = \xi_{F1} + i\xi_{F2}$, induced in a ferromagnet due to the proximity effect is equal to several nanometers ($\xi_{F1} \approx$ 1.2–4.6 nm,). These values are much smaller than the typical lengths $\xi_N \approx$ 10–100 nm of the superconductivity penetration into a normal metal (N). These lengths (ξ_{F1} and ξ_{F2}) determine the typical scale of decreasing the critical current I_C of the SFS junctions with an increase in the interelectrode distance L and oscillation period $I_C(L)$. Such small ξ_{F1} and ξ_{F2} values significantly complicate the technology of manufacturing the SFS junctions with reproducible parameters and lead to the degradation of the high-frequency properties of such junctions. The probability of finding a technological F material whose H value is an order of magnitude smaller is relatively low [20]. This fact stimulates the search for other solutions to this problem. One of them is an "effective" decrease in H in the composite NF structures. In this work, it is shown that this effect exists and can lead to an increase in the effective ξ_{F1} and ξ_{F2} values to the scale of ξ_N lengths.

In this Chapter the critical current Ic of S–(FN)–S Josephson structures has been calculated as a function of the distance L between superconducting (S) electrodes using the Usadel quasiclassical equations for the case of specifying the supercurrent in the direction parallel to the interface between the ferromagnetic (F) and normal (N) films of the composite

weak-link region. It has been shown that, owing to the interaction between F and N films, both the typical decrease scale $I_C(L)$ and the period of the critical current oscillations can be much larger than the respective quantities for the SFS junctions. The conditions have been determined under which these lengths are on the order of the effective depth ξ_N of superconductivity penetration to a normal metal.

2.1 Structure of S-FN-S junction and its mathematical description

In this Chapter S-FN-S Josephson junction (Fig. 2.1) is considered, that consists of two massive superconducting electrodes connected to each other by a bilayer NF structure. The width of F layer is $d_F$and of N layer is d_N. It is suggested that the "dirty" limit conditions are satisfied in the N and F materials, and exchange energy $H = 0$ in the normal metal and Magnetization vector is perpendicular to SF interface in F film. The origin of the coordinate system is in the middle of the structure and the x and y axes are perpendicular and parallel to the NF interface, respectively (Fig. 2.1).

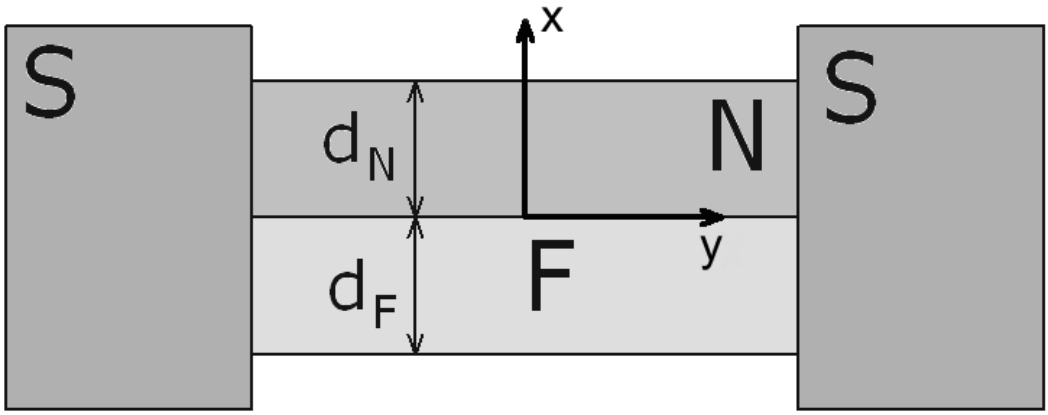

Figure 2.1. Structure of S-FN-S Josephson junction.

It is suggested that the structure is completely symmetric and the suppression parameters $\gamma_{BN} = R_{B1}\mathcal{A}_{B1}/\rho_N\xi_N$ and $\gamma_{BF} = R_{B2}\mathcal{A}_{B2}/\rho_F\xi_F$ characterizing the NS and FS interfaces, respectively, are large

$$\gamma_{BN} \gg \max\left\{1, \frac{\rho_S\xi_S}{\rho_N\xi_N}\right\}, \quad \gamma_{BF} \gg \max\left\{1, \frac{\rho_S\xi_S}{\rho_F\xi_F}\right\},$$

so that the suppression of superconductivity in S electrodes can be disregarded. Here, R_{B1}, R_{B2} and $\mathcal{A}_{B1}, \mathcal{A}_{B2}$ - are the resistance and area of the SN (SF) interface, respectively, ρ_S, ρ_F, ρ_N and $\xi_S = (D_S/2\pi T_C)^{1/2}$, $\xi_F = (D_F/2\pi T_C)^{1/2}$, $\xi_N = (D_N/2\pi T_C)^{1/2}$ are

the resistivities and coherence lengths of the materials, respectively; $D_{S,N,F}$ - are the diffusion coefficients of the respective materials; and , T_C - is the critical temperature of the superconducting electrodes.

Under the above assumptions, it can be suggested that the Green's functions G_S and Φ_S in superconducting electrodes are equal to their equilibrium values $G_S = \omega/\sqrt{\omega^2 + \Delta^2}$, $\Phi_S = \Delta \exp\{\pm i\varphi/2\}$, where Δ and φ -are the absolute value and phase difference of the order parameters of the superconducting electrodes. The properties of the weak-link region can be described by using the linearized Usadel equation [17]. In the Φ - parameterization, they are represented in the form [18]:

$$\xi_N^2 \left\{ \frac{\partial^2}{\partial x^2} + \frac{\partial^2}{\partial y^2} \right\} \Phi_N - \frac{|\omega|}{\pi T_c} \Phi_N = 0, \tag{2.1}$$

$$\xi_F^2 \left\{ \frac{\partial^2}{\partial x^2} + \frac{\partial^2}{\partial y^2} \right\} \Phi_F - \frac{\widetilde{\omega}}{\pi T_c} \Phi_F = 0, \tag{2.2}$$

where $\omega = T\pi(2n+1)$ -are the Matsubara frequencies and $(n = 0, \pm 1, \pm 2...)$, $\widetilde{\omega} = |\omega| + iH \operatorname{sgn}\omega$. The boundary conditions at the SN and SF interfaces (for $y = \pm L/2$) have the form [18], [30]

$$\gamma_{BN}\xi_N \frac{\partial}{\partial y}\Phi_N = \pm G_S \Delta \exp\{\pm i\varphi/2\}, \tag{2.3}$$

$$\gamma_{BF}\xi_F \frac{\partial}{\partial y}\Phi_F = \pm \frac{\widetilde{\omega}}{|\omega|} G_S \Delta \exp\{\pm i\varphi/2\}. \tag{2.4}$$

The boundary conditions at the FN interface (for $x = 0$) have the form [18], [30]:

$$\frac{\xi_N}{|\omega|}\frac{\partial}{\partial x}\Phi_N = \gamma \frac{\xi_F}{\widetilde{\omega}}\frac{\partial}{\partial x}\Phi_F, \tag{2.5}$$

$$\gamma_B \xi_F \frac{\partial}{\partial x}\Phi_F + \Phi_F = \frac{\widetilde{\omega}}{|\omega|}\Phi_N, \tag{2.6}$$

$$\gamma_B = R_{B3}\mathcal{A}_{B3}/\rho_F\xi_F, \quad \gamma = \rho_N\xi_N/\rho_F\xi_F,$$

where R_{B3} and $\mathcal{A}_{B3}$ - are the resistance and area of the NF interface, respectively. The conditions at the free boundaries of the weak-link region at $x = d_N$ and $x = -d_F$ reduce to the equations

$$\frac{\partial \Phi_F}{\partial x} = 0, \quad \frac{\partial \Phi_N}{\partial x} = 0, \tag{2.7}$$

which ensure the absence of the current through these boundaries.

For further simplification of the problem, the thicknesses of the F and N films are assumed to be sufficiently small:

$$d_N \ll \xi_N, \quad d_F \ll \xi_F. \tag{2.8}$$

and the solution of the boundary value problem given by (5.1)-(2.7) is sought in the form of the expansion in small parameters (d_N/ξ_N) and (d_F/ξ_F). In the first approximation, the functions Φ_N and Φ_F

$$\Phi_N(x,y) = A(y), \Phi_F(x,y) = B(y) \tag{2.9}$$

are independent of the coordinate x. In the next approximation, taking into account (2.7) we arrive at the expressions

$$\Phi_N = A(y) + \left\{ \frac{|\omega|}{\pi T_c \xi_N^2} A(y) - \frac{\partial^2}{\partial y^2} A(y) \right\} \frac{(x-d_N)^2}{2}, \tag{2.10}$$

$$\Phi_F = B(y) + \left\{ \frac{\widetilde{\omega}}{\pi T_c \xi_F^2} B(y) - \frac{\partial^2}{\partial y^2} B(y) \right\} \frac{(x+d_F)^2}{2}. \tag{2.11}$$

The substitution of (2.10), (2.11) into boundary conditions (2.5), (2.6) yields the following system of two equations for the functions $A(y)$ and $B(y)$:

$$\left[\zeta_F^2 \frac{\partial^2}{\partial y^2} - (\gamma_F \frac{\widetilde{\omega}}{\pi T_c} + 1) \right] B(y) + \frac{\widetilde{\omega}}{|\omega|} A(y) = 0, \tag{2.12}$$

$$B(y) \frac{|\omega|}{\widetilde{\omega}} + \left[\zeta_N^2 \frac{\partial^2}{\partial y^2} - (\gamma_N \frac{|\omega|}{\pi T_c} + 1) \right] A(y) = 0, \tag{2.13}$$

where

$$\zeta_F = \sqrt{\gamma_F} \xi_F, \quad \zeta_N = \sqrt{\gamma_N} \xi_N, \tag{2.14}$$

$$\gamma_F = \gamma_B \frac{d_F}{\xi_F}, \quad \gamma_N = \frac{\gamma_B}{\gamma} \frac{d_N}{\xi_N}. \tag{2.15}$$

The solution of this system of equations is represented in the form

$$A(y) = A_1 \cosh q_1 y + A_2 \sinh q_1 y + A_3 \cosh q_2 y + A_4 \sinh q_2 y,$$

$$B(y) = B_1 \cosh q_1 y + B_2 \sinh q_1 y + B_3 \cosh q_2 y + B_4 \sinh q_2 y,$$

where coefficients are related as follows:

$$B_1 = -\frac{1}{\zeta_F^2} \beta \frac{\widetilde{\omega}}{|\omega|} A_1, B_2 = -\frac{1}{\zeta_F^2} \beta \frac{\widetilde{\omega}}{|\omega|} A_2, \tag{2.16}$$

$$B_3 = \zeta_N^2 \frac{1}{\beta} \frac{\widetilde{\omega}}{|\omega|} A_3, B_4 = \zeta_N^2 \frac{1}{\beta} \frac{\widetilde{\omega}}{|\omega|} A_4,$$

Here, q_1 and q_2 are the roots of the characteristic equation

$$q_{1,2}^2 = \frac{1}{2} \left[u^2 + v^2 \pm \sqrt{(u^2 - v^2)^2 + 4\zeta_F^{-2} \zeta_N^{-2}} \right], \tag{2.17}$$

$$u^2 = \frac{1}{\zeta_N^2} + \frac{\Omega}{\xi_N^2}, \quad v^2 = \frac{1}{\zeta_F^2} + \frac{\Omega}{\xi_F^2} + i \frac{h}{\xi_F^2}, \tag{2.18}$$

and parameter β is:

$$\beta = \frac{2}{\left[u^2 - v^2 + \sqrt{\left(u^2 - v^2\right)^2 + 4\zeta_F^{-2}\zeta_N^{-2}}\right]}, \tag{2.19}$$

and $\Omega = |\omega| \setminus \pi T_C$, $\widetilde{\Omega} = \widetilde{\omega} \setminus \pi T_C$, $h = H/\pi T_C \operatorname{sgn}(\omega)$.

The integration constants A_1, A_2, A_3, A_4 are determined from boundary conditions (2.3), (2.4):

$$A_1 = \frac{1 - s\beta\frac{\xi_N}{\xi_F}\zeta_N^{-2}}{\gamma_{BN}(1+\kappa^2)} \frac{G_S\Delta\sin(\varphi/2)}{\xi_N q_1 \cosh q_1\frac{L}{2}}, \tag{2.20}$$

$$A_2 = i\frac{1 - s\beta\frac{\xi_N}{\xi_F}\zeta_N^{-2}}{\gamma_{BN}(1+\kappa^2)} \frac{G_S\Delta\cos(\varphi/2)}{\xi_N q_1 \sinh q_1\frac{L}{2}}, \tag{2.21}$$

$$A_3 = \frac{1 + \beta\frac{\xi_F}{\xi_N\zeta_F^2 s}}{\gamma_{BF}(1+\kappa^2)} \frac{G_S\Delta\cos(\varphi/2)}{\xi_F q_2 \sinh q_2\frac{L}{2}}, \tag{2.22}$$

$$A_2 = i\frac{1 + \beta\frac{\xi_F}{\xi_N\zeta_F^2 s}}{\gamma_{BF}(1+\kappa^2)} \frac{G_S\Delta\sin(\varphi/2)}{\xi_F q_2 \cosh q_2\frac{L}{2}}, \tag{2.23}$$

Here $s = \gamma_{BN}/\gamma_{BF}$, $\kappa = \beta(\zeta_F\zeta_N)^{-1}$.

The substitution of the solution obtained in the form of into the expression J_S for the superconducting current

$$\begin{aligned} J_S &= \frac{i\pi T\mathcal{A}_{B2}}{2e\rho_F}\sum_{\omega=-\infty}^{\infty}\frac{1}{\widetilde{\omega}^2}\left[B_\omega\frac{\partial}{\partial y}B^*_{-\omega} - B^*_{-\omega}\frac{\partial}{\partial y}B_\omega\right] + \\ &+\frac{i\pi T\mathcal{A}_{B1}}{2e\rho_N}\sum_{\omega=-\infty}^{\infty}\frac{1}{\omega^2}\left[A_\omega\frac{\partial}{\partial y}A^*_{-\omega} - A^*_{-\omega}\frac{\partial}{\partial y}A_\omega\right] \end{aligned} \tag{2.24}$$

yields the sinusoidal dependence $J_S = I_C\sin\varphi$. It is convenient to represent the critical current $I_C = I_{C1} + I_{C2}$ as the sum of two terms:

$$I_{C2} = \frac{2\pi T}{eR_{BF}\gamma_{BF}}\operatorname{Re}\sum_{\omega>0}^{\infty}\frac{G_S^2\Delta^2\omega^{-2}(1+\beta s^{-1}\frac{\xi_F}{\xi_N\zeta_F^2})^2}{(1+\kappa^2)\,\xi_F q_2\sinh Lq_2}, \tag{2.25}$$

$$I_{C1} = \frac{2\pi T}{eR_{BN}\gamma_{BN}}\operatorname{Re}\sum_{\omega>0}^{\infty}\frac{G_S^2\Delta^2\omega^{-2}(1-\beta s\frac{\xi_N}{\xi_F\zeta_N^2})^2}{(1+\kappa^2)\,\xi_N q_1\sinh Lq_1}. \tag{2.26}$$

Expressions (6.47)-(2.19), (5.12), (2.26) specify a general expression for the critical current of the S–(FN)–S Josephson junctions under investigation. According to these relations, by complete analogy with oscillatory systems with two degrees of freedom, the S–(FN)–S structure under consideration can be characterized in terms of the partial coherence lengths $u,\ v$ and the proper coherence lengths

$$q_1 = \xi_{11}^{-1} + i\xi_{21}^{-1},\ q_2 = \xi_{12}^{-1} + i\xi_{22}^{-1} \tag{2.27}$$

The parameters ζ_F^{-1} and ζ_N^{-1} are the coupling constants. It is easy to see that the amplitude distribution coefficients at the proper coherence lengths, which are proportional to β are determined only by the material constants of the structure and are independent of the boundary conditions at the SN and SF interfaces, respectively. The way of current injection in the weak- link region (through the ratio γ_{BN}/γ_{BF}) is taken into account in (6.45)-(2.23), (5.12), (2.26) by the coefficient s, and the subsequent redistribution of the injected current between the F and N films is determined by the ratio γ_F/γ_N. The approach developed above is applicable when the all characteristic lengths in the problem are much larger than the thicknesses of the normal and ferromagnetic films:

$$\xi_{11},\ \xi_{21}\ \xi_{12},\ \xi_{22} \gg d_F, d_N. \tag{2.28}$$

2.2 Analysis of inverse coherence lengths and critical current

Analysis of expressions (5.12), (2.26) for the critical current components and inverse coherence lengths are simplified for a number of limiting cases.

2.2.1 The limit of a high resistance of the FN weak-link interface

In the limit of a high resistance of the FN weak-link interface

$$\zeta_N \gg \xi_N, \quad \zeta_F \gg \xi_F \tag{2.29}$$

the coupling constants between the F and N films are small. In the first approximation in ζ_N^{-1} and ζ_F^{-1} , the supercurrent in the structure flows through two independent channels and formulas for I_{C1} and I_{C2} are transformed to the expressions for the critical currents [18], [24], [31], that were previously obtained for two-barrier SIFIS and SINIS junctions:

$$\frac{eR_{B2}I_{C2}}{2\pi T_C} = \frac{T}{\gamma_{BF}T_C}\sum_{\omega>0}^{\infty}\mathrm{Re}\left\{\frac{G_S^2\Delta^2}{\omega^2\xi_F q_2 \sinh Lq_2}\right\}, \tag{2.30}$$

$$\frac{eR_{B1}I_{C1}}{2\pi T_C} = \frac{T}{\gamma_{BN}T_C}\sum_{\omega>0}^{\infty}\frac{G_S^2\Delta^2}{\omega^2\xi_N q_1 \sinh Lq_1}, \tag{2.31}$$

where

$$q_2^2 = q_{20}^2 = \frac{\Omega}{\xi_F^2} + i\frac{h}{\xi_F^2}, q_1^2 = q_{10}^2 = \frac{\Omega}{\xi_N^2}. \tag{2.32}$$

In the next approximation, the proper inverse coherence lengths are easily expressed as

$$q_1^2 = q_{10}^2 + \frac{1}{\zeta_N^2} + \frac{\xi_F^2(\Omega + ih)}{\zeta_F^2\zeta_N^2\left(h^2 + \Omega^2\right)}, \tag{2.33}$$

$$q_2^2 = q_{20}^2 + \frac{1}{\zeta_F^2} - \frac{\xi_F^2(\Omega + ih)}{\zeta_F^2\zeta_N^2\left(h^2 + \Omega^2\right)}. \tag{2.34}$$

According to (2.33), (2.34)the proximity effect between the N and F films leads to a small decrease in the effective exchange energy in the F film. The physical meaning of these changes is obvious. An electron for a certain time can be in the N part of the FN film of the structure. This is equivalent to the subjection of electrons to the effective exchange energy averaged over the thickness of the FN film, which is obviously lower than the exchange energy in the ferromagnetic part of the structure. Changes in the damping of the superconductivity in the N film are more significant. In this case, the exponential decrease law changes to damping oscillations. However, their period in this approximation is much larger than ξ_N

$$\Lambda = 4\pi\xi_N \frac{\sqrt{\Omega}\zeta_F^2\zeta_N^2\left(h^2 + \Omega^2\right)}{\xi_N^2\xi_F^2 h} \gg \xi_N, \tag{2.35}$$

It increases infinitely for $h \to 0$ and is proportional to h for $h \gg \Omega$. This means that the term I_{C2} in this case in the expression for the critical current is negligibly small and $I_C \approx I_{C1}$. In contrast to similar SNS junctions without F films, the dependence $I_{C1}(L)$ has the form of damping oscillations. This effect is a consequence of the double proximity effect, because the superposition between the superconducting correlations induced from superconductors and spin ordering from the ferromagnet occurs in the N film. However, the oscillation period is very large; for this reason, the experimental observation of the transition to the π-state is complicated in the case considered above.

2.2.2 The limit of small resistance of the FN weak-link interface

In the opposite limiting case $\zeta_F \ll \xi_F$ and $\zeta_N \ll \xi_N$, strong coupling between the F and N films occurs in the weak-link region. In this case, the inverse proper coherence lengths are easily obtained in the form

$$q_{1+\theta(\zeta_N-\zeta_F)} = \frac{\sqrt{\zeta_N^2 + \zeta_F^2}}{\zeta_N\zeta_F} + \frac{\Omega\zeta_N\zeta_F}{2(\zeta_F^2 + \zeta_N^2)^{3/2}}\left(\frac{\zeta_F^2}{\xi_N^2} + \frac{\zeta_N^2}{\xi_F^2} + ih\frac{\zeta_N^2}{\xi_F^2}\right), \tag{2.36}$$

$$q_{2-\theta(\zeta_N-\zeta_F)} = \frac{1}{\sqrt{\zeta_N^2 + \zeta_F^2}}\sqrt{\left(\frac{\zeta_F^2}{\xi_F^2} + \frac{\zeta_N^2}{\xi_N^2}\right)\Omega + ih\frac{\zeta_F^2}{\xi_F^2}}, \tag{2.37}$$

where θ - Hevecide function. From (2.36), (2.37) it follows that the ferromagnetic film in the limit $\zeta_F \gg \zeta_N$ additionally suppresses superconductivity induced in the N region, so that

$$q_1 = \frac{1}{\zeta_N} + \frac{\Omega\zeta_N}{2\zeta_F^2}\left(\frac{\zeta_F^2}{\xi_N^2} + \frac{\zeta_N^2}{\xi_F^2}\right) + ih\frac{\Omega\zeta_N^3}{2\zeta_F^2\xi_F^2}, \tag{2.38}$$

$$q_2 = \sqrt{\frac{\Omega + ih}{\xi_F^2} + \frac{\zeta_N^2\Omega}{\zeta_F^2\xi_N^2}}. \tag{2.39}$$

It is seen that the coherence length and oscillation period of the term I_{C2} in this case coincides in the first approximation with the respective quantities for the SFS junctions, whereas the term I_C in I_{C1} damps at lengths $(\mathrm{Re}(q_1))^{-1} \approx \zeta_N \ll \xi_N$.

In the limit $\zeta_N \gg \zeta_F$ the processes in the N film are determining, so that

$$q_2 = \frac{1}{\zeta_F} + \frac{\Omega\zeta_F}{2\xi_F^2} + ih\frac{\Omega\zeta_F}{2\xi_F^2}, \tag{2.40}$$

$$q_1 = \sqrt{\frac{\Omega}{\xi_N^2}\left(1 + \frac{\zeta_F^2\xi_N^2}{\zeta_N^2\xi_F^2}\right) + i\frac{h}{\xi_F^2}\frac{\zeta_F^2}{\zeta_N^2}}. \tag{2.41}$$

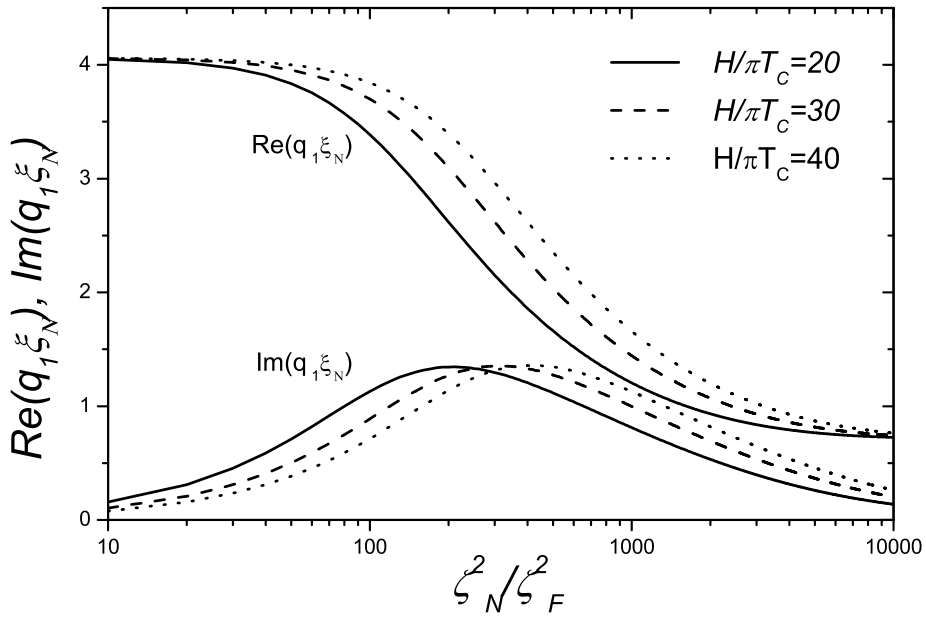

Figure 2.2. Real and imaginary parts of inverse coherence length q_2 versus the parameter $z = (\zeta_N/\zeta_F)^2$ at $\xi_N/\zeta_N = 4$, $\xi_N/\xi_F = 10$, $T = 0.5T_C$, and $h = 20, 30, 40$.

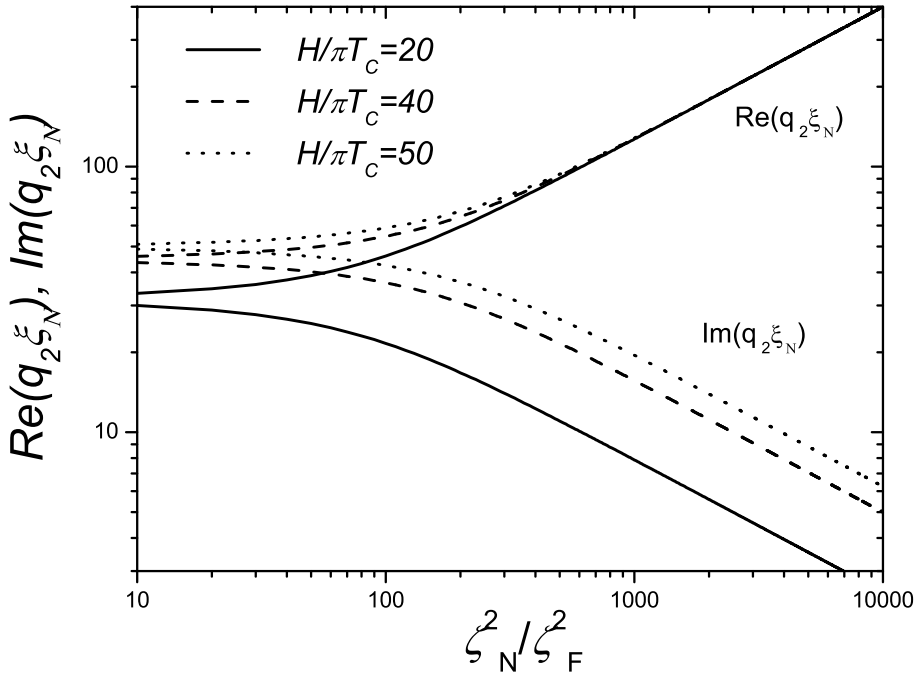

Figure 2.3. Real and imaginary parts of inverse coherence length q_1 versus the parameter $z = (\zeta_N/\zeta_F)^2$ at $\xi_N/\zeta_N = 4$, $\xi_N/\xi_F = 10$, $T = 0.5T_C$, and $h = 20, 40, 50$.

Therefore, the term I_{C2} in the critical current decreases more sharply than I_{C1}. In particular, the typical damping scale for superconducting correlations is approximately equal to $\xi_{N\Omega} = \xi_N/\sqrt{\Omega}$, whereas the effective exchange energy decreases by a factor of $z^{-1} = \zeta_F^2/\zeta_N^2 \ll 1$.

Thus, when $\zeta_F \ll \zeta_N \ll \xi_N$ both the damping scale and oscillation period of $I_C(L)$ in the S–(FN)– S structures under consideration are much larger than the respective values in similar SFS junctions, where the normal film is absent. This statement is illustrated by the numerical calculation results shown in Figs.2.2 - 2.6.

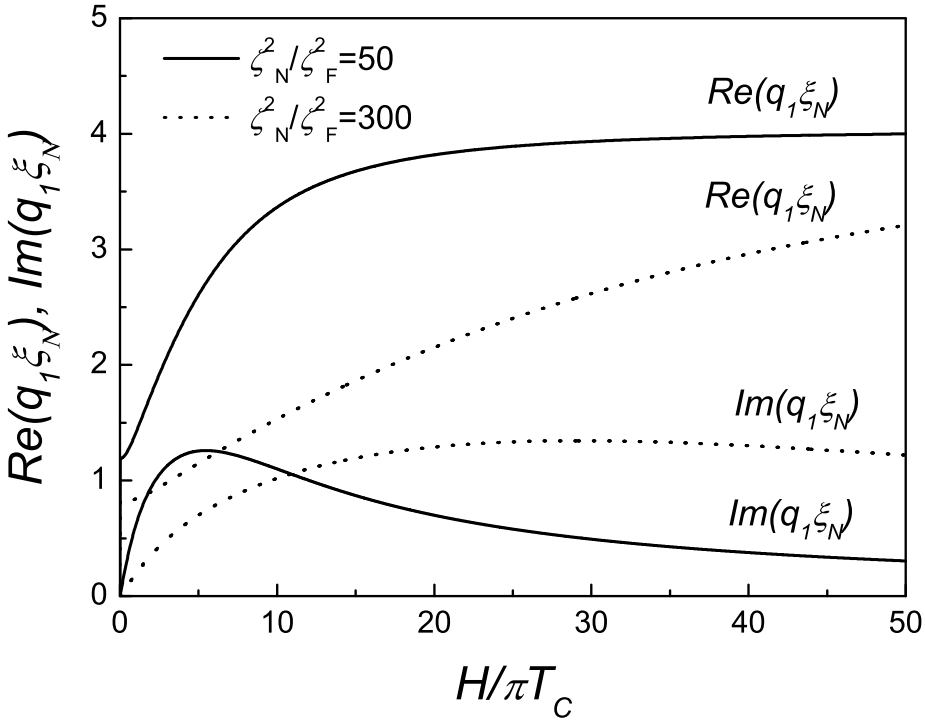

Figure 2.4. Real and imaginary parts of inverse coherence length q_1 at $H/\pi T_C$, $\xi_N/\zeta_N = 4$, $\xi_N/\xi_F = 10$, $T = 0.5T_C$, and $z = (\zeta_N/\zeta_F)^2 = 50, 300$.

Figures 2.2 and 2.3 show the real and imaginary parts of q_2 and q_1 respectively, as functions of $(\zeta_N/\zeta_F)^2$, for $T = 0.5T_C$, $h = 20, 30, 40$ and $\xi_N = 10\xi_F$ and $\xi_N = 4\zeta_N$. it is seen that for $h = 30$ $\mathrm{Im}(q_2\xi_N)$ has maximum at $(\zeta_N/\zeta_F)^2 \approx 300$. The oscillation period of the critical current near this maximum is $\Lambda = 2\pi(\mathrm{Im}(q_2)^{-1} \approx 1.5\pi\xi_N$, and its damping length is $(\mathrm{Re}(q_2))^{-1} \approx 0.4\xi_N$ The damping scale of the second term in the expression for the critical current is $(\mathrm{Re}(q_2))^{-1} \approx 0.014\xi_N$ which is two orders of magnitude smaller. Such strong difference between the damping lengths, allows observation of the transition to the π state in the structures, where the distance between the electrodes is an order of magnitude larger than that in the available structures.

Fig. 2.4 shows dependences of real and imaginary parts of q_1 on exchange energy for parameter $z = 50, 300$. At small H critical current decrease without oscillations. With H increase the period of oscillations is decreased. It is seen that the imaginary part of q_1 has a maximum as function exchange energy and, with increase of z this maximum moves towards large values of H. The value of this maximum increases with growth of z, and at $z \sim 50$ leaves on saturation. Simultaneously the damping length decreases with increase of H.

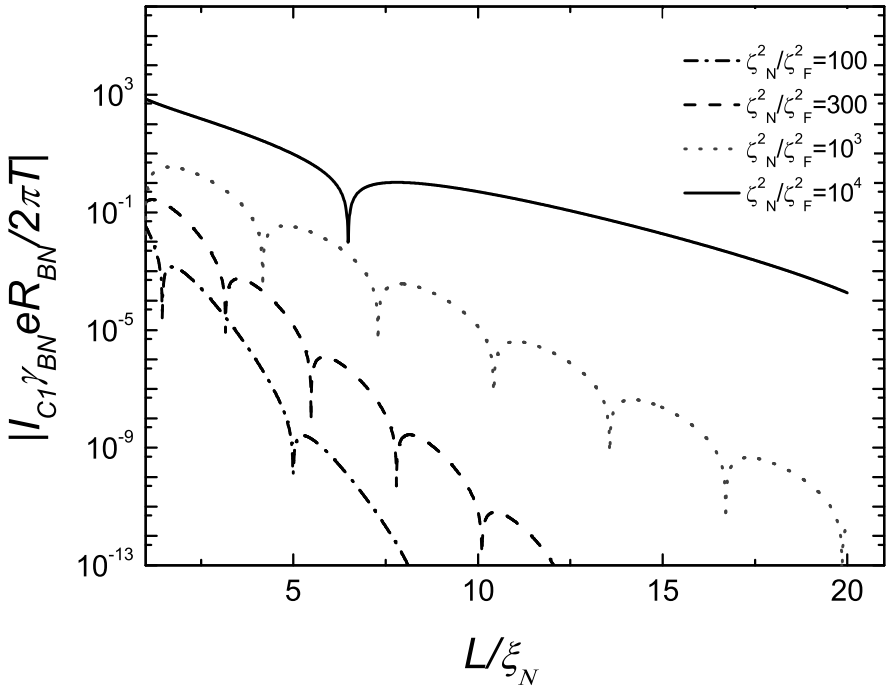

Figure 2.5. Normalized value of part of criticul current I_{C1} versus the distance L/ξ_N between the superconducting electrodes for $h = 30$, $\xi_N/\zeta_N = 4$, $\xi_N/\xi_F = 10$, $T = 0.5T_C$, $s = 1$, and $z = (\zeta_N/\zeta_F)^2 = 100, 300, 1000, 10000$.

Figs. 2.5 and 2.6 show the critical current components I_{C1} and I_{C2} as functions of the distance L between electrodes for $T = 0.5T_C$ and various values of the parameter $z = (\zeta_N/\zeta_F)^2$.

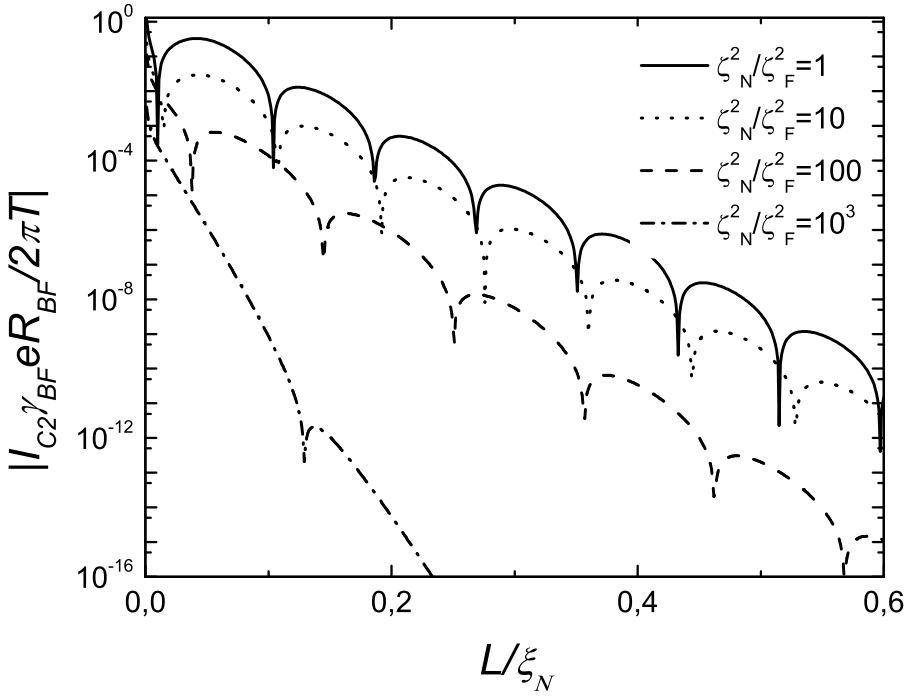

Figure 2.6. Normalized value of part of critical current I_{C2} of the critical current versus the distance L/ξ_N between the superconducting electrodes for $h = 30$, $\xi_N/\zeta_N = 4$, $\xi_N/\xi_F = 10$, $T = 0.5T_C$, $s = 1$, and $z = (\zeta_N/\zeta_F)^2 = 1, 10, 100, 1000$.

It is easy to see that the component I_{C2} at the given parameters decreases sharply with an increase in L and, in agreement with expectations, its contribution to I_C is negligibly small already at $L \approx 0.5$, i.e., long before the appearance of the first minimum in I_{C2}. It is interesting that the oscillation period in $I_C \approx I_{C2}$ is a nonmonotonic function of the parameter z. It has the minimum at $z \approx 300$.

2.3 Conclusion

Thus, it has been shown that the use of a bilayer thin-film FN structure as a weak-link material can lead to the effective decrease in H and to a significant increase in both the damping length and oscillation period of the dependence $I_C(L)$ of the S–(FN)–S junctions as compared to the respective values for similar structures containing only the ferromagnetic film.

Bibliography

[1] V. V. Ryazanov, V. A. Oboznov, A. Yu. Rusanov, A. V. Veretennikov, A. A. Golubov, and J. Aarts, Phys. Rev. Lett. **86**, 2427 (2001).

[2] A. A. Golubov, M. Yu. Kupriyanov, and E. Il'ichev, Rev. Mod. Phys. **76**, 411 (2004).

[3] A. I. Buzdin, Rev. Mod. Phys. **77**, 935 (2005).

[4] F. S. Bergeret, A. F. Volkov, K. B. Efetov, Rev. Mod. Phys. **77**, 1321 (2005).

[5] S. M. Frolov, D. J. Van Harlingen, V. A. Oboznov, V. V. Bolginov, and V. V. Ryazanov, Phys. Rev. B **70**, 144505 (2004).

[6] S. M. Frolov, D. J. Van Harlingen, V. V. Bolginov, V. A. Oboznov, and V. V. Ryazanov, Phys. Rev. B **74**, 020503 (2006).

[7] T. Kontos, M. Aprili, J. Lesueur, et al., Phys. Rev. Lett. **89**, 137007 (2002).

[8] H. Sellier, C. Baraduc, F. Lefloch, and R. Calemczuck, Phys. Rev. B **68**, 054531 (2003).

[9] Y. Blum, A. Tsukernik, M. Karpovski, et al., Phys. Rev. B **70**, 214501 (2004).

[10] C. Surgers, T. Hoss, C. Schonenberger, et al., J. Magn. Magn. Mater. **240**, 598 (2002).

[11] C. Bell, R. Loloee, G. Burnell, and M. G. Blamire Phys. Rev. B **71**, 180501 (R) (2005).

[12] V. Shelukhin, A. Tsukernik, M. Karpovski, Y. Blum, K. B. Efetov, A. F. Volkov, T. Champel, M. Eschrig, T. Löfwander, G. Schö

[13] V. A. Oboznov, V. V. Bol'ginov, A. K. Feofanov, V. V. Ryazanov, and A. Buzdin, Phys. Rev. Lett. **96**, 197003 (2006).

[14] M. Weides, K. Tillmann, and H. Kohlstedt, Physica C 437-438, 349-352 (2006).

[15] M. Weides, M. Kemmler, H. Kohlstedt, A. Buzdin, E. Goldobin, D. Koelle, R. Kleiner, Appl. Phys. Lett. **89**, 122511 (2006).

[16] M. Weides, M. Kemmler, E. Goldobin, H. Kohlstedt, R. Waser, D. Koelle, R. Kleiner, cond-mat/0605656, submitted to PRL.

[17] H. Sellier, C. Baraduc, F. Lefloch, and R. Calemczuck, Phys. Rev. Lett. **92**, 257005 (2004).

[18] F. Born, M. Siegel, E. K. Hollmann, H. Braak, A. A. Golubov, D. Yu. Gusakova, and M. Yu. Kupriyanov, Phys. Rev. B. **74**, 140501 (2006).

[19] J. W. A. Robinson, S. Piano, G. Burnell, C. Bell, and M. G. Blamire, Phys. Rev. Lett. **97**, 177003 (2006)

[20] M. Yu. Kupriyanov, A. A. Golubov, M. Siegel, Proc. SPIE **6260** p. 227-238 (2006).

[21] L. Usadel, Phys. Rev. Lett. textbf{25}, 507 (1970).

[22] M. Yu. Kuprianov and V. F. Lukichev, Zh. Eksp. Teor. Fiz. **94**, 139 (1988) [Sov. Phys. JETP **67**, 1163 (1988)].

[23] E. A. Koshina and V. N. Krivoruchko, Fiz. Nizk. Temp. 26, **157** (2000) [Low Temp. Phys. **26**, 115 (2000)].

[24] A. A. Golubov, M. Yu. Kupriyanov, Pis'ma Zh. Eksp.Teor.Fiz., **75**, 709 (2002) [JETP Letters, **75**, 588 (2002)].

[25] A. I. Buzdin, Pis'ma Zh. Eksp.Teor.Fiz., **78**, 1073 (2003) [JETP Letters, **78**, 583 (2003)].

Chapter 3

Critical current in S-FNF-S Josephson junctions with collinear magnetization vectors of ferromagnetic films

Introduction

The possibility of controlling the critical current of Josephson junctions, i.e., creating a Josephson transistor, was actively discussed previously in application to structures with a two-dimensional gas or semiconductor as a weak-link material [1]. The theoretical estimates and experimental investigations (see [2] and references in this work) show that the gain of such a device is usually much smaller than one and, therefore, this device is not attractable for applications. In recent theoretical works [3, 4], it was shown that the critical current in Josephson structures containing ferromagnetic (F) materials can also be efficiently controlled by varying the angle between the magnetization directions in these F layers by means of an external magnetic field. In particular, in SFIFS structures [5–7], where two sandwiches consisting of superconducting (S) and ferromagnetic (F) films are separated by an insulator (I), change of the parallel orientation of the magnetizations of the F layers to the antiparallel orientation can give rise to the transformation of a state with a finite critical current not only to a state with zero critical current but also to a state with a negative critical current. Unfortunately, the geometry of the SFIFS structures makes the implementation of change in the angle very difficult. From this point of view, SFSF structures investigated in [8–10], where one of the F films is screened from the external film by a superconducting electrode, are more convenient. The triplet component of the critical current appears in such contacts at the angle $\alpha \neq 0, \pi$. The characteristic damping length of this component in the F layer is much larger than the characteristic damping length of the critical current at $\alpha = 0$ or π. This circumstance allows one to control the parameters of the structure by varying the angle α. Unfortunately, in order to implement such control, it is necessary to separate the ferromagnetic layers by a sufficiently thin S electrode. This gives rise to the degradation of its critical temperature [11] and to the significant connect-

edness of the magnetization directions of the F films, which hinders independent change in their orientations. The second general demerit of the SFS Josephson structures with traditional geometry [12–26] is a very small characteristic length $\xi = \xi_1 + i\xi_2$ of penetration of superconducting correlations induced in a ferromagnet owing to the proximity effect. It is equal to several nanometers and is much smaller than the typical lengths ξ_N of superconductivity penetration into a normal (N) metal. In this Chapter it is shown that both these disadvantages can be overcome in S–FNF–S contacts by specifying the supercurrent in the direction parallel to the FN interface of the composite weak-link region. In such structures, the direction of the magnetization of one of the F layers can be pinned by using an antiferromagnetic substrate. The efficient decrease in the exchange energy investigated previously [27] can simultaneously be used not only for the increase in ξ_{F1} and ξ_{F2} to the ξ_N scale but also for the efficient control over the critical current in such junctions.

3.1 Structure of S-FNF-S junction and its mathematical description

In this Chapter Josephson junctions of S-FNF-S type are analyzed (Fig. 3.1). This junction consists of two superconducting electrodes which are connected by FNF trilaer structure. Width of F films are equal and they are d_F and width of normal film is $2d_N$. In such structure current flows parallel to FN interface of the weak-link region. Direction of magnetization of lower ferromagnetic film is fixed (exchange energy is H_1) and the value and sign of magnetization of the upper ferromagnetic film can be changed by value and sign (exchange energy is H_2). The origin of the coordinate system is in the middle of the structure and the x and y axes are perpendicular and parallel to the NF interface, respectively Fig. 3.1.

It is also suggested that the structure is completely symmetric and the suppression parameters characterizing the NS and FS interfaces, respectively, are large so that the suppression of superconductivity in the S electrodes can be disregarded.

Under the above assumptions, it can be suggested that the Green's functions G_S and Φ_S in superconducting electrodes are equal to their equilibrium values $G_S = \omega/\sqrt{\omega^2 + \Delta^2}$, $\Phi_S = \Delta \exp\{\pm i\varphi/2\}$, where Δ and φ - are the absolute value and phase difference, respectively, of the order parameters of the superconducting electrodes. The properties of the weak-link region can be described via the linearized Usadel equations [17]. If the mag-

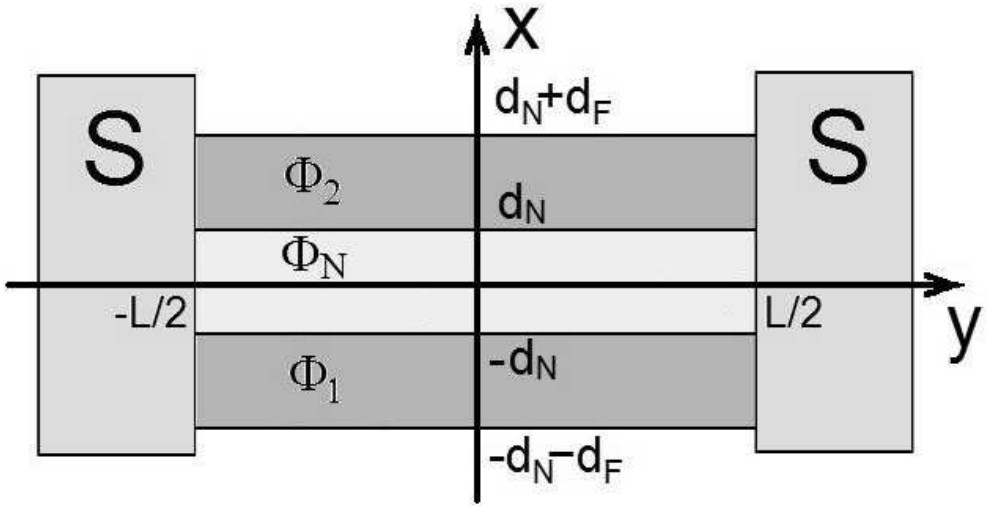

Figure 3.1. Structure of S-FNF-S junction.

netization vectors of F films are perpendicular to the FS interfaces, the triplet component is absent in the system and linearized Usadel equations in the Φ parameterization are represented in the form

$$\xi_N^2 \left\{ \frac{\partial^2}{\partial x^2} + \frac{\partial^2}{\partial y^2} \right\} \Phi_N - \frac{|\omega|}{\pi T_c} \Phi_N = 0, \tag{3.1}$$

$$\xi_F^2 \left\{ \frac{\partial^2}{\partial x^2} + \frac{\partial^2}{\partial y^2} \right\} \Phi_{1,2} - \frac{\widetilde{\omega}_{1,2}}{\pi T_c} \Phi_{1,2} = 0, \tag{3.2}$$

where Φ_N, $\Phi_{2,1}$ - are the Green's functions in the normal metal and in the upper and lower ferromagnetic layers, respectively; $\omega = \pi T(2n+1)$ -are the Matsubara frequencies; $\widetilde{\omega}_1 = |\omega| + iH_1 \operatorname{sgn}\omega$, $\widetilde{\omega}_2 = |\omega| + iH_2 \operatorname{sgn}\omega$.

The boundary conditions at the SN and SF interfaces (for $y = \pm L/2$) have the form [18], [30]

$$\gamma_{BN}\xi_N \frac{\partial}{\partial y}\Phi_N = \pm\delta \exp\{\pm i\varphi/2\}, \tag{3.3}$$

$$\gamma_{BF}\xi_F \frac{\partial}{\partial y}\Phi_{1,2} = \pm\delta \frac{\widetilde{\omega}_{1,2}}{|\omega|} \exp\{\pm i\varphi/2\}, \tag{3.4}$$

where $\delta = G_S\Delta$.

The boundary conditions at the FN interface (for $x = \pm d_N$) have the form:

$$\frac{\xi_N}{|\omega|}\frac{\partial}{\partial x}\Phi_N = \gamma \frac{\xi_F}{\widetilde{\omega}_{2,1}}\frac{\partial}{\partial x}\Phi_{2,1}, \tag{3.5}$$

$$\mp\Phi_{2,1} + \gamma_B\xi_F \frac{\partial}{\partial x}\Phi_{2,1} = \frac{\widetilde{\omega}_{2,1}}{|\omega|}\Phi_N, \tag{3.6}$$

$$\gamma_B = R_{B3}\mathcal{A}_{B3}/\rho_F\xi_F, \quad \gamma = \rho_N\xi_N/\rho_F\xi_F,$$

where R_{B3} and $\mathcal{A}_{B3}$ - are the resistance and area of the NF interface, respectively. The conditions at the free boundaries $x = \pm(d_N + d_F)$ have the form

$$\frac{\partial \Phi_1}{\partial x} = 0, \quad \frac{\partial \Phi_2}{\partial x} = 0, \tag{3.7}$$

and ensure the absence of the current through these boundaries.

For further simplification of the problem, the thicknesses of the F and N films are assumed to be sufficiently small,

$$d_N \ll \xi_N, \quad d_F \ll \xi_F, \tag{3.8}$$

and the solution of the boundary value problem given by Eqs. (3.1)-(3.7) is sought in the form of the expansion in small parameters (d_N/ξ_N) and (d_F/ξ_F). In the first approximation, the functions Φ_N and $\Phi_{1,2}$ are independent of the coordinate x:

$$\Phi_N = A(y), \quad \Phi_1 = B(y), \quad \Phi_2 = C(y). \tag{3.9}$$

In the next approximation at $x = \pm d_N$ taking into account Eq. (3.7) we have:

$$\frac{\partial \Phi_N}{\partial x}|_{d_N -} \qquad \frac{\partial \Phi_N}{\partial x}|_{-d_N} = 2d_N \left[\frac{\Omega}{\xi_N^2} - \frac{\partial^2}{\partial y^2}\right] A(y), \tag{3.10}$$

$$\frac{\partial \Phi_1}{\partial x} = d_F \left[\frac{\widetilde{\Omega}_1}{\xi_F^2} - \frac{\partial^2}{\partial y^2}\right] B(y), \tag{3.11}$$

$$\frac{\partial \Phi_2}{\partial x} = -d_F \left[\frac{\widetilde{\Omega}_2}{\xi_F^2} - \frac{\partial^2}{\partial y^2}\right] C(y), \tag{3.12}$$

where $\Omega = |\omega| \setminus \pi T_C$, $\widetilde{\Omega}_{1,2} = \widetilde{\omega}_{1,2} \setminus \pi T_C$. The substitution of Eqs. (3.10) - (3.12) into boundary conditions (6.5), (3.6) yields the following system of three equations for the functions $A(y)$, $B(y)$ and $C(y)$

$$\begin{aligned}
\left\{\frac{\Omega\zeta_N^2}{\xi_N^2} + 1 - \zeta_N^2 \frac{\partial^2}{\partial y^2}\right\} A(y) &= \frac{\Omega C(y)}{2\widetilde{\Omega}_2} + \frac{\Omega B(y)}{2\widetilde{\Omega}_1}, \\
\left\{\widetilde{\Omega}_2 \frac{\zeta_F^2}{\xi_F^2} + 1 - \zeta_F^2 \frac{\partial^2}{\partial y^2}\right\} C(y) &= \frac{\widetilde{\Omega}_2}{\Omega} A(y), \\
\left\{\widetilde{\Omega}_1 \frac{\zeta_F^2}{\xi_F^2} + 1 - \zeta_F^2 \frac{\partial^2}{\partial y^2}\right\} B(y) &= \frac{\widetilde{\Omega}_1}{\Omega} A(y).
\end{aligned} \tag{3.13}$$

$$\zeta_F = \sqrt{\gamma_F}\xi_F, \quad \zeta_N = \sqrt{\gamma_N}\xi_N, \tag{3.14}$$

$$\gamma_F = \gamma_B \frac{d_F}{\xi_F}, \quad \gamma_N = \frac{\gamma_B}{\gamma}\frac{d_N}{\xi_N}. \tag{3.15}$$

The solution of the system of equations(3.13) is represented in the form

$$\begin{aligned} A(y) &= \sum_{i=1,2,3} (A_{2i-1}\cosh(q_i y) + A_{2i}\sinh(q_i y)), \\ B(y) &= \sum_{i=1,2,3} (B_{2i-1}\cosh(q_i y) + B_{2i}\sinh(q_i y)), \\ C(y) &= \sum_{i=1,2,3} (C_{2i-1}\cosh(q_i y) + C_{2i}\sinh(q_i y)). \end{aligned} \tag{3.16}$$

The coefficients in Eqs. (3.16) are related as

$$B_{1,2} = A_{1,2}\frac{\widetilde{\Omega}_1}{\Omega}\zeta_N^2\beta_1, \quad C_{1,2} = A_{1,2}\frac{\widetilde{\Omega}_2}{\Omega}\zeta_N^2\epsilon_1, \tag{3.17}$$

$$B_{3,4} = A_{3,4}\frac{\widetilde{\Omega}_1}{\Omega}\zeta_N^2\beta_2, \quad C_{3,4} = A_{3,4}\frac{\widetilde{\Omega}_2}{\Omega}\zeta_N^2\epsilon_2, \tag{3.18}$$

$$B_{5,6} = -A_{5,6}\frac{\widetilde{\omega}_1}{\omega}\frac{1}{\zeta_F^2}\frac{\epsilon_2}{k+\epsilon_2(u^2-q_1^2)}, \tag{3.19}$$

$$C_{5,6} = -A_{5,6}\frac{\widetilde{\omega}_2}{\omega}\frac{1}{\zeta_F^2}\frac{\beta_2}{k+\beta_2(u^2-q_1^2)}, \tag{3.20}$$

$$\beta_{1,2} = \frac{k}{v_1^2-q_{1,2}^2}, \quad \epsilon_{1,2} = \frac{k}{v_2^2-q_{1,2}^2}, \tag{3.21}$$

where $k = \zeta_F^{-2}\zeta_N^{-2}$, and the inverse characteristic lengths q_i are the roots of the sixth order equation

$$2k^{-1}\left(q^2-u^2\right)\left(q^2-v_1^2\right)\left(q^2-v_2^2\right) = 2q^2-v_2^2-v_1^2, \tag{3.22}$$

$$u^2 = \frac{1}{\zeta_N^2}+\frac{\Omega}{\xi_N^2}, \quad v_{1,2}^2 = \frac{1}{\zeta_F^2}+\frac{\Omega}{\xi_F^2}+i\frac{h_{1,2}}{\xi_F^2}, \tag{3.23}$$

where $h_{1,2} = H_{1,2}/\pi T_C$ are normalized exchange energies.

Following the procedure described in Chapter 1, from boundary conditions (6.2), (6.4) the integration constants $A_1, A_2, A_3, A_4, A_5, A_6$ are determined in the form

$$A_{1,3} = \frac{\delta\cos(\varphi/2)}{q_{1,2}\sinh(q_{1,2}L/2)\zeta_N^2\gamma_{BF}\xi_F}\frac{r+(u^2-q_{1,2}^2)}{k+\left\{\epsilon_{1,2}^2+\beta_{1,2}^2\right\}/2}, \tag{3.24}$$

$$A_5 = \frac{\delta\cos(\varphi/2)}{q_3\sinh(q_3L/2)\gamma_{BN}\xi_N}\frac{1+(u^2-q_3^2)r^{-1}}{1+\eta}, \tag{3.25}$$

$$A_{2,4,6} = iA_{1,3,5}\tan(\varphi/2)\tanh(q_{1,2,3}L/2), \tag{3.26}$$

$$r = \frac{\gamma_{BF}}{\gamma_{BN}}\frac{\xi_F}{\xi_N\zeta_F^2},$$

$$\eta = \frac{k}{2}\left\{\left(\frac{\beta_2}{k+\beta_2(u^2-q_1^2)}\right)^2+\left(\frac{\epsilon_2}{k+\epsilon_2(u^2-q_1^2)}\right)^2\right\}$$

The substitution of the solution obtained in the form of Eqs. (3.16) into the standard expression for the superconducting current J_S, yields to the sinusoidal dependence $J_S(\varphi) = I_C \sin\varphi$. It is convenient to represent the critical current I_C as the sum of three terms

$$I_C = I_{C1} + I_{C2} + I_{C3}, \tag{3.27}$$

$$I_{C1} = \frac{8\pi T}{e\xi_F \gamma_{BF} R_{BF}} \mathrm{Re} \sum_{\omega>0} \frac{a_1^2 (\delta/\omega)^2}{(2k + \epsilon_1^2 + \beta_1^2) q_1 \sinh q_1 L},$$

$$I_{C2} = \frac{8\pi T}{e\xi_F \gamma_{BF} R_{BF}} \mathrm{Re} \sum_{\omega>0} \frac{a_2^2 (\delta/\omega)^2}{(2k + \epsilon_2^2 + \beta_2^2) q_2 \sinh q_2 L},$$

$$I_{C3} = \frac{2\pi T}{e\xi_N \gamma_{BN} R_{BN}} \mathrm{Re} \sum_{\omega>0} \frac{a_3^2 (\delta/\omega)^2}{r^2 (1+\eta) q_3 \sinh q_3 L},$$

where $a_i = r + u^2 - q_i^2, i = 1, 2, 3$. The developed approach is applicable when all the characteristic lengths of the problem are larger than the thicknesses of the normal and ferromagnetic films. Expressions (3.22), (6.48), (3.27) specify a general expression for the critical current of the S–FNF–S Josephson junctions under investigation.

3.2 The analysis of inverse coherence lengths vectors and critical current

When $h_1 \neq h_2$, the system is similar to an oscillatory system with three degrees of freedom, with the partial inverse lengths given by Eqs. (6.48) and with own inverse lengths $q_{1,2,3}$, that are determined from Eq. (3.22). When the magnetizations of the ferromagnetic films coincide in magnitude and direction, $h_1 = h_2 = h$, the situation is similar to that considered in Chapter 1. In this case, according to Eqs. (3.22), (3.27) the expressions for the critical current components I_{C1} and I_{C3} are transformed into the results obtained in Chapter 1 for the critical current in the S–FN–S Josephson junctions and $I_{C2} = 0$.

Analysis of expressions (3.27) for the critical-current components is simplified for a number of limiting cases.

3.2.1 The limit of high resistance of the FN interface

In the limit of high resistance of the FN interface

$$\zeta_N \gg \xi_N, \quad \zeta_F \gg \xi_F \tag{3.28}$$

coupling between the F and N films is small in the three-layer FNF structure. In this approximation, it follows from Eq. (3.22) that the proper coherence lengths coincide with

the partial coherence lengths. As a result, the system is decomposed into three independent supercurrent flow channels. In this case, Eqs. (3.27) are transformed into the expressions for the critical current in two-barrier SINIS and SIFIS junctions [18], [31].

3.2.2 The limit of "strong" normal film

In the limit of "strong" normal film,

$$\zeta_N >> \zeta_F \tag{3.29}$$

and for the limit $\xi_N >> \xi_F$ from (3.22) it follows that inverse coherence lengths in the next approximation are given by the expressions

$$q_1^2 = v_{1+\theta(h_1-h_2)}^2, \quad q_2^2 = v_{1-\theta(h_1-h_2)}^2, \tag{3.30}$$

$$q_3^2 = u^2 - \frac{v_1^2 + v_2^2}{2v_1^2 v_2^2 \zeta_F^2 \zeta_N^2}, \tag{3.31}$$

where $\theta(x)$ -is the Heaviside step function.

According to Eqs. (3.27), (3.30), (3.31) the critical-current components I_{C1}, I_{C2} decrease in a length of $(\mathrm{Re}(q_{1,2}))^{-1} << \xi_N$ with increasing L. At the same time, the term I_{C3} decreases in a length comparable with ξ_N. The period of spatial oscillations $I_{C3}(L)$ depends strongly on the relation between h_1 and h_2.

3.2.3 Antiferromagmetic configuration of vectors of magnetization

Figure 3.2 shows the imaginary and real parts of q_3 calculated as functions of the exchange energy h_2 of one of the ferromagnetic layers at the given energy $h_1 = 30$, of the other ferromagnetic layer for the parameters $z = (\zeta_N/\zeta_F)^2 = 50, 150, 300, 600$ and $\xi_N/\zeta_N = 4$, $\xi_N/\xi_F = 10$. It is seen that $\mathrm{Im}\, q_3$ for the antiparallel orientation of the magnetizations of the F films vanishes strictly at $h_2 = -h_1$ for all the parameter values.

$$q_3^2 = \frac{\Omega}{\xi_N^2} + \frac{(h^2 + \Omega^2)\zeta_F^2 + \Omega\xi_F^2}{\zeta_N^2 \zeta_F^2 (h^2 + (\xi_F^2 \zeta_F^{-2} + \Omega)^2)}. \tag{3.32}$$

The absence of oscillations is explained by the compensating action of opposite magnetizations. According to Fig. 3.2 $h_1 = -h_2$ the imaginary part of q_3 vanishes but also at

$$h_1 = -\frac{1}{\gamma_F^2 h_2}. \tag{3.33}$$

The position of the second point on the h_2, axis at which $\mathrm{Im}\, q_3 = 0$, depends on the parameter z and can be located both to the left and to the right from the value $h_2 = -h_1$.

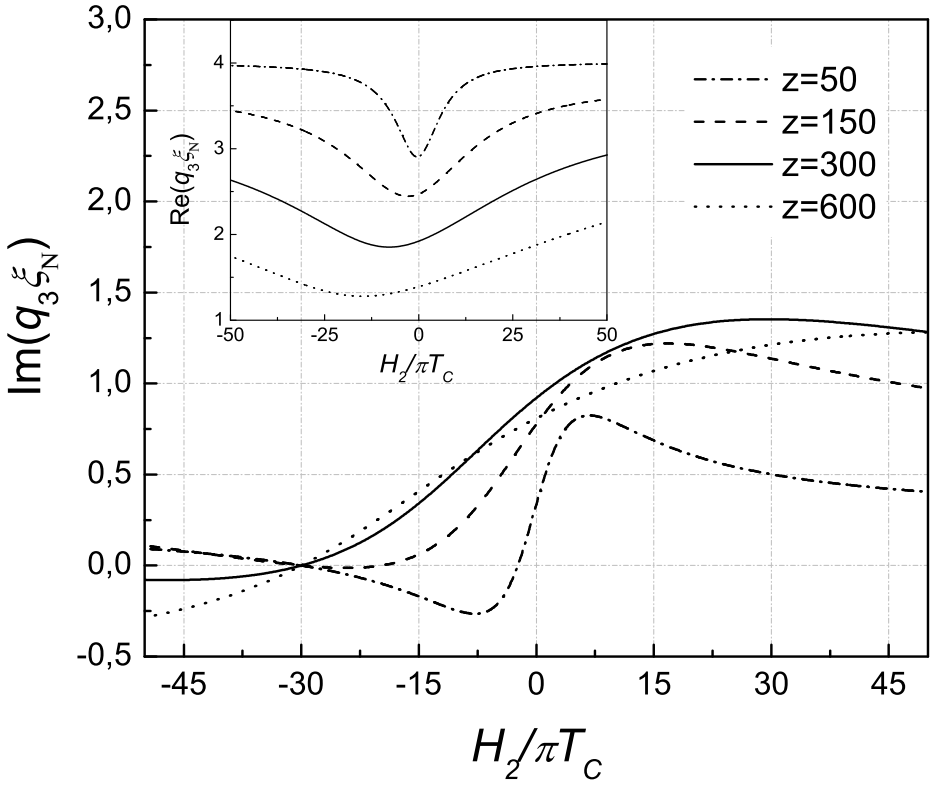

Figure 3.2. Imaginary part of inverse coherence length q_3 vs. the normalized exchange energy $H_2/\pi T_C$, for the parameters $z = (\zeta_N/\zeta_F)^2 = 50, 150, 300, 600$ at $\xi_N/\zeta_N = 4$, $\xi_N/\xi_F = 10$, $T = 0.5T_C$, $H_1/\pi T_C$; Inset shows dependence of real part of q_3 for the same parameters.

3.2.4 Ferromagnetic configuration of vectors of magnetization

Expressions (3.30), (3.31) are simplified for $h_1 = h_2 = h$ and reduce to

$$q_1^2 = q_2^2 = \frac{1}{\zeta_F^2} + \frac{\Omega}{\xi_F^2} + i\frac{h}{\xi_F^2}, \tag{3.34}$$

$$q_3^2 = \frac{\Omega}{\xi_N^2} + \frac{(h^2+\Omega^2)\zeta_F^2 + \Omega\xi_F^2 + ih\xi_F^2}{\zeta_N^2\zeta_F^2(h^2 + (\xi_F^2\zeta_F^{-2} + \Omega)^2)}. \tag{3.35}$$

At parallel magnetization junction can be as in 0 state so in π state (Chapter1).

3.2.5 Synchronization

It is interesting that synchronization, $\mathrm{Im}\, q_1 = \mathrm{Im}\, q_2$, occurs in the system at small h_1, h_2 values even when h_1 is not identically equal to h_2. . The relative width of the synchronization region, $\mu = (|h_1| - |h_2|)/|h_1|$ at $h_1 \approx 1$, at the parameters $h_1 \approx 1$ and $z = (\zeta_N/\zeta_F)^2 = 100$, $\xi_N/\zeta_N = 4$, $\xi_N/\xi_F = 10$ is equal to about 30 and decreases with a further increase in h_1.

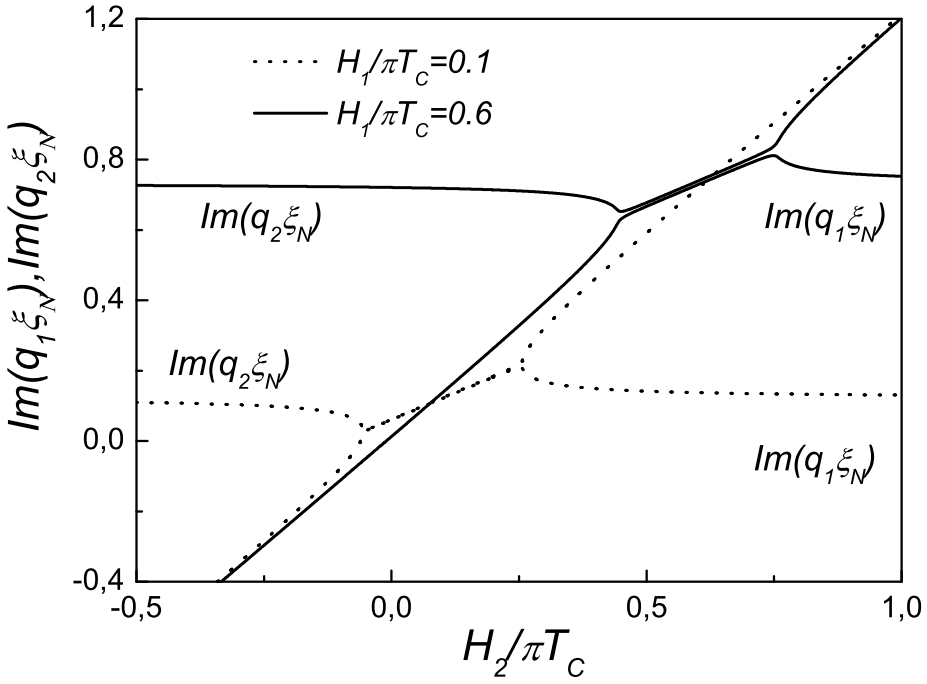

Figure 3.3. Dependence of imaginary parts of q_2 and q_3 on normalized value of exchange energy $H_2/\pi T_C$, for $z = (\zeta_N/\zeta_F)^2 = 100$ and $H_1/\pi T_C = 0.1, 0.6$, $\xi_N/\zeta_N = 4$, $\xi_N/\xi_F = 10$, $T = 0.5T_C$.

3.2.6 Critical current

Figure 3.4 shows the critical-current components of the structure calculated numerically as functions of the distance between the superconducting electrodes for the parameters $h_1 = 30$, $z = (\zeta_N/\zeta_F)^2 = 300$, $\xi_N/\zeta_N = 4$, $\xi_N/\xi_F = 10$, $T = 0.5T_C$, $\gamma_{BF}/\gamma_{BN} = 1$, and $h_2 = 30, -10, -30, -78.4$.

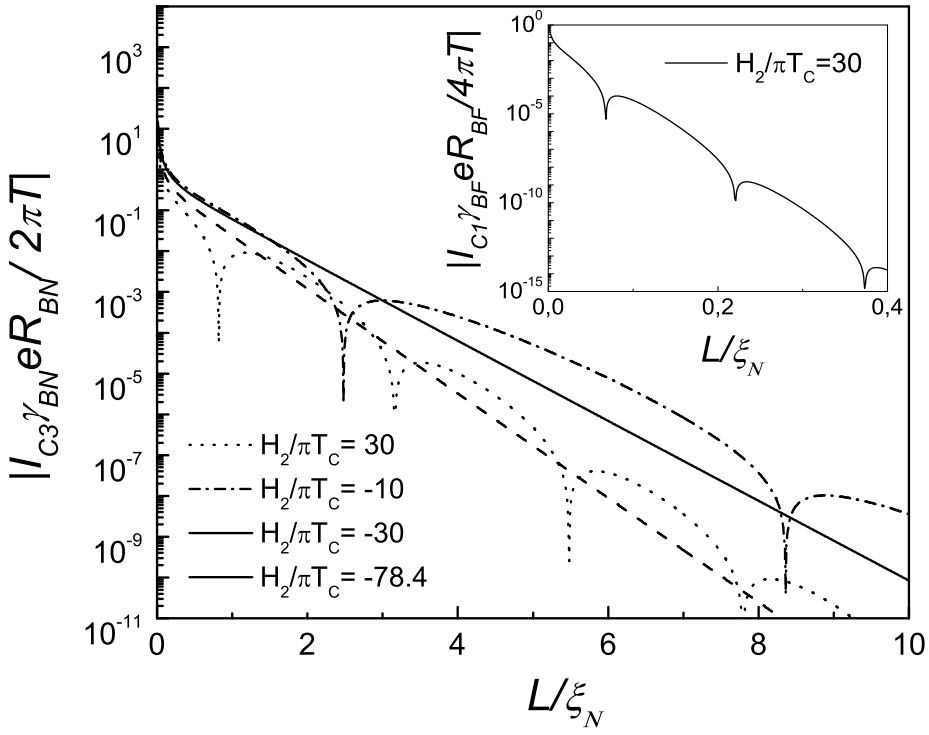

Figure 3.4. Dependence of normalized part of critical current $|I_{C3}\gamma_{BN}eR_{BN}/2\pi T|$ (and (inset) shows part of critical current $|I_{C1}\gamma_{BF}eR_{BF}/4\pi T|$) vs. the distance between the superconducting electrodes L/ξ_N for the parameters $h_1 = 30$, $z = (\zeta_N/\zeta_F)^2 = 300$, $\xi_N/\zeta_N = 4$, $\xi_N/\xi_F = 10$, $T = 0.5T_C$, $\gamma_{BF}/\gamma_{BN} = 1$, and $h_2 = 30, -10, -30, -78.4$.

The inset shows the normalized part of the critical current I_{C1}, calculated at $h_2 = 30$ with the same parameters. According to Fig.3.4 the critical current components $I_{C1,2}$ in the case under consideration are much smaller than the component I_{C3} and decrease much more rapidly with increasing L . For the case $L \gtrsim \xi_N$ interesting for applications, the contribution to the critical current from $I_{C1,2}$ is negligibly small, so that $I_C = I_{C3}$ with a good accuracy. The critical current decreases exponentially with increasing L and undergoes oscillations associated with the transition of the structure from the 0 state to the π state at a length of $\xi_N \gg \xi_F$. In complete agreement with Fig.3.2 the oscillations disappear at $h_2 = -h_1$ and $h_2 = -(\gamma_F^2 h_1)^{-1} \approx -78.4$.

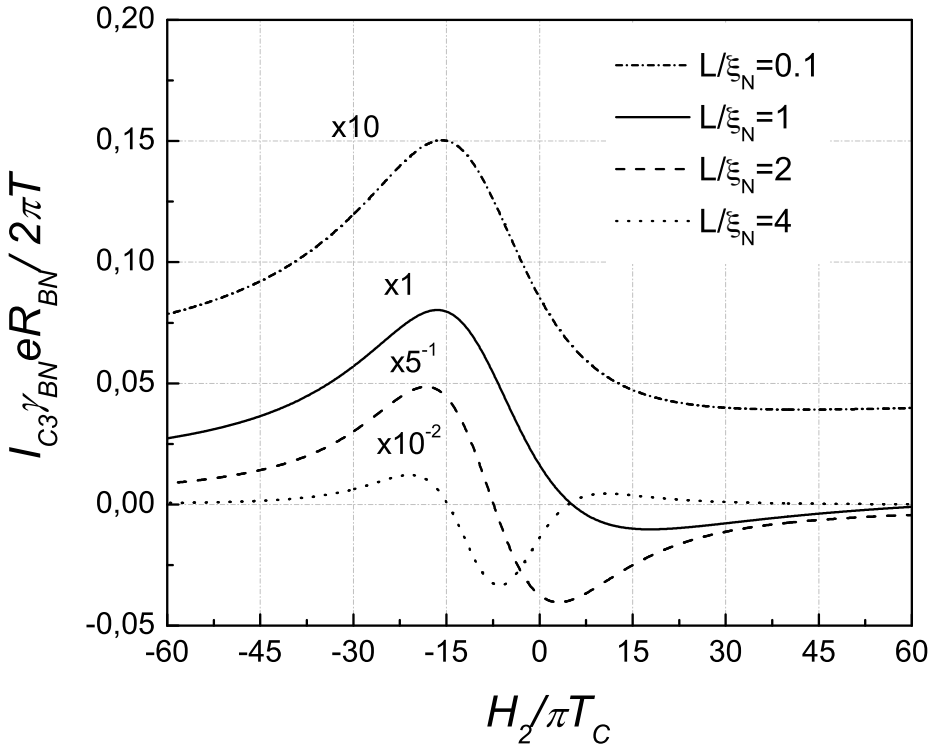

Figure 3.5. Dependence of normalized part of critical current $I_{C3}\gamma_{BN}eR_{BN}/2\pi T$ vs. the normalized exchange energyh_2 for the parameters $h_1 = 30$, $z = (\zeta_N/\zeta_F)^2 = 300$, $\xi_N/\zeta_N = 4$, $\xi_N/\xi_F = 10$, $T = 0.5T_C$, $\gamma_{BF}/\gamma_{BN} = 1$, and $L/\xi_N = 0.1, 2, 3, 4$, plotted with scales of $10, 1, 0.2, 0.01$ respectively.

Figure 3.5 shows the $I_{C3}(h_2)$ dependence calculated numerically at $h_1 = 30$ for the distances between the superconducting electrodes $L/\xi_N = 0.1, 1, 2, 4$. The parameter $z = 300$ is taken such that the period of the critical-current oscillations at $h_2 = h_1$ is minimal (see Fig. 3.2). According to Fig.3.4 the structure at $L/\xi_N = 0.1$ always is in the 0-state. For this reason, change from $h_2 = h_1$ to $h_2 = -h_1$ does not lead to change in the sign of I_{C3}, but triples the critical current. At $h_2 = h_1$ and $L/\xi_N = 1, 2$ the Josephson junction is in the π-state (see Fig. 3.4). In this case, change from $h_2 = h_1$ to $h_2 = -h_1$ gives rise to the transition from theπ- state to the 0-state. After this transition, the critical current increases by factors of 7 for $L/\xi_N = 1$ and3 for $L/\xi_N = 2$. Finally, the system is in the 0-state for $L/\xi_N = 4$ at $h_2 = h_1$. It is seen that the transition from the 0 state to the π-state is possible if h_2 lies in the range from 4 to 15. A change from $h_2 = h_1$ to $-h_1$ results in the increase in the critical current by a factor of about 6.

Figures 3.4 and 3.5 show that the transition from the ferromagnetic configuration ($h_2 = h_1$) to the antiferromagnetic configuration ($h_2 = -h_1$) can be accompanied by a

significant increase in the critical current of the structure, particularly near the transition between the "0" state and "π" state. Far from the transition points, the gain can be equal to ten owing to change in the characteristic damping length of the critical current (see the inset in Fig. 3.2).

3.3 Conclusion

The critical current of S–FNF–S Josephson structures has been calculated as a function of the distance between the superconducting (S) electrodes, L, via the Usadel quasiclassical equations for the case of specifying the supercurrent in the direction parallel to the interface between the ferromagnetic (F) and normal (N) films of the composite weak-link region. It has been shown that, owing to the interaction between the F and N films, both the typical decrease scale of the critical current and the period of its oscillations to lengths of the scale ξ_N can be much larger than the respective quantities for the SFS junctions. Moreover, this interaction changes both the magnitude and sign of the critical current. It has been shown that the critical current in a structure with the collinear magnetization vectors of the films can be significantly different from the critical current in a structure with the antiparallel magnetization of the F films.

Note that these calculations are valid if the magnetization of the film changes without the turn of the magnetization in the film plane; i.e., remagnetization occurs through the decrease in the magnetic moment to zero and the further increase in the direction opposite to the initial direction. If the transition from the ferromagnetic configuration to the antiferromagnetic one occurs by means of the turn of the magnetization, e.g., with the conservation of its absolute value, then the critical current component that corresponds to the triplet pairing and decreases at lengths independent of H must be generated in the structure.

Bibliography

[1] A. W. Kleinsasser and W. J. Gallagher, Modern Superconductor Devices, Academic Press, Boston, (1990).

[2] D. V. Goncharov, I. A. Devyatov, and M. Yu. Kupriyanov, Nelin. Mir 3, **92** (2005).

[3] F. S. Bergeret, A. F. Volkov, K. B. Efetov, Rev. Mod. Phys. **77**, 1321 (2005).

[4] A. A. Golubov, M. Yu. Kupriyanov, and E. Il'ichev, Rev. Mod. Phys. **76**, 411 (2004).

[5] F. S. Bergeret, A. F. Volkov, and K. B. Efetov, Phys. Rev. Lett. **86**, 3140 (2001).

[6] V. N. Krivoruchko and E. A. Koshina, Phys. Rev. B **63**, 224515 (2001); **64**, 172511 (2001).

[7] A. A. Golubov, M. Yu. Kupriyanov, and Ya. V. Fominov, JETP Letters **75** 223 (2002).

[8] A. F. Volkov, F. S. Bergeret, and K. B. Efetov, Phys. Rev. Lett. **90**, 117006 (2003).

[9] A. F. Volkov, F. S. Bergeret, and K. B. Efetov, Phys. Rev. B **64**, 134506 (2001);

[10] F. S. Bergeret, A. F. Volkov, and K. B. Efetov, Phys. Rev. B **68**, 064513 (2003);

[11] A. A. Golubov, M. Yu. Kupriyanov, and Ya. V. Fominov, JETP Letters **77** 609 (2003).

[12] S. M. Frolov, D. J. Van Harlingen, V. A. Oboznov, V. V. Bolginov, and V. V. Ryazanov, Phys. Rev. B **70**, 144505 (2004).

[13] S. M. Frolov, D. J. Van Harlingen, V. V. Bolginov, V. A. Oboznov, and V. V. Ryazanov, Phys. Rev. B **74**, 020503 (2006).

[14] T. Kontos, M. Aprili, J. Lesueur, et al., Phys. Rev. Lett. **89**, 137007 (2002).

[15] H. Sellier, C. Baraduc, F. Lefloch, and R. Calemczuck, Phys. Rev. B **68**, 054531 (2003).

[16] Y. Blum, A. Tsukernik, M. Karpovski, et al., Phys. Rev. B **70**, 214501 (2004).

[17] C. Surgers, T. Hoss, C. Schonenberger, et al., J. Magn. Magn. Mater. **240**, 598 (2002).

[18] C. Bell, R. Loloee, G. Burnell, and M. G. Blamire Phys. Rev. B **71**, 180501 (R) (2005).

[19] V. Shelukhin, A. Tsukernik, M. Karpovski, Y. Blum, K. B. Efetov, A. F. Volkov, T. Champel, M. Eschrig, T. Löfwander, G. Schö

[20] V. A. Oboznov, V. V. Bol'ginov, A. K. Feofanov, V. V. Ryazanov, and A. Buzdin, Phys. Rev. Lett. **96**, 197003 (2006).

[21] M. Weides, K. Tillmann, and H. Kohlstedt, Physica C **437-438**, 349-352 (2006).

[22] M. Weides, M. Kemmler, H. Kohlstedt, A. Buzdin, E. Goldobin, D. Koelle, R. Kleiner, Appl. Phys. Lett. **89**, 122511 (2006).

[23] M. Weides, M. Kemmler, E. Goldobin, H. Kohlstedt, R. Waser, D. Koelle, R. Kleiner, cond-mat/0605656, submitted to PRL.

[24] H. Sellier, C. Baraduc, F. Lefloch, and R. Calemczuck, Phys. Rev. Lett. **92**, 257005 (2004).

[25] F. Born, M. Siegel, E. K. Hollmann, H. Braak, A. A. Golubov, D. Yu. Gusakova, and M. Yu. Kupriyanov, Phys. Rev. B. **74**, 140501 (2006).

[26] J. W. A. Robinson, S. Piano, G. Burnell, C. Bell, and M. G. Blamire, Phys. Rev. Lett. **97**, 177003 (2006)

[27] T. Y. Karminskaya, M. Yu. Kupriyanov, JETP Letters **85** 343 (2007).

[28] L. Usadel, Phys. Rev. Lett. **25**, 507 (1970).

[29] M. Yu. Kuprianov and V. F. Lukichev, Zh. Eksp. Teor. Fiz. **94**, 139 (1988) [Sov. Phys. JETP **67**, 1163 (1988)].

[30] E. A. Koshina and V. N. Krivoruchko, Fiz. Nizk. Temp. **26**, 157 (2000) [Low Temp. Phys. **26**, 115 (2000)].

[31] A. I. Buzdin, Pis'ma Zh. Eksp.Teor.Fiz., **78**, 1073 (2003) [JETP Letters, **78**, 583 (2003)].

Chapter 4

Critical current in S-FNF-S Josephson junctions with noncollinear magnetization vectors of ferromagnetic films

Introduction

The experimental investigations of the processes in Josephson junctions with the ferromagnetic materials have been focused on the structures in which the weak coupling region is a weak single-domain ferromagnet (see, e.g., [1]) or a fully spin-polarized metal [2]. As shown in [3, 4], in the Josephson junctions, where the weak-coupling region is a multilayer structure consisting of the alternating layers of normal (N) and ferromagnetic (F) metals, it is possible not only to significantly increase the characteristic damping and oscillation scale in the dependence of the critical current I_C on the ferromagnet thickness, but also to efficiently control both the magnitude and sign of I_C. The control was achieved by the remagnetization of one of the ferromagnetic layers, i.e., by changing the magnitude and direction of the magnetization vector M through the transition from the ferromagnetic orientation ($M_1 \uparrow\uparrow M_2$) to the antiferromagnetic orientation ($M_1 \uparrow\downarrow M_2$) of the magnetization vectors of the ferromagnetic films. It is qualitatively clear that control over the magnitude and the sign of I_C by means of the rotation of the magnetization vector $\mathbf{M}_1$ of one of the ferromagnetic films at a certain angle α with respect to $\mathbf{M}_2$ is much more energetically favorable than its complete remagnetization, i.e., the transition from $\mathbf{M}_1$ to $-\mathbf{M}_1$ by means of a change in the magnitude of this vector. In this Chapter it is shown that the effective control in such a spin gate is achieved at a relatively small misorientation angles α if the rotation is performed from the antiferromagnetic configuration. Moreover, this approach can provide a significantly larger difference between the critical currents in the 0 ($I_C > 0$) and π ($I_C < 0$) states than that in the case of the remagnetization by means of a change in this vector from $\mathbf{M}_1$. to $-\mathbf{M}_1$

4.1 Structure of S-FNF-S junction and its mathematical description

Figure 4.1 shows the schematic view of the S–FNF–S junction under investigation. It consists of a normal metal film with the thickness $2d_N$, that is sandwiched between two ferromagnetic films each with the thickness d_F. The superconducting electrodes are joined to the ends of such an FNF multilayer structure. Let the coordinate origin be at the middle of the structure and the x and y axes be directed across and along the NF interfaces, respectively.

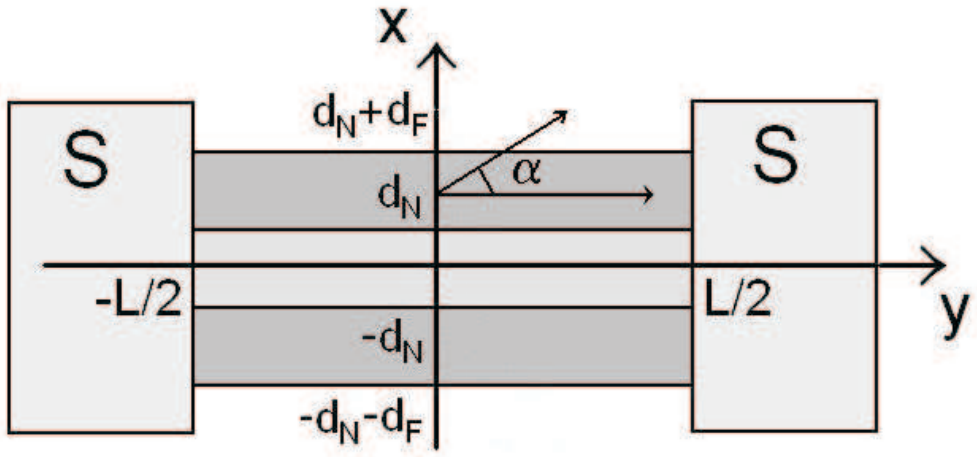

Figure 4.1. Structure of S-FNF-S junction.

Below only the case where the vectors $\mathbf{M}_1, \mathbf{M}_2$ lie in the plane of the ferromagnetic films will be considered. For definiteness, we choose the direction of the magnetizations of the lower and upper ferromagnetic layers along the y axis and at the angle α to this axis. Let the "dirty" limit conditions be satisfied in the normal and ferromagnetic materials, their effective electron–phonon coupling constant be zero, and exchange energy $H = 0$ in the normal metal. Then, let us assume that the structure is completely symmetric and the suppression parameters are large so that the suppression of superconductivity in the superconducting electrodes can be neglected.

Under the above assumptions, the anomalous Green's functions in the upper and lower ferromagnets, as well as in the normal layer, can be considered as the matrices $(\hat{f})$,

$(\hat{p})$ and $(\hat{n})$, that satisfy the linearized Usadel equations [4], [6]:

$$\xi_F^2\left\{\frac{\partial^2}{\partial x^2}+\frac{\partial^2}{\partial y^2}\right\}\hat{f}-\Omega\hat{f}-\frac{i}{2}h(\hat{f}\hat{H}_1^*+\hat{H}_1\hat{f})=0, \tag{4.1}$$

$$\xi_F^2\left\{\frac{\partial^2}{\partial x^2}+\frac{\partial^2}{\partial y^2}\right\}\hat{p}-\Omega\hat{p}-\frac{i}{2}h(\hat{p}\hat{H}_2^*+\hat{H}_2\hat{p})=0, \tag{4.2}$$

$$\xi_N^2\left\{\frac{\partial^2}{\partial x^2}+\frac{\partial^2}{\partial y^2}\right\}\hat{n}-\Omega\hat{n}=0, \tag{4.3}$$

$\Omega=|\omega|/(\pi T_C)$, ω -are the Matsubara frequencies, $h=H/\pi T_c$, $\hat{H}_1=\hat{\sigma}_2\sin\alpha+\hat{\sigma}_3\cos\alpha$, and $\hat{H}_2=\hat{\sigma}_3$, ($\hat{\sigma}_i$-are the Pauli matrices).

System of equations (4.1)-(4.3) should be supplemented by the boundary conditions. At the free interfaces of the structure ($x=d_N+d_F, x=-d_N-d_F$) they have the form

$$\frac{\partial\hat{f}}{\partial x}=0,\quad \frac{\partial\hat{p}}{\partial x}=0. \tag{4.4}$$

The boundary conditions at the FN interface (for $x=\pm d_N$) have the form [18], [8]:

$$\xi_N\frac{\partial}{\partial x}\hat{n}=\gamma\xi_F\frac{\partial}{\partial x}\hat{f},\quad -\gamma_B\xi_F\frac{\partial}{\partial x}\hat{f}+\hat{f}=\hat{n}, \tag{4.5}$$

$$\xi_N\frac{\partial}{\partial x}\hat{n}=\gamma\xi_F\frac{\partial}{\partial x}\hat{p},\quad \gamma_B\xi_F\frac{\partial}{\partial x}\hat{p}+\hat{p}=\hat{n}. \tag{4.6}$$

Finally, the boundary conditions at the SF and SN interfaces have the form

$$\begin{gathered}\gamma_{BN}\xi_N\frac{\partial}{\partial y}\hat{n}=\pm\hat{f}_S,\quad y=\pm L/2,\\ \gamma_{BF}\xi_F\frac{\partial}{\partial y}\hat{f}=\pm\hat{f}_S,\quad y=\pm L/2,\\ \gamma_{BF}\xi_F\frac{\partial}{\partial y}\hat{p}=\pm\hat{f}_S,\quad y=\pm L/2.\end{gathered} \tag{4.7}$$

Under the above assumptions, the anomalous Green's functions in the superconducting electrodes in Eqs. (4.7) can be represented in the form $\hat{f}_S(\pm L/2)=\hat{\sigma}_3\Delta\exp(\pm i\varphi/2)/\sqrt{\omega^2+\Delta^2}$, where Δ and φ - are the absolute value and phase difference of their order parameters.

When the normal and ferromagnetic films are sufficiently thin,

$$d_N\ll\xi_N,\quad d_F\ll\xi_F \tag{4.8}$$

the boundary value problem given by Eqs. (4.1)-(4.7) is significantly simplified and reduces to the solution of the equations for the x independent components $\hat{f}(y)$, $\hat{p}(y)$ and $\hat{n}(y)$ of

the initial functions of the problem:

$$(u_N - \frac{\partial^2}{\partial y^2})\hat{n}(y) = \frac{\hat{f}(y) + \hat{p}(y)}{2\zeta_N^2}, \tag{4.9}$$

$$(u_F - \frac{\partial^2}{\partial y^2})\hat{f}(y) - \frac{ih(\hat{f}(y)\hat{H}_1^* + \hat{H}_1\hat{f}(y))}{2\xi_F^2} = \frac{\hat{n}(y)}{\zeta_F^2}, \tag{4.10}$$

$$(u_F - \frac{\partial^2}{\partial y^2})\hat{p}(y) - \frac{ih(\hat{p}(y)\hat{H}_2^* + \hat{H}_2\hat{p}(y))}{2\xi_F^2} = \frac{\hat{n}(y)}{\zeta_F^2}, \tag{4.11}$$

where $u_N = \Omega\xi_N^{-2} + \zeta_N^{-2}$, $u_F = \Omega\xi_F^{-2} + \zeta_F^{-2}$, $\zeta_F = \gamma_F\xi_F^2$, $\zeta_N = \gamma_N\xi_N^2$.

The matrices $\hat{f}(y)$, $\hat{p}(y)$ and $\hat{n}(y)$ can be represented in the Pauli matrix basis:

$$\hat{f}(y) = f_0\hat{\sigma}_0 + f_1\hat{\sigma}_1 + f_2\hat{\sigma}_2 + f_3\hat{\sigma}_3, \tag{4.12}$$

$$\hat{p}(y) = p_0\hat{\sigma}_0 + p_1\hat{\sigma}_1 + p_2\hat{\sigma}_2 + p_3\hat{\sigma}_3, \tag{4.13}$$

$$\hat{n}(y) = n_0\hat{\sigma}_0 + n_1\hat{\sigma}_1 + n_2\hat{\sigma}_2 + n_3\hat{\sigma}_3. \tag{4.14}$$

Substituting Eqs. (4.12)-(4.14) into Eqs. (4.9)-(4.11) and taking into account Eqs. (4.7) one can easily see that this boundary value problem has only the trivial solution $f_2 = 0$, $p_2 = 0$, $n_2 = 0$, so that matrix equations (4.9)-(4.11) reduce to the system of nine differential equations

$$\begin{gathered}
(u_N - \frac{\partial^2}{\partial y^2})n_j = \frac{f_j + p_j}{2\zeta_N^2}, \quad j = 0, 1, 3, \\
(u_F - \frac{\partial^2}{\partial y^2})f_0 + ih_f \cos\alpha f_3 = \frac{n_0}{\zeta_F^2}, \\
(u_F - \frac{\partial^2}{\partial y^2})f_1 - h_f \sin\alpha f_3 = \frac{n_1}{\zeta_F^2}, \\
(u_F - \frac{\partial^2}{\partial y^2})f_3 + h_f \sin\alpha f_1 + ih_f \cos\alpha f_0 = \frac{n_3}{\zeta_F^2}, \\
(u_F - \frac{\partial^2}{\partial y^2})p_{0,3} + ih_f p_{3,0} = \frac{n_{0,3}}{\zeta_F^2}, \\
(u_F - \frac{\partial^2}{\partial y^2})p_1 = \frac{n_1}{\zeta_F^2}.
\end{gathered} \tag{4.15}$$

Here, $h_f = h/\xi_F^2$, $f_0 \sim \langle\psi_\uparrow\psi_\downarrow\rangle + \langle\psi_\downarrow\psi_\uparrow\rangle$ and $f_3 \sim \langle\psi_\uparrow\psi_\downarrow\rangle - \langle\psi_\downarrow\psi_\uparrow\rangle$ are the triplet and singlet parts of the condensate function, respectively; and $f_1 \sim \langle\psi_\uparrow\psi_\uparrow\rangle \sim \langle\psi_\downarrow\psi_\downarrow\rangle$ is the triplet component.

We seek the solution of system (4.15) in the form of the sums:

$$\begin{aligned} f_i &= \sum_{j=1}^{9}(f_{ij}^{(c)}\cosh(q_j y) + f_{ij}^{(s)}\sinh(q_j y)), \\ p_i &= \sum_{j}^{9}(p_{ij}^{(c)}\cosh(q_j y) + p_{ij}^{(s)}\sinh(q_j y)), \\ n_i &= \sum_{j}^{9}(n_{ij}^{(c)}\cosh(q_j y) + n_{ij}^{(s)}\sinh(q_j y)), \end{aligned} \tag{4.16}$$

where $i = 0, 1, 3$, and inverse lengths q_j satisfy the dispersion equation:

$$\begin{aligned} (a_j^3 b_j^2 - 4a_j^2 b_j + a_j k^2 b_j^2 + 4a_j - k^2 b_j + k^2 b_j \cos\alpha) * \\ (b_j a_j^3 - 2a_j^2 + a_j k^2 b_j - k^2 - k^2\cos\alpha) = 0, \end{aligned}$$

where $k = \zeta_F^2 h_f$, $b_j = 2\zeta_N^2(u_N - q_j^2)$ and $a_j = \zeta_F^2(u_F - q_j^2)$.

It can be shown that, for q_j, which are solutions of the equation

$$(b_j a_j^3 - 2a_j^2 + a_j k^2 b_j - k^2 - k^2\cos\alpha) = 0 \tag{4.17}$$

the coefficients $f_{ij}^{(c,s)}$, $p_{ij}^{(c,s)}$, and $n_{ij}^{(c,s)}$ are zero. Hence, sums (4.16) contain only five nonzero terms, and their coefficients are related as

$$\begin{aligned} f_{0j}^{(c,s)} &= n_{0j}^{(c,s)}\frac{\cos\alpha(b_j a_j - 1) + 1}{a_j(\cos\alpha + 1)}, \\ p_{0j}^{(c,s)} &= n_{0j}^{(c,s)}\frac{b_j a_j - 1 + \cos\alpha}{a_j(\cos\alpha + 1)}, \\ f_{3j}^{(c,s)} = \frac{in_{0j}^{(c,s)}(b_j a_j - 2)}{k(\cos\alpha + 1)},\ & p_{3j}^{(c,s)} = \frac{in_{0j}^{(c,s)}(b_j a_j - 2)}{k(\cos\alpha + 1)}, \\ f_{1j}^{(c,s)} = \frac{in_{0j}^{(c,s)}\sin\alpha(b_j a_j - 1)}{a_j(\cos\alpha + 1)},\ & p_{1j}^{(c,s)} = \frac{in_{0j}^{(c,s)}\sin\alpha}{a_j(\cos\alpha + 1)}, \\ n_{1j}^{(c,s)} = \frac{in_{0j}^{(c,s)}\sin\alpha}{\cos\alpha + 1},\ & n_{3j}^{(c,s)} = \frac{2in_{0j}^{(c,s)}(a_j b_j - 2)}{b_j k(\cos\alpha + 1)}. \end{aligned} \tag{4.18}$$

Substituting Eqs. (4.16), (4.18) into Eq. (4.7), we obtain five linearly independent equations for the coefficients n_{0j}.

4.2 The limit of strong normal film

For further simplification of the problem the case of strong normal film will be discussed

$$\zeta_N >> \zeta_F, \xi_N >> \xi_F. \tag{4.19}$$

In this approximation, the equation for the inverse characteristic lengths q_j

$$a_j^3 b_j^2 - 4a_j^2 b_j + a_j k^2 b_j^2 + 4a_j - k^2 b_j + k^2 b_j \cos\alpha = 0 \tag{4.20}$$

can be solved analytically:

$$q_{1,2}^2 = u_N - \frac{4u_F^2 + h_f^2(1-\cos\alpha)}{4u_F(u_F^2+h_f^2)\zeta_N^2\zeta_F^2} \pm$$
$$\pm \frac{h_f\sqrt{h_f^2(1-\cos\alpha)^2 - 8u_F^2(1+\cos\alpha)}}{4u_F(u_F^2+h_f^2)\zeta_N^2\zeta_F^2}, \tag{4.21}$$

$$q_{3,4}^2 = u_F \pm i h_f, \quad q_5^2 = u_F. \tag{4.22}$$

At $\alpha = 0$ and $\alpha = \pi$, the expressions for $q_{1,2}$coincide with those previously derived in chapter 2 for the case of strong normal film (4.19):

$$q_1^2 = \frac{\Omega}{\xi_N^2} + \frac{(h^2+\Omega^2)\zeta_F^2 + \Omega\xi_F^2 + ih\xi_F^2}{\zeta_N^2\zeta_F^2(h^2 + (\xi_F^2\zeta_F^{-2} + \Omega)^2)}, \alpha = 0, \tag{4.23}$$

$$q_2^2 = (q_1^2)^*, \quad \alpha = 0. \tag{4.24}$$

$$q_1^2 = \frac{\Omega}{\xi_N^2} + \frac{(h^2+\Omega^2)\zeta_F^2 + \Omega\xi_F^2}{\zeta_N^2\zeta_F^2(h^2 + (\xi_F^2\zeta_F^{-2} + \Omega)^2)}, \alpha = \pi, \tag{4.25}$$

The real parts of the last three inverse lengths q_3, q_4, and q_5 are much larger than $Re(q_1)$, so that, to determine the total current in approximation (4.19) it is sufficient to determine $n_{01}^{(c,s)}$ and $n_{02}^{(c,s)}$

$$n_{01,02}^{(s)} = i n_{01,02}^{(c)} \tan(\varphi/2)\tanh(q_{1,2}L/2), \tag{4.26}$$

$$n_{01,02}^{(c)} = \frac{\mp i h_f(\cos\alpha+1)\cos(\varphi/2)}{8q_{1,2}\sinh(q_{1,2}L/2)\zeta_N^4} \frac{b_{1,2}\left[\delta_f t_{1,2}^f - \delta_n t_{1,2}^n\right]}{(u_F^2+h_f^2)^2(q_2^2-q_1^2)},$$

where $\delta_{f,n} = \Delta/(\sqrt{\omega^2+\Delta^2}\gamma_{BF,BN}\xi_{F,N})$ and

$$\begin{aligned} t_{1,2}^f &= (u_F^2+h_f^2)b_{1,2}u_N\zeta_F^2 + 2(u_F^2+h_f^2-2u_F q_{1,2}^2), \\ t_{1,2}^n &= (u_F^2+h_f^2)^2 b_{1,2}\zeta_F^2\zeta_N^2. \end{aligned}$$

The expression for the superconducting current flowing through the junction has the form

$$I_S = \frac{-2i\pi Tw}{e}\left[\frac{d_F}{\rho_F}(I_{F1}+I_{F2}) + \frac{2d_N}{\rho_N}I_N\right],$$

$$I_N = \sum_{\omega>0}^{\infty}(n_0\frac{d}{dy}n_0 + n_3\frac{d}{dy}n_3 - n_1\frac{d}{dy}n_1),$$

$$I_{F1} = \sum_{\omega>0}^{\infty}(f_0\frac{d}{dy}f_0 + f_3\frac{d}{dy}f_3 - f_1\frac{d}{dy}f_1),$$

$$I_{F2} = \sum_{\omega>0}^{\infty}(p_0\frac{d}{dy}p_0 + p_3\frac{d}{dy}p_3 - p_1\frac{d}{dy}p_1).$$

The substitution of functions (4.16), (4.18), (4.21), (4.26) into the above expression yields the sinusoidal dependence $I_S(\varphi)$, where the critical current is represented in the form

$$I_C = I_{C1} + I_{C2}, \tag{4.27}$$

$$I_{Ci} = \frac{\pi T\Delta\zeta_F^{-4}\zeta_N^{-8}}{eR_{BN}\gamma_{BN}\xi_N}\sum_{\omega>0}^{\infty}\frac{A_i b_i^2(s\frac{\xi_N}{\xi_F}t_i^f + t_i^n)^2}{32q_i\sinh(q_iL)(\Delta^2+\omega^2)}.$$

Here, $s = \gamma_{BN}/\gamma_{BF}$, and $i = 1, 2,$, and

$$\begin{aligned} A_i &= \frac{2\left\{2(a_ib_i-2)^2 - h_f^2\zeta_F^4 b_i^2(\cos\alpha_1+1)\right\}}{b_i^2(u_F^2+h_f^2)^4(q_2^2-q_1^2)^2} - \\ &-\frac{2h_f^2(b_ia_i-1)(\cos\alpha_1+1) + (a_ib_i-2)^2(h_f^2-\frac{a_i^2}{\zeta_F^4})}{a_i^2\zeta_N^2\zeta_F^{-6}(u_F^2+h_f^2)^4(q_2^2-q_1^2)^2}. \end{aligned}$$

Expression (4.27) describes the behavior of I_C of the junction under investigation in approximation (4.19) and will be used, together with Eq. (4.21) in analysis whose results are shown in Figs. 4.2 -4.5.

4.3 Analysis of inverse coherence lengths.

The real and imaginary parts of the inverse characteristic lengths $q_{1,2}$ calculated at $\xi_N/\zeta_N = 4$ are shown in Figs. 4.2 and 4.3 , respectively, as functions of the angle α for the normalized exchange energy $h = 30$ (the solid and dashed lines for q_1 and q_2, respectively) and $h = 15$ (the dash–dotted and dotted lines for q_1 and q_2, respectively). The insets show the same quantities calculated at $h = 30$ and $\xi_N/\zeta_N = 4$ (the solid and dashed lines for q_1 and q_2, respectively) and q_1 and q_2 (the dash–dotted and dotted lines for q_1 and q_2, respectively)

It is seen that the dependences $Re(q_{1,2})$ and $Im(q_{1,2})$ are symmetric with respect to the angle $\alpha = \pi$. As the angle $\alpha = 0$ increases from to $\alpha = \alpha'$

$$\alpha' = \arccos(1 + 4u_F/h_f^2(u_F - \sqrt{u_F^2+h_f^2})), \tag{4.28}$$

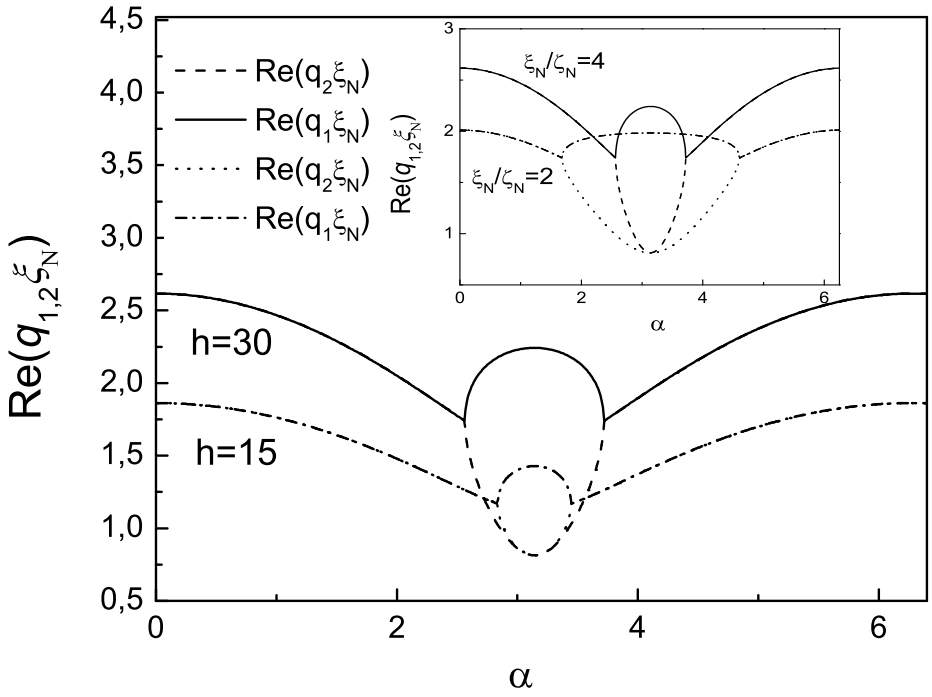

Figure 4.2. $q_{1,2}$ versus the misorientation angle α of the vectors $\mathbf{M}_{1,2}$ at $\xi_N/\zeta_N = 4$, $\xi_N/\xi_F = 10$, $\zeta_N^2/\zeta_F^2 = 300$, $T = 0.5T_C$, $\omega = \pi T$ and h: $h = 30$, $h = 15$. The inset shows the same dependence for $\xi_N/\zeta_N = 4$ and $\xi_N/\zeta_N = 2$ at $h = 30$, $\xi_N/\xi_F = 10$, $\zeta_N^2/\zeta_F^2 = 300$, $T = 0.5T_C$, $\omega = \pi T$.

both the imaginary and real parts of q_1 decrease smoothly, and $q_2 = q_1^*$. According to Fig. 4.3 the imaginary parts $Im(q_{1,2})$ vanish at $\alpha = \alpha'$, thus, q_1 and $q_2$are real. As α further increases to $\alpha = \pi$ the imaginary parts $Im(q_{1,2})$ remain zero. The real part of q_1 increases and reaches a local maximum given by Eq. (4.25) at $\alpha = \pi$ whereas q_2 decreases to

$$q_2^2 = \Omega(\frac{1}{\xi_N^2} + \frac{\zeta_F^2}{\zeta_N^2(\xi_F^2 + \Omega\zeta_F^2)}), \quad \alpha = \pi. \tag{4.29}$$

It can be shown that the coefficient A_2 in Eq.(4.27) tends to zero at $\alpha \to \pi$, so that the contribution I_{C2} to the critical current of the junction vanishes. A similar vanishing of the pre-exponential factor in one of the components of the critical current was previously pointed out in [9].

According to Fig. 4.2 and (4.29) q_2 in the region $\alpha' \leq \alpha \leq 2\pi - \alpha'$ depends weakly on h. Such behavior is typical of the solutions generated by the triplet component, which is odd in ω and even in the momentum. This component is responsible for the existence of the angle range $\alpha' \leq \alpha \leq 2\pi - \alpha'$, where $Im(q_{1,2}) = 0$. This is also confirmed by calculations

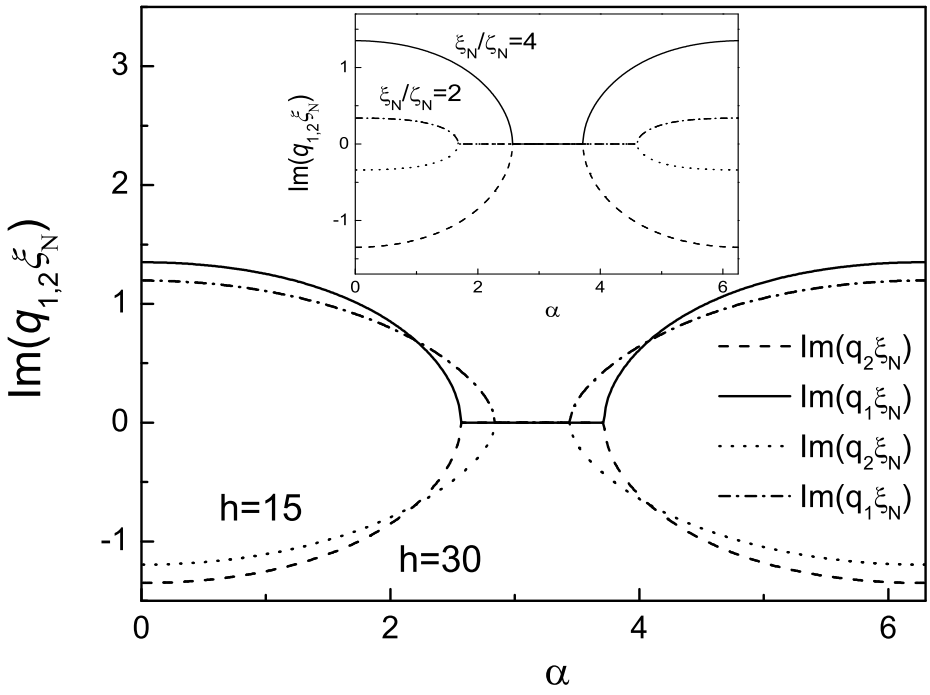

Figure 4.3. $q_{1,2}$ versus the misorientation angle α of the vectors $\mathbf{M}_{1,2}$ at $\xi_N/\zeta_N = 4$, $\xi_N/\xi_F = 10$, $\zeta_N^2/\zeta_F^2 = 300$, $T = 0.5T_C$, $\omega = \pi T$ and h - $h = 30$ and $h = 15$. The inset shows the same dependence for $\xi_N/\zeta_N = 4$ and $\xi_N/\zeta_N = 2$ at $h = 30$, $\xi_N/\xi_F = 10$, $\zeta_N^2/\zeta_F^2 = 300$, $T = 0.5T_C$, $\omega = \pi T$.

within the framework of the approach developed in [10], which ignores the existence of such a triplet component. In the last case, the imaginary part of q vanishes strictly at $\alpha = \pi$, is absent. Thus, the existence of q_2. clearly indicates that the triplet component odd in ω exists in the system; this component decreases with an increase in the distance from the superconductors at a characteristic length much longer than a similar length for the components even in ω. The insets in Figs.4.2 and 4.3 show that, as the transparency of the FN interface, i.e., the ratio ξ_N/ζ_N, decreases, the range $\alpha^{'} \leq \alpha \leq 2\pi - \alpha^{'}$, where the imaginary parts of $q_{1,2}$ vanish, expands, and q_2 approaches the value $\sqrt{\Omega}/\xi_N$. Note that the range where $Im(q_{1,2}) = 0$, also expands with an increase in h. The above calculations were performed with the parameters $\omega = \pi T$, $\xi_N/\xi_F = 10$, $T = 0.5T_C$. This set of parameters at $\xi_N/\zeta_N = 4$, and $h = 30$ corresponds to the minimum period of the spatial oscillations of the critical current. For this reason, $Im(q_{1,2})$ approaches zero both with a further increase in the magnetization $h = 30$, and with a decrease in the ratio ξ_N/ζ_N.

4.4 Critical current

At Fig. 4.4 the critical current calculated by Eqs. (4.27), (4.20) with $\xi_N/\xi_F = 10$, $T = 0.5T_C$, $\xi_N/\zeta_N = 4$, and $h = 30$ at the distances between superconducting electrodes $L/\xi_N = 0.5, 1, 2, 4$ is shown as a function of the rotation angle α of the vectors $\mathbf{M}_{1,2}$. For a more convenient comparison of the shapes of the curves, the I_c, values calculated for $L/\xi_N = 1$ and $L/\xi_N = 2$ were multiplied by a factor of 3, and I_c calculated for $L/\xi_N = 4$ -was multiplied by a factor of 20.

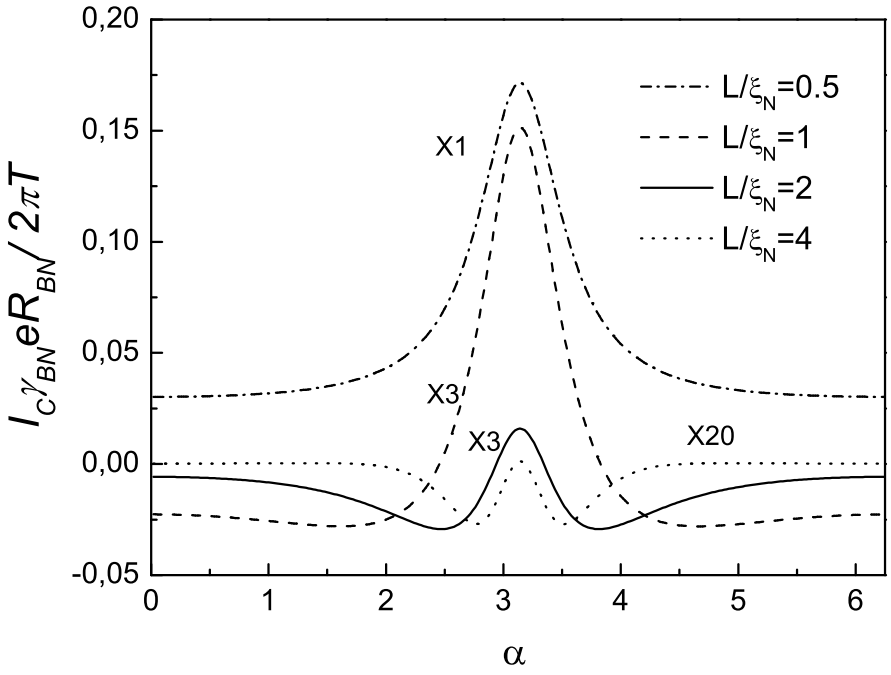

Figure 4.4. $I_C\gamma_{BN}eR_{BN}/2\pi T$ versus the angle α at $h = 30$, $\xi_N/\zeta_N = 4, \xi_N/\xi_F = 10, s = 1, T = 0.5T_C$, $\zeta_N^2/\zeta_F^2 = 300$ and $L/\xi_N = 0.5, 1, 2, 4$ .The dependences for $L/\xi_N = 1, 2, 3$ are multiplied by factors 3, 3 and 20, respectively.

It is seen that the junction at $L/\xi_N = 0.5$ is in the 0-state at any misorientation angle α of the vectors $\mathbf{M}_{1,2}$. The junction at $L/\xi_N = 1$ is in the π - and 0 states at $\alpha = 0$ and π-, respectively.

When the angle α varies from $\alpha = 0$ to $\alpha = \pi$ the state with the negative critical current holds up to $\alpha = 2.46$ and the critical current in the π-state is maximal at $\alpha = 1.62$ rather than at the parallel orientation of the magnetizations. The behavior of $I_c(L)$ at $L/\xi_N = 2$ is the same. In this case, the π state holds up to $\alpha = 2.95$, and the critical current in theπ state is maximal at $\alpha = 2.45$.

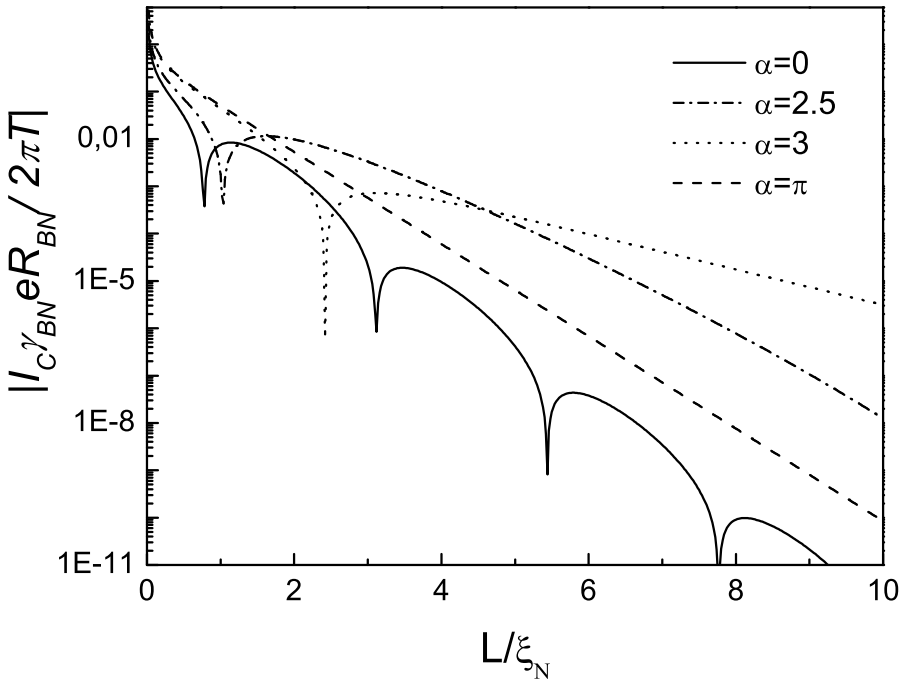

Figure 4.5. $|I_C\gamma_{BN}eR_{BN}/2\pi T|$ versus the distance between the superconducting electrodes L/ξ_N for the parameters $h = 30$ and $\xi_N/\zeta_N = 4, \xi_N/\xi_F = 10, s = 1, T = 0.5T_C$, $\zeta_N^2/\zeta_F^2 = 300$, $\alpha = 0, 2.5, 3, \pi$.

Finally, at $L/\xi_N = 4$ and $\alpha = 0$ the junction is in the 0 state. As α increases, the critical current decreases and the junction at $\alpha = 1.75$ passes to the π-state, which in turn changes to the 0-state at $\alpha = 3.1$. The maximum of the critical current in the π-state is also shifted towards π ($\alpha = 2.76$). With a further increase in the distance between the superconducting electrodes, additional regions of the 0 and π-states appear between $\alpha = 0$ and $\alpha = \pi$. However, an increase in L s accompanied by the exponential decrease in the critical current.

This behavior is illustrated in Fig. 4.5, which shows the dependence $I|_C(L)|$ calculated with the parameters $\alpha = 0, 2.5, 3, \pi$, $\xi_N/\xi_F = 10$, $T = 0.5T_C$, $\xi_N/\zeta_N = 4$, and $h = 30$. As the misorientation angle α increases from 0 to $\alpha^{'}$ the oscillation period increases and is formally infinity at $\alpha = \alpha^{'}$.

The further evolution of $I_C(L)$ with an increase in α (in the range $[\alpha^{'}; 2\pi - \alpha^{'}]$) is determined by the competition of two contributions to $I_C(L)$. The first contribution (I_{C1}) is due to the components with zero projection of the magnetic moment of Cooper pairs is always positive. The second contribution (I_{C2}) is always negative and is due to the existence

of the triplet component with nonzero projection of the magnetic moment of Cooper pairs in the weak-coupling region. At $\alpha = \pi$ $I_{C2} = 0$ and the critical current I_C (shown by the dotted line in Fig. 4.5) is always positive. At $\alpha \neq \pi$ the contribution I_C appears in $I_{C2}(L)$, this contribution is negative, and its absolute value decreases with an increase in L much more slowly than $I_{C1}(L)$. Owing to the difference between $Re(q_1)$ and $Re(q_2)$ in the range $\alpha' \leq \alpha \leq 2\pi - \alpha'$ there is only one length L, beginning with which theπ state appears in the junction and holds with a further increase in L. At $\alpha \to \pi$ the transition to the π state occurs at the length tending to infinity.

4.5 Conclusion

Thus, a new type of "triplet" π junction is possible in the S–FNF–S structures. The possibility of the existence of the triplet π junction was previously discussed in [11]- [17], where it was shown that the triplet superconducting component, whose contribution to I_C can be both negative and positive, is generated in the structures containing one or several ferromagnetic layers with noncollinear magnetizations. For this reason, the π state in such structures can be due not only to the oscillatory decrease in the singlet component and triplet component with zero projection of the magnetic moment of Cooper pairs, but also to the superposition of this combination with the contribution from the triplet component with nonzero projection of the magnetic moment of Cooper pairs to I_C. It is important that the characteristic scale of the decrease in all these components, ξ_F is deter- mined by the transport parameters of the ferromagnet. In contrast to [11]- [17] it was shown that the π state appears in the structures under investigation as a result of the interaction between two spatially nonoscillating contributions to the critical current; each contribution decreases at lengths about the coherent length of the normal metal, which is normally much longer than the length ξ_F. This is illustrated by the dash–dotted curves in Fig. 4.5. In particular, the transition to the π-state at $\alpha = 3$ occurs at $L/\xi_N = 2.4$. As the difference of α from π increases, the 0 - π transition point is shifted towards smaller L values. Note that the existence of the triplet π junction allows one to effectively control the critical current of the S–FNF–S spin gate by means of the rotation of the magnetization vectors of the ferromagnetic films from its initial antiferromagnetic configuration by a relatively small angle. In this case, the difference between the critical currents in the "0" ($I_c > 0$) and "π" ($I_c < 0$) states can be much larger than that in the case where the magnetization direction

of one of the ferro- magnetic films is changed through its remagnetization, i.e., through the transition from $\mathbf{M}_1$ to $\mathbf{-M}_1$ by means of a change in the length of this vector.

Bibliography

[1] V. V. Ryazanov, V. A. Oboznov, A. Yu. Rusanov, A. V. Veretennikov, A. A. Golubov, and J. Aarts, Phys. Rev. Lett. **86**, 2427 (2001).

[2] R. S. Keizer, S. T. V. Goennenwein, T. M. Klapwijk, G. Miao, G. Xiao, and A. Gupta, Nature (London) **439**, 825 (2006).

[3] T. Y. Karminskaya, M. Y. Kupriyanov, JETP Lett. **85**, 343 (2007) [JETP Lett. **85**, 286 (2007)].

[4] T. Y. Karminskaya, M. Y. Kupriyanov, JETP Lett. **86**, 65 (2007) [JETP Lett. **86**, 61 (2003)]. JETP Lett.

[5] F. S. Bergeret, A. F. Volkov, K. B. Efetov, Rev. Mod. Phys. **77**, 1321 (2005).

[6] A. F. Volkov, F. S. Bergeret, K. B. Efetov, Phys. Rev. Lett. **90**, 117006 (2003).

[7] M. Yu. Kuprianov and V. F. Lukichev, Zh. Eksp. Teor. Fiz. **94**, 139 (1988) [Sov. Phys. JETP **67**, 1163 (1988)].

[8] Ya. V. Fominov, A. A. Golubov, and M. Yu. Kupriyanov, JETP Lett. **77**, 609 (2003) [JETP Lett. **77**, 510 (2003)].

[9] M. Faure, A. I. Buzdin, A. A. Golubov, and M. Yu. Kupriyanov, Phys. Rev. B **73**, 064505 (2006).

[10] L. Baladie, A. Buzdin, N. Ryzhanova, and A. Vedyayev, Phys. Rev. B **63**, 054513 (2001).

[11] M. Eschrig, J. Kopu, J. C. Cuevas, and Gerd Schön, Phys. Rev. Lett. **90**, 137003 (2003).

[12] Ya. V. Fominov, A. F. Volkov, K. B. Efetov, Phys. Rev. B **75**, 104509 (2007).

[13] V. Braude and Yu. V. Nazarov, Phys. Rev. Lett. **98**, 077003 (2007).

[14] Y. Asano, Y. Tanaka, and A. A. Golubov, Phys. Rev. Lett. **98**, 107002 (2007).

[15] M. Houzet and A. I. Buzdin, Phys. Rev. B **76**, 060504(R) (2007).

[16] M. Eschrig, T. Löfwander, Nature physics, **4**, 138 (2008).

[17] A. V. Galaktionov, M. S. Kalenkov, A. D. Zaikin, Phys. Rev. B **77**, 094520, (2008).

Chapter 5

Josephson effect in S-FN-S structures with arbitrary thickness of ferromagnetic and normal layers

Introduction

In the last few years, noticeable progress was achieved in the development of special techniques for fabricating superconducting spintronic devices based on SF-structures (S- superconductor, F- ferromagnetic metal). Among them are arrays of Nb/CuNi π-junctions [1], S/F1/N/F2 spin valves consisting on V/Fe superlattices [6], Nb/CuNi nanostructures with a high-quality S-F interface, exhibiting re-entrant and double re-entrant $T_C(d_F)$ behavior [2], [3].

The results obtained in [8] - [10] are essentially based on the assumption that the thicknesses, d_N, d_F, of all the films in FNF multilayer are small compared to their decay lengths. This assumption allows one to simplify the problem and to reduce two dimensional problem to one dimensional.

In real structures the requirement $d_N \ll \xi_N$ can be easily fulfilled, while the inequality $d_F \ll \xi_F$ is difficult to achieve due to the smallness of ξ_F and finite roughness of NF interfaces. Therefore the solution of two dimensional problem is needed. The structures with two dimensional geometry were examined in [8] for two-domain junction, in [5] for multidomain SF structures, and in [6] for junction with helicoidal spin modulation.

It is worth to note that the solution of two dimensional problem arising in the "in plane" geometry, when the domain wall is perpendicular to SF interface [8], [7], is simplified by a natural for this problem suggestion that domain walls consist of materials differing only by the direction of their magnetization.

In this Chapter the properties of a generic S-FN-S junction and perform the calculation of its critical current beyond the limits of small F and N film thicknesses for two dimensional geometry will be discussed. Contrary to [8], [7] in our approach we shall consider that NF interface has finite transparency and that N and F metals have different

transport parameters. Under these conditions, the solution of the two dimensional problem should be found, which is essentially more complicated compared to that discussed in [8], [7].

5.1 Junction model

Consider a symmetric multilayered structure, which consists of a superconducting (S) electrode contacting the end-wall of a bilayer. This bilayer consists of ferromagnetic (F) film and normal metal (N) having a thickness d_F, and d_N respectively (see Fig.5.1). It is supposed also that the condition of a dirty limit is fulfilled for all metals and that effective electron-phonon coupling constant is zero in F and N films. For simplicity it will be suggested below that the parameters γ_{BN} and γ_{BF} which characterize the transparency of NS and FS interfaces

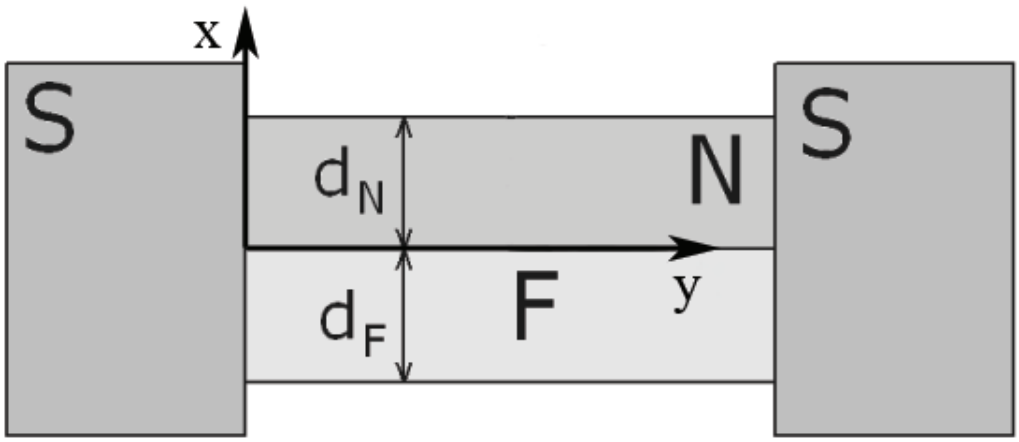

Figure 5.1. FIG. 1. Schematic view of the$S-(NF)-S$ junction.

are large enough to neglect the suppression of superconductivity in S part of the proximity system and to permit the use of the linearized Usadel equations in F and N films of the structure. Under the above conditions the problem of calculation of the critical current in the structure reduces to solution of the set of 2 -dimensional linearized Usadel equations [17], [18], [4]

$$\xi_N^2\left\{\frac{\partial^2}{\partial x^2}+\frac{\partial^2}{\partial y^2}\right\}\Phi_N-\frac{|\omega|}{\pi T_c}\Phi_N=0, \tag{5.1}$$

$$\xi_F^2\left\{\frac{\partial^2}{\partial x^2}+\frac{\partial^2}{\partial y^2}\right\}\Phi_F-\frac{\widetilde{\omega}}{\pi T_c}\Phi_F=0, \tag{5.2}$$

where $\xi_{N,F}^2=(D_{N,F}/2\pi T_c)$, $D_{N,F}$, are diffusion coefficients, $\omega=\pi T(2n+1)$ are Matsubara frequencies, $\widetilde{\omega}=|\omega|+iH\,\mathrm{sgn}\,\omega$, H, is exchange energy of ferromagnetic material. The

boundary conditions at SN and SF interfaces [18] are

$$\gamma_{BN}\xi_N\frac{\partial}{\partial y}\Phi_N = \pm G_0\Delta\exp\left\{\pm i\frac{\varphi}{2}\right\},\ y = L,\ 0, \tag{5.3}$$

$$\gamma_{BF}\xi_F\frac{\partial}{\partial y}\Phi_F = \pm\frac{\widetilde{\omega}}{|\omega|}G_0\Delta\exp\left\{\pm i\frac{\varphi}{2}\right\},\ y = L,\ 0, \tag{5.4}$$

where L is the distance between superconducting electrodes, $G_0 = \omega/\sqrt{\omega^2+\Delta^2}$, Δ is the modulus of the order parameter of superconducting electrodes.

At the FN interface ($x = 0$) we also have [18]

$$\frac{\xi_N}{|\omega|}\frac{\partial}{\partial x}\Phi_N = \gamma\frac{\xi_F}{\widetilde{\omega}}\frac{\partial}{\partial x}\Phi_F, \tag{5.5}$$

$$\gamma_B\xi_F\frac{\partial}{\partial x}\Phi_F + \Phi_F = \frac{\widetilde{\omega}}{|\omega|}\Phi_N, \tag{5.6}$$

where $\gamma_B = R_{B3}\mathcal{A}_{B3}/\rho_F\xi_F$, $\quad\gamma = \rho_N\xi_N/\rho_F\xi_F$, R_{B3} and $\mathcal{A}_{B3}$ are the resistance and area of the NF interface. The boundary conditions at free interfaces

$$\frac{\partial}{\partial x}\Phi_N = 0,\ x = d_N, \tag{5.7}$$

$$\frac{\partial}{\partial x}\Phi_F = 0,\ x = -d_F. \tag{5.8}$$

come from the demand of an absence a current across them.

It is convenient to write the general solution of the boundary value problem (5.1)-(6.8) in the form [8]

$$\Phi_N(x,y) = \Phi_N(y) + \sum_{n=-\infty}^{\infty} A_n(x)\cos\frac{\pi n(y-L)}{L}, \tag{5.9}$$

$$\Phi_F(x,y) = \Phi_F(y) + \sum_{n=-\infty}^{\infty} B_n(x)\cos\frac{\pi n(y-L)}{L}, \tag{5.10}$$

where $\Phi_N(y)$ and $\Phi_F(y)$ are asymptotic solutions of Eq.(5.9),(5.10) at the distance far from FN interface

$$\Phi_N(y) = \frac{G_0\Delta}{\sqrt{\Omega}\gamma_{BN}}\left(\frac{\cos\frac{\varphi}{2}\cosh\frac{L-2y}{2\xi_{N\Omega}}}{\sinh\frac{L}{2\xi_{N\Omega}}} - \frac{i\sin\frac{\varphi}{2}\sinh\frac{L-2y}{2\xi_{N\Omega}}}{\cosh\frac{L}{2\xi_{N}\Omega}}\right),$$

$$\Phi_F(y) = \frac{\sqrt{\widetilde{\Omega}}G_0\Delta}{\Omega\gamma_{BF}}\left(\frac{\cos\frac{\varphi}{2}\cosh\frac{L-2y}{2\xi_{F\Omega}}}{\sinh\frac{L}{2\xi_{F\Omega}}} - \frac{i\sin\frac{\varphi}{2}\sinh\frac{L-2y}{2\xi_{F\Omega}}}{\cosh\frac{L}{2\xi_{F\Omega}}}\right), \qquad \text{where } \xi_{N\Omega} = \xi_N/\sqrt{\Omega},\ \xi_{F\Omega} = \xi_F/\sqrt{\widetilde{\Omega}},$$

while functions $A_n(x)$ and $B_n(x)$ are solutions of appropriate one dimensional boundary problem. The details of $A_n(x)$ and $B_n(x)$ determination are given in Appendix.

Substitution of the expressions (5.9),(5.10) into formula for the supercurrent, I_S, after routine calculations and several simplifications presented in Appendix in the most interesting from the practical point of view situation is when

$$H \gg \pi T_C,\ \xi_F \ll \xi_N, \tag{5.11}$$

results in sinusoidal dependence $I_S = I_C \sin\varphi$, where

$$I_C = \frac{2\pi T}{e}\frac{d_N}{\xi_N}\frac{W}{\gamma_{BN}^2\rho_N}\,\mathrm{Re}\sum_{\omega>0}^{\infty}\frac{G_0^2\Delta^2}{\omega^2 q\xi_N\sinh(qL)}, \tag{5.12}$$

and inverse coherence length is given by

$$q = \frac{1}{\xi_N}\sqrt{\frac{\xi_N}{d_N}\frac{\gamma\sqrt{\widetilde{\Omega}}}{\gamma_B\sqrt{\widetilde{\Omega}}+\coth\left\{\frac{d_F}{\xi_F}\sqrt{\widetilde{\Omega}}\right\}}+\Omega}. \tag{5.13}$$

It is necessary to note that in general the expression for the critical current except summation over ω contains also summation over infinite number of inverse coherence lengths which are the eigenvalues of boundary problem (5.1)-(6.8). As it is followed from estimations given in Appendix under the restrictions on the distance L between superconductors

$$L >> \mathrm{Re}\left(\frac{1}{q}\,\mathrm{arctanh}\,\frac{1}{\gamma_{BN}q\xi_N}\right) \tag{5.14}$$

and on thickness of the N layer

$$\frac{\xi_F^2}{\eta h\xi_N^2} << \frac{d_N}{\xi_N} << \eta, \tag{5.15}$$

where

$$\eta = \begin{cases} \frac{1}{\gamma}\sqrt{\gamma_B^2+\gamma_B\sqrt{2h^{-1}}+h^{-1}}, \\ fracd_F\xi_F >> 1/\sqrt{h}, \\ \frac{1}{\gamma}\sqrt{\gamma_B^2+2\gamma_B\frac{\xi_F}{d_F}\frac{\Omega}{h^2}+\frac{\xi_F^2}{d_F^2h^2}},\ \frac{d_F}{\xi_F} << 1/\sqrt{h}. \end{cases} \tag{5.16}$$

and $h = H/\pi T_C$ the main contribution to I_C comes from the item corresponding to the first eigenvalue, q, which is given by expression (6.24) and for I_C one can get formula (5.12).

From Eq. (5.11) it follows that q weakly depends on temperature. As a result a change of temperature should weakly influence on decay length and period of I_C oscillations and mainly controls only the absolute value of the critical current (5.12). Neglecting in the first approximation the dependence of q on Matsubara frequency one can easily get that $I_C(T) \propto f(T) = \Delta\tanh(\Delta/T)$.

It is necessary to point out that the experimentally studied parameters such as decay length of I_C as a function of L and period of I_C oscillations should be mainly controlled by the real and imaginary parts of inverse coherence length q calculated at $\omega = \pi T$.

Below here will be detailed examination of behavior of inverse coherence length q as a functions of geometrical and transport parameters of weak link. The calculated dependencies do not only provide the knowledge, which is necessary to take into account for design of S-FNF-S structures with input properties, but also will be useful for understanding the features of $I_C(L, d_F)$ dependencies.

5.2 Properties of inverse coherence length q.

In the limit of thin F film $d_F/\xi_F << 1/\sqrt{h}$ expression (6.24) for q transforms into result obtained in [8] in the limit $\zeta_N >> \zeta_F$:

$$q^2 = \frac{\Omega}{\xi_N^2} + \frac{(h^2+\Omega^2)\zeta_F^2 + \Omega\xi_F^2 + ih\xi_F^2}{\zeta_N^2\zeta_F^2(h^2 + (\xi_F^2\zeta_F^{-2} + \Omega)^2)}, \tag{5.17}$$

where $\zeta_F^2 = \gamma_B d_F/\xi_F,\ \zeta_N^2 = \gamma_B d_N/(\xi_N\gamma)$.

In the opposite case $d_F/\xi_F >> 1/\sqrt{h}$ from (6.24) we get

$$q = \frac{1}{\xi_N}\sqrt{\Omega + \frac{\xi_N}{d_N}\gamma\sqrt{\frac{h}{2}}\frac{i+1+\sqrt{2}\gamma_B\sqrt{h}}{\sqrt{h}\gamma_B(\sqrt{2}+\gamma_B\sqrt{h})+1}}. \tag{5.18}$$

At temperature $T = 0.5T_C$. the main contribution into the critical current is provided by the term corresponding to the first Matsubara frequency ($n = 0$). For this reason in this paragraph we will study the properties of inverse coherence length q for $\Omega = 0.5$ that is the value of Ω for $(n = 0)$ and $T/T_C = 0.5$.

In Figs. 5.2 and 5.3 solid curves show the real and imaginary parts of inverse coherence length q as a function of d_F/ξ_F calculated from (6.24) for two ratios of normal film thickness $d_N/\xi_N = 0.01$ and $d_N/\xi_N = 0.1$.

The dotted lines in these figures are the same dependencies, which are followed from asymptotic formula (5.17). All calculations were done for a set of parameters $\xi_N/\xi_F = 10$, $\gamma = 0.03$, $\gamma_B = 0.2$, $h = 30$ which in accordance with analysis done in [8] provide the maximum value for imaginary part of q at $d_F/\xi_F = 0.1$, $d_N/\xi_N = 0.01$ and $d_N/\xi_N = 0.1$.

It is clearly seen that the solid and dotted curves are in close agreement for $d_F/\xi_F \lesssim 0.1$. At $d_F/\xi_F \gtrsim 0.4$ the inverse coherence length starts to be practically independent of d_F reaching the value determined by (5.18). This fact is very important from practical point of view. It says that the parameters of S-FN-S junctions do not deteriorate with increase of d_F, as it follows from the previously obtained [8] result (5.17) (see the dashed lines in Fig.5.2, Fig.5.3). Moreover imaginary parts of q become very robust against the fluctuation of ferromagnetic film thickness in the practically important interval $d_F/\xi_F \gtrsim 0.4$. From Figs.5.2,5.3 one can also see that taking into account finite value of thicknesses of films leads to some increase of decay length.

In Fig. 5.4 solid and dotted lines show the real and imaginary parts of inverse coherence length q as function of d_N/ξ_N calculated from (6.24) and (5.17), respectively, for two ratio of ferromagnetic film thickness $d_F/\xi_F = 0.1$ and $d_F/\xi_F = 1$ and at the same set of other parameters ($\xi_N/\xi_F = 10$, $\gamma = 0.03$, $\gamma_B = 0.2$, $\Omega = 0.5$, $h = 30$).

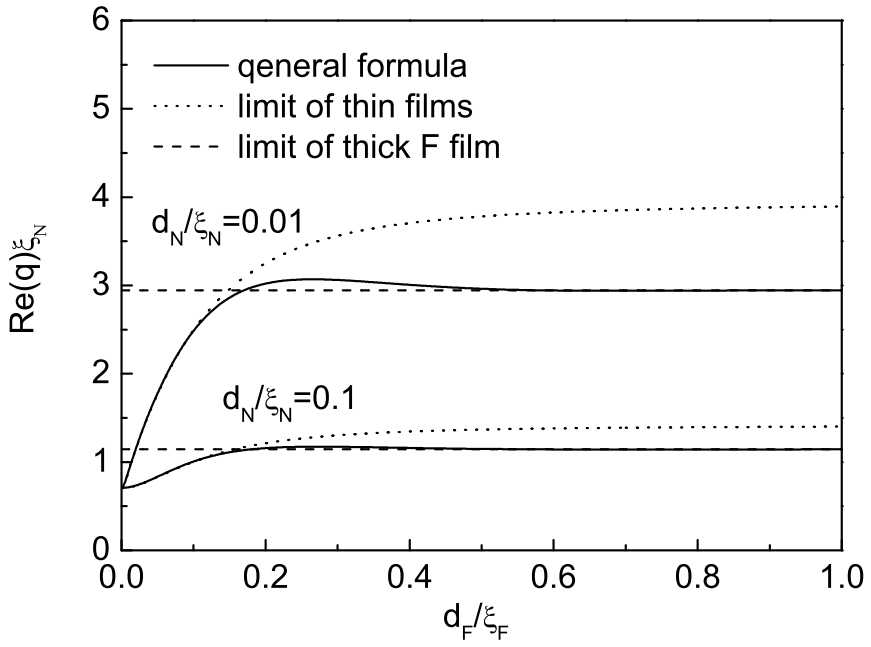

Figure 5.2. Real part of q versus the thickness of F film d_F/ξ_F for two values of $d_N/\xi_N = 0.1, 0.01$ (solid lines for q calculated from (6.24), dotted limes for q calculated from formula for thin films [8], dashed lines correspond to the limit oh thick F film (5.18)) at $\xi_N/\xi_F = 10$, $\Omega = 0.5$, $h = 30$, $\gamma_B = 0.2$, $\gamma = 0.03$.

From the data it follows that an increase of thickness of normal film leads to an increase of period of oscillations, which tends to infinity at large d_N. The decay length also increases with d_N and for $d_F/\xi_F = 0.1$ it practically approaches the value $\xi_N/\sqrt{\Omega}$, that is the decay length of the single normal film.

Figs. 5.5 and 5.6 show the real and imaginary parts of inverse coherence length q as a function of γ and γ_B calculated at $d_N/\xi_N = 0.05$ for $\xi_N/\xi_F = 10$, $\Omega = 0.5$, $h = 30$. In Fig. 5.5, $\gamma_B = 0.1$ and inset shows the same dependencies calculated for $\gamma_B = 0.01$. In Fig. 5.6, $\gamma = 0.1, 0.03$.

There is significant discrepancy between the curves calculated from the general expression (6.24) for q and from asymptotic dependence (5.17) for q previously obtained in [8]. This discrepancy the larger the smaller is the suppression parameter γ_B. This result is obvious since the expression (5.17) is not valid at small γ_B. From direct comparison of the curves we can conclude that in practically important range of $\gamma \gtrsim 0.1$ within the accuracy of 20% we may use the results of [8]- [10] for $\gamma_B \gtrsim 0.2$.

Figure 5.7 shows the dependencies of real and imaginary parts of q upon thickness

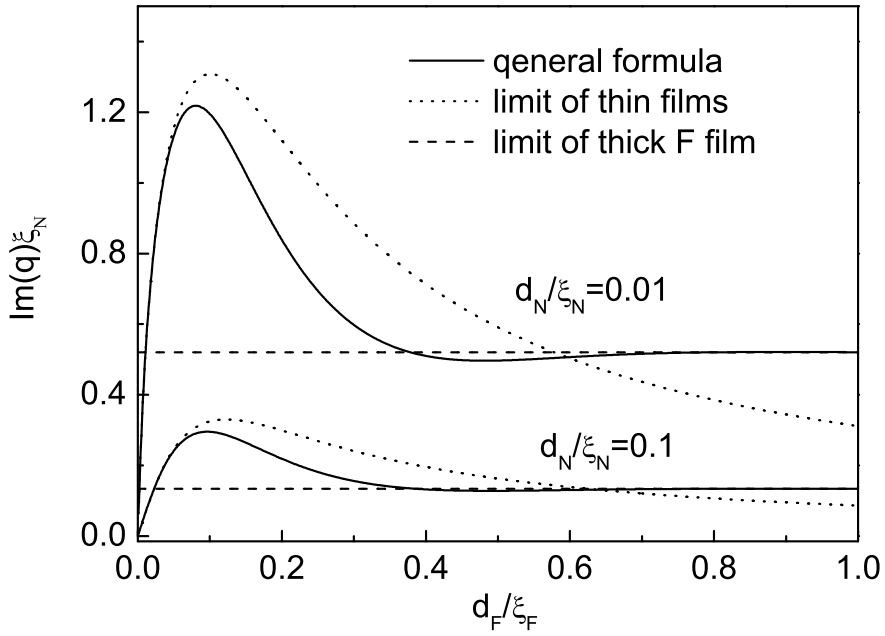

Figure 5.3. Imaginary part of q versus the thickness of F film d_F/ξ_F for two values of $d_N/\xi_N = 0.1, 0.01$ (solid lines for q calculated from (6.24), dotted limes for q calculated from formula for thin films [8], dashed lines correspond to the limit oh thick F film (5.18)) at $\xi_N/\xi_F = 10$, $\Omega = 0.5$, $h = 30$,$\gamma_B = 0.2$, $\gamma = 0.03$.

of F film calculated for $\xi_N/\xi_F = 10$, $\Omega = 0.5$, $h = 30$, $\gamma = 0.03$, $d_N/\xi_N = 0.05$ and the set of parameters $\gamma_B = 0.2, 0.1, 0.01$ (solid lines, dashed lines, dotted lines, respectively). Inset in this figure shows the same dependencies obtained for smaller value of exchange energy $h = 5$. It is clearly seen that $\mathrm{Im}(q)$ has a maximum as a function of d_F/ξ_F. The position of the maximum shifts to larger F layer thickness with γ_B decrease. At $\gamma_B = 0.2$ the maximum of imaginary part has the value $\max(\mathrm{Im}(q)) \approx 0.5\xi_N$, which is achieved at $d_F/\xi_F \approx 0.1$. For smaller suppression parameters $\gamma_B = 0.1$ ($\gamma_B = 0.01$) the maximum of imaginary part equals to $\mathrm{Im}(q) \approx 2/3\xi_F$ ($\max(\mathrm{Im}(q)) \approx \xi_F$) and is achieved at $d_F/\xi_F \approx 0.13$ and $d_F/\xi_F \approx 0.2$, respectively. Inset in Fig.5.7 also demonstrates that both position of the maximum of $\mathrm{Im}(q)$ and its absolute value depend on exchange energy h. Decrease of h shifts $\max(\mathrm{Im}(q))$ to larger ratio d_F/ξ_F and simultaneously suppresses the value of this maximum. From the structure of expression (6.24) for q it follows that its imaginary part $\mathrm{Im}(q)$ has a maximum as a function of exchange energy h. Indeed, at $h \to 0$ the period of $I_C(L)$ oscillation tends to infinity, which is equivalent to $\mathrm{Im}(q) \to 0$. At large h the imaginary part $\mathrm{Im}(q) \propto h^{-1/2}$, that is also goes to zero with h increase. At $d_F/\xi_F \gtrsim 0.4$

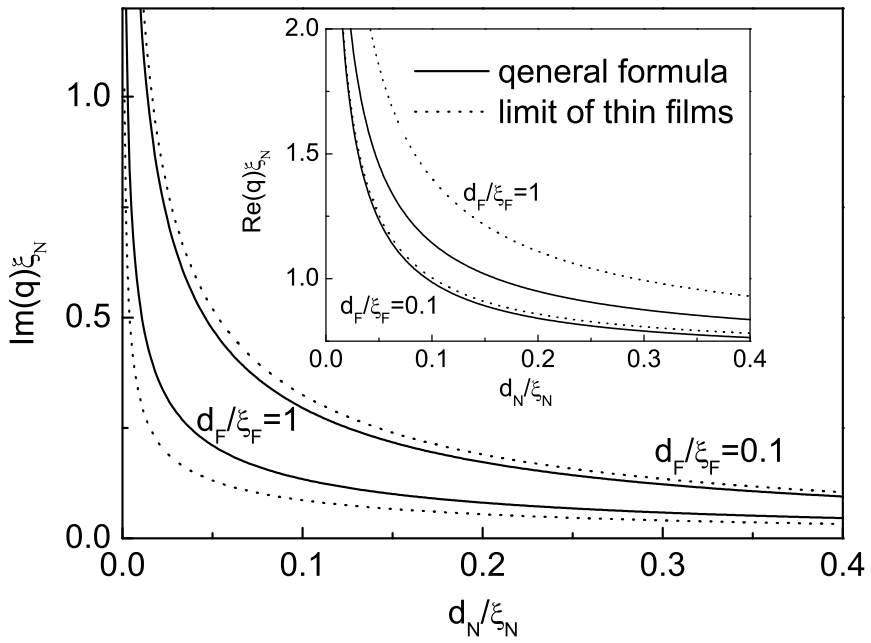

Figure 5.4. Imaginary part of q versus the thickness of N film d_N/ξ_N for two values of $d_F/\xi_F = 0.1, 1$ (solid lines for q calculated from (6.24) and dotted limes for q calculated from formula for thin films [8]) at $\xi_N/\xi_F = 10$, $\Omega = 0.5$, $h = 30$, $\gamma_B = 0.2$, $\gamma = 0.03$. Inset shows real part of q versus the thickness of N film d_N/ξ_N at the same parameters.

both $\mathrm{Im}(q)$ and $\mathrm{Re}(q)$ saturate and practically become independent on F layer thickness.

Figure 5.8 shows the dependence of $\mathrm{Im}(q)/\,\mathrm{Re}(q)$ as a function of d_F/ξ_F. The calculations have been done for $\gamma_B = 0.01$, $\xi_N/\xi_F = 10$, $\Omega = 0.5$, and for two values of suppression parameter $\gamma = 0.03$ (solid line), $\gamma = 0.1$ (dotted line). The values of exchange energy h have been equal to 10 and 30, as it is marked in Fig.5.8 by arrows. The curves presented in Fig.5.8 can be also used for minimization of period of I_C oscillations. Actually, the maximum of ratio $\mathrm{Im}(q)/\,\mathrm{Re}(q)$ corresponds to the minimum decay per one period. It is obvious that this maximum is located near maximum of $\mathrm{Im}\, q$. Therefore the position of this maximum shifts to smaller d_F with increase of exchange energy or suppression parameter γ.

If we want to fix the value of $\max(\mathrm{Im}\, q)$ in the vicinity of ξ_N and to shift this maximum to the largest d_F, we should choose suppression parameter γ_B in the range of 0.01 (for large d_F) and perform the fitting procedure in order to estimate suppression parameter γ and exchange energy h. For instance, we may find that for $h = 30$ maximum of $\mathrm{Im}(q)$ is of the order of ξ_N and it is achieved for $\gamma = 0.03$ at $d_F/\xi_F \approx 0.18$, while for

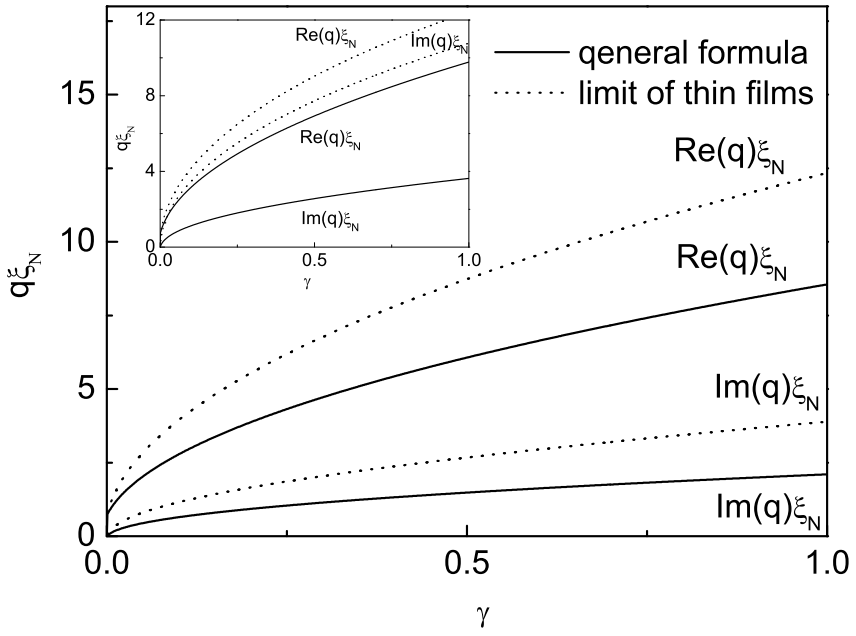

Figure 5.5. Real and imaginary parts of q versus the parameter γ (solid lines for q calculated from (6.24) and dotted limes for q calculated from formula for thin films [8]) at $\xi_N/\xi_F = 10$, $\Omega = 0.5$, $h = 30$, $d_F/\xi_F = 0.5$, $d_N/\xi_N = 0.05$ and $\gamma_B = 0.1$. Inset shows the same dependence at $\gamma_B = 0.01$ and the same other parameters.

$h = 10$, $\gamma = 0.03$ the maximum is shifted to $d_F/\xi_F \approx 0.3$. The smaller the exchange energy the thicker should be the thickness of F film to get $\mathrm{Im}(q)$ in the range of ξ_N. Thus for $h = 5$, $\gamma = 0.09$ the maximum is achieved at $d_F/\xi_F = 0.45$. From the data presented in

Fig.5.7 and Fig.5.8 it follows that for all mentioned above sets of parameters the ratio $\mathrm{Im}(q)/\,\mathrm{Re}(q) \approx 0.6$ and does not exceed this value.

For thick F film $d_F/\xi_F >> 1/\sqrt{h}$ the maximum of $Im(q)/Re(q)$ is achieved at small $\gamma_B \to 0$, $h >> \Omega$ and $\gamma\xi_N/d_N\sqrt{h/2} >> \Omega$ and this maximum relation is $Im(q)/Re(q) \sim 0.4$.

5.3 Thickness dependence of the critical current.

The critical current (5.12) of the studied S-FN-S Josephson junction (see Fig.5.9) is a function of two arguments. They are the distance between superconducting electrodes L/ξ_N and the thickness of ferromagnetic film d_F/ξ_F. The dependence of $I_C(L/\xi_N, d_F/\xi_F)$ have shown in Fig.5.9. It has been calculated from (5.12), (6.24) for $h = 10$, $d_N/\xi_N = 0.05$, $\gamma_B = 0.01$, $\gamma = 0.03$, $\gamma_{BF}/\gamma_{BN} = 1$ and $T = 0.5T_C$.

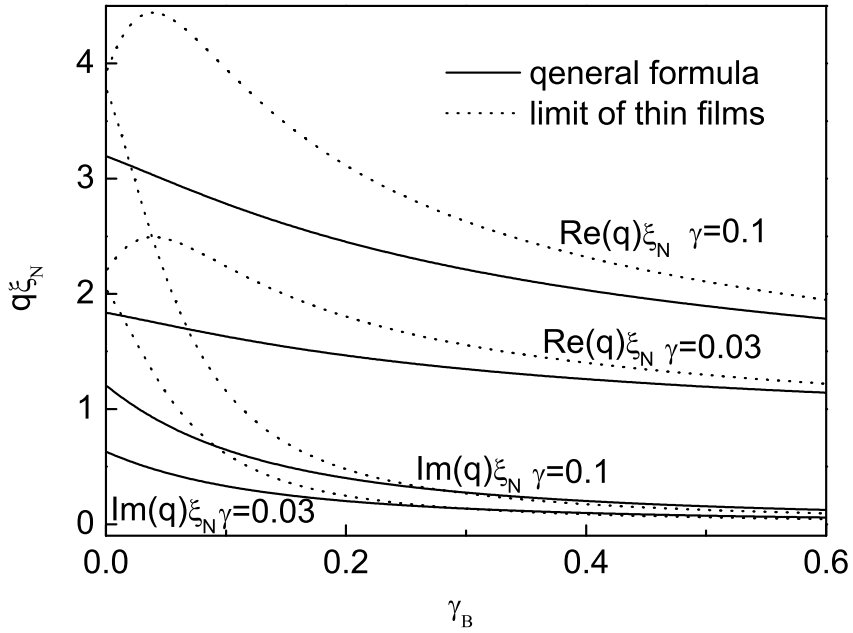

Figure 5.6. Real and imaginary parts of q versus the parameter γ_B (solid lines for q calculated from (6.24) and dotted limes for q calculated from formula for thin films [8]) at $\xi_N/\xi_F = 10$, $\Omega = 0.5$, $h = 30$, $d_F/\xi_F = 0.5$, $d_N/\xi_N = 0.05$ and two values of $\gamma = 0.1, 0.03$.

In the limit $d_F \to 0$ period of critical current oscillations tends to infinity (see Fig. 5.9) and I_C decays monotonically with L, as it must be for SNS Josephson junctions. With d_F, increase (see Fig. 5.10) the dependence of critical current as a function of L/ξ_N has the form of damped oscillations. The decay length of these oscillations is different for different thickness of F film. The most intensive suppression is localized in the vicinity of $d_F/\xi_F \approx 0.6$ since $\mathrm{Re}(q)$ has maximum at this thickness of F layer. It is seen that the suppression of I_C is smaller for thicker ($d_F > 0.6\xi_F$) and thinner ($d_F < 0.6\xi_F$) F films. Period of I_C oscillations decreases with d_F achieving the smallest value at $d_F/\xi_F \approx 0.3$. Further increase of d_F results in increase of this period. Finally in the range of thickness $d_F/\xi_F > 0.5$ both period of I_C oscillations and decay length are nearly constant. In the interval of F layer thickness $d_F/\xi_F \gtrsim 1$ the position of zeros of $I_C(L, d_F)$ undergoes oscillations as a function of d_F (see insert in Fig.5.10). They take place around values $L = L_n$, under which $I_C(L_n, d_F) = 0$ at $d_F \gg \xi_F$. The amplitude of these oscillations decays with increase of d_F. It is interesting to mention that the larger is L_n, the more intensive are the amplitudes of the oscillations. This behavior can be easily understood from the form of $q(d_F)$ dependence (6.24). In the vicinity of $L = L_n$ the critical current is small due to the 0-π transition of I_C as a function of L.

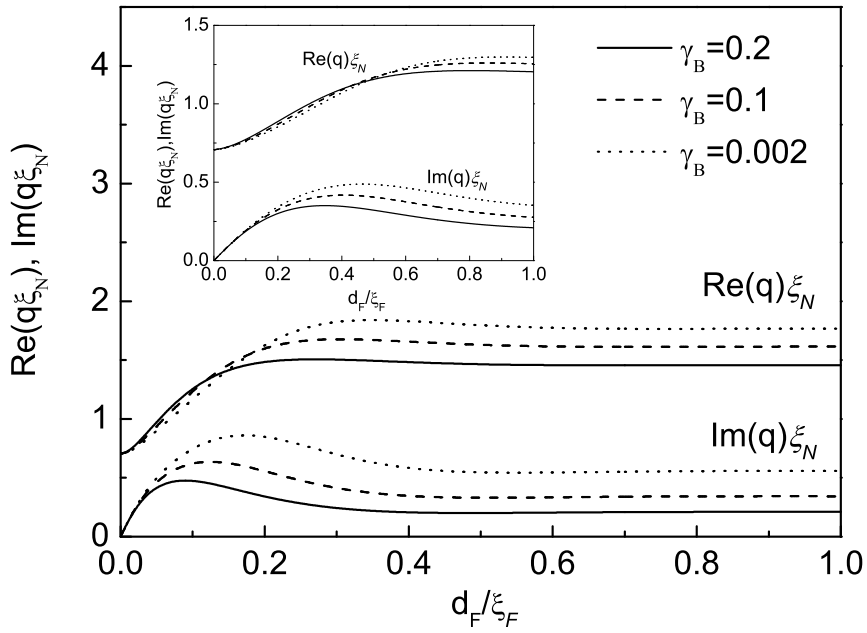

Figure 5.7. Real and imaginary parts of q versus the thickness of F film d_F/ξ_F for $\gamma_B = 0.2, 0.1, 0.01$ (solid, dashed and dotted lines) at $\xi_N/\xi_F = 10$, $\Omega = 0.5$, $h = 30$, $\gamma = 0.03$, $d_N/\xi_N = 0.05$. Inset shows the same dependence for $h = 5$.

Under this condition any small variations of q, which occur due to factor $\coth\left(d_F\sqrt{\widetilde{\Omega}}/\xi_F\right)$ in (6.24) start to be important giving rise to the discussed $I_C(L, d_F)$ behavior.

Figure 5.11 shows the $I_C(L, d_F)$ dependencies calculated at fixed values of L under $h = 10$, $d_N/\xi_N = 0.05$, $\gamma_B = 0.01$, $\gamma = 0.03$, $\gamma_{BF}/\gamma_{BN} = 1$ and $T = 0.5T_C$.

In the small L domain the properties of the S-FN-S junction do not depend on the structure of weak link region. The critical current I_C is practically independent on d_F, so that there is no transition from zero to π state on $I_C(d_F)$. With the increase of L the $I_C(d_F)$ dependence becomes apparent (see Fig.5.9) resulting in suppression of I_C. This suppression is different for different thicknesses of F film. The strongest suppression is realized in the vicinity of $d_F/\xi_F \approx 0.3$. This fact is illustrated in Fig.5.11(a) by the line corresponding to the ratio $L/\xi_N = 1.3$. It is seen that at this value of L/ξ_N the suppression of I_C is smaller for thicker ($d_F > 0.3\xi_F$) and thinner ($d_F < 0.3\xi_F$) F films. At $L/\xi_N \approx 1.67$ and $d_F \approx 0.3\xi_F$ the magnitude of critical current for the first time reaches zero, while the sign of I_C does not change.

With further increase of L the L/ξ_N, d_F/ξ_F plane starts to be subdivided into two regions separated by the line along which the junction critical current is equal to zero. The

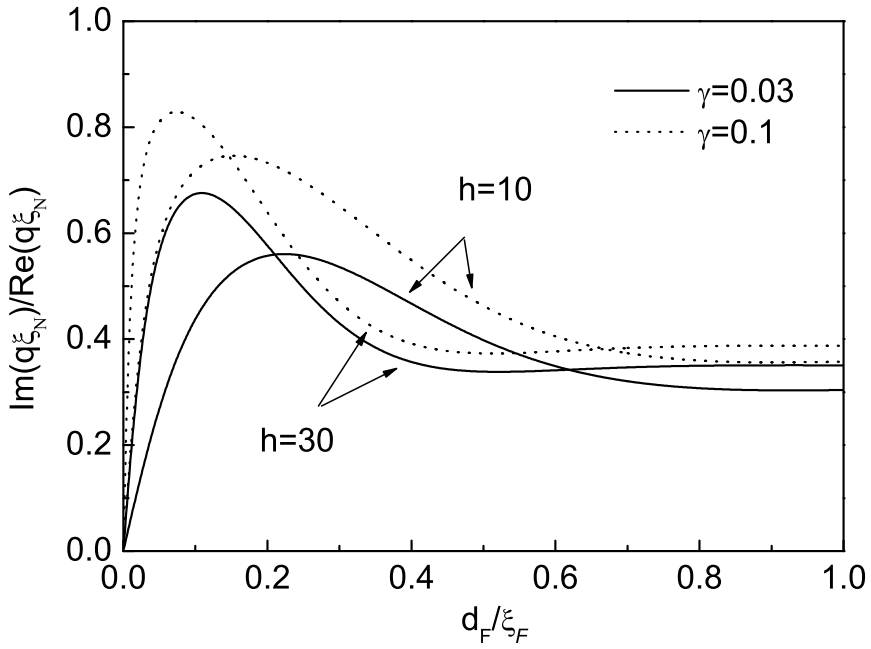

Figure 5.8. Ratio of imaginary part of q to its real part versus the thickness of F film d_F/ξ_F for two values of $\gamma = 0.03, 0.1$ (solid and dotted lines) at $\xi_N/\xi_F = 10, \gamma_B = 0.01, d_N/\xi_N = 0.05$, $\Omega = 0.5$, and $h = 30, 10$.

boundary between the regions has two branches (see Fig.5.12). The first one is located at $d_F < 0.3\xi_F$. It starts from the first critical point $(L_{c1}/\xi_N, d_{F,c1}/\xi_F) \approx (1.67, 0.3)$ and $d_{F,c1}$ the smaller the larger is L. The second branch located at $d_F > 0.3\xi_F$. It starts from the same critical point and for large d_F asymptotically verge towards the line $L = L_1$ exhibiting damped oscillation around it. As a result, any cross-section presented in Fig.5.9 dependence of $I_C(L/\xi_N, d_F/\xi_F)$ by a perpendicular to L axis plane in the region $1.67 < L/\xi_N < 2.87$ should give a dependence of $I_C(d_F)$ having the typical shape shown by solid line ($L/\xi_N = 1.8$) in Fig.5.11(a). It demonstrates that in this range of distances between S electrodes ($1.67 < L/\xi_N < 2.87$) for any given L there is a nucleation of only one π state in between of two zero states in $I_C(d_F)$ dependence. The interval of d_F in which the π state exists, becomes wider the larger the L. Note also that for $1.67 < L/\xi_N < 2.87$ only 0 -state can be realized for large $d_F/\xi_F \gtrsim 0.8$.

The number of transitions between zero and π states in $I_C(d_F)$ increases by asymptotically approaching the line $L = L_1$. This is illustrated in Fig.5.11(b). At ($L/\xi_N = 2.6$) there are still only two transitions, namely, from 0-state to π-state and from π to zero state. At ($L/\xi_N \approx 2.8702$) in the zero state domain there is nucleation of the next critical point at

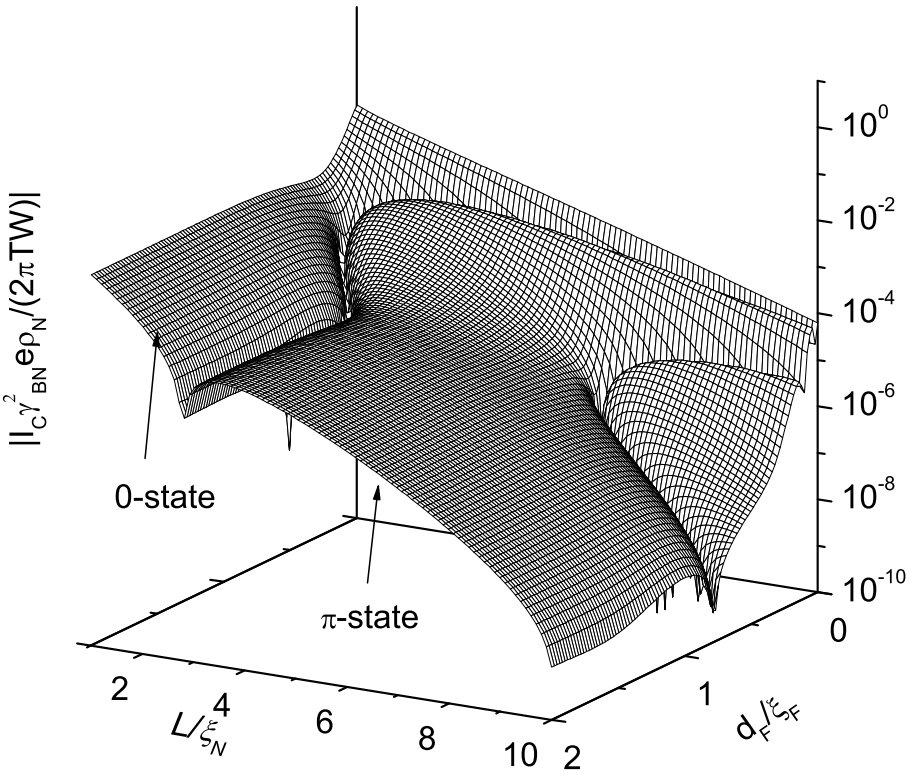

Figure 5.9. Normalized absolute value of critical current versus the thickness of F film d_F/ξ_F and distance between the superconducting electrodes L/ξ_N for $\gamma = 0.03, \gamma_B = 0.01$, $\xi_N/\xi_F = 10, d_N/\xi_N = 0.05$, $h = 10$, $\gamma_{BN}/\gamma_{BF} = 1, T = 0.5T_C$.

$d_F/\xi_F \approx 1.7$. In it $I_C = 0$, while the sign of I_C is kept positive for all $d_F/\xi_F \gtrsim 0.8$. Further increase of L leads to generation of additional π state in the vicinity of $d_F/\xi_F \approx 1.7$ as it is shown in Fig.5.11(b) by solid line. The closer L to L_1 the larger is the amount of zero to π transitions. As it was already pointed above, this behavior of critical current at $L/\xi_N \approx L_1$ is a result of small oscillations of $\mathrm{Im}(q)$ which occur at large d_F. Note that in the region $L = L_1 - 0$ S-FN-S junction always is in the zero state at $d_F \to \infty$.

Contrary to that, for $L = L_1 + 0$ it is π state that is finally established in the limit of large d_F (see the dotted line for $L/\xi_N = 2.8729$ in Fig.5.11(c)). Further increase of L leads to the reduction of thickness intervals in which the zero states exists. They collapse one by one with L. The last stage of this process is shown in Fig. 5.11(c). It is seen that transition from $(L/\xi_N = 2.8729)$ to $(L/\xi_N = 2.92)$ leads to reduction of the zero state located in vicinity of $d_F/\xi_F = 1$. At $(L/\xi_N \approx 2.95)$ it completely shrinks, so that I_C becomes always negative at $d_F/\xi_F \gtrsim 0.2$. As a result in the distance interval $3.5 \lesssim L/\xi_N \lesssim 6.5$ the typical shape of $I_C(d_F)$ dependence for a fixed L has the form of the curve presented in Fig.5.11(c) by the line calculated for $L/\xi_N \approx 3.5$. There is only one 0-π transition, which occurs at

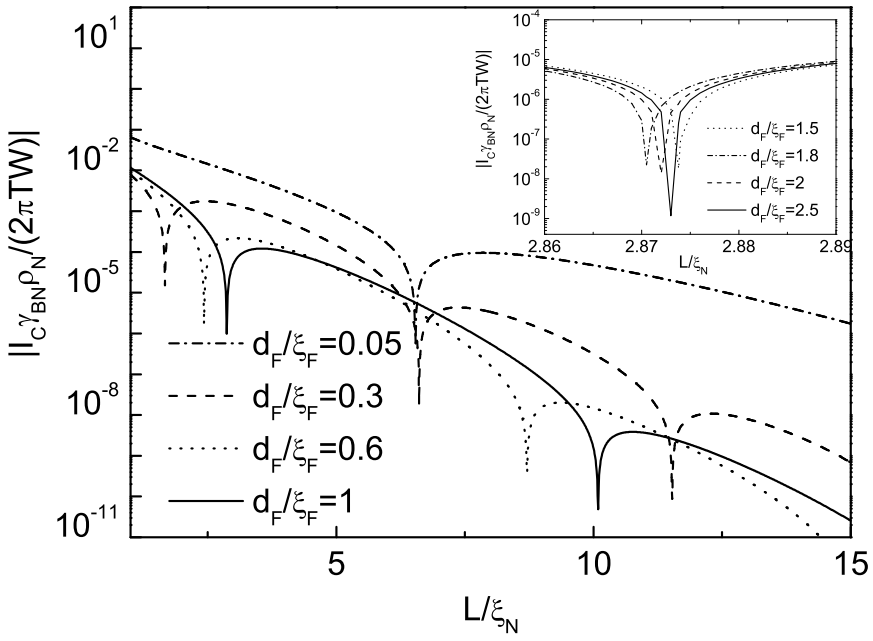

Figure 5.10. Normalized absolute value of critical current versus the distance between electrodes L/ξ_N for $\gamma = 0.03, \gamma_B = 0.01$, $\xi_N/\xi_F = 10, d_N/\xi_N = 0.05$, $h = 10$, $\gamma_{BN}/\gamma_{BF} = 1$, $T = 0.5T_C$ for several thicknesses of F film $d_F/\xi_F = 0.05, 0.3, 0.6, 1$.Insert shows the same dependence for $d_F/\xi_F = 1.5, 1.8, 2, 2.2$.

$d_F/\xi_F \approx 0.2$. It is the first branch of the locus of point at which $I_C = 0$ on $L/\xi_N, d_F/\xi_F$ plane.

It is seen from Fig.5.9, Fig.5.12 that at $L/\xi_N \approx 6.5$ and $d_F/\xi_F \approx 0.32$ there is a nucleation of the next critical point. Again the two branches start to propagate from it. They produce the next boundary on $L/\xi_N, d_F/\xi_F$ plane, thus subdividing this plane into three regions.

The first branch is located at $d_F/\xi_F \lesssim 0.32$. It propagates along L nearly parallel to the already existing in this domain branch generated at critical point $L_{c1}/\xi_N, d_{F,c1}/\xi_F) \approx (1.67, 0.3)$. In the narrow zone between these branches the junction is in the π state. The second branch is located at $d_F > 0.32\xi_F$. Starting from the second critical point for large d_F it asymptotically verges towards the line $L = L_2 = 10.089$ exhibiting damped oscillations around it. Quantitatively the behavior of $I_C(L, d_F)$ in the vicinity of $L = L_2$ and at slightly larger L is the same as we discuss above. There is increasing number of zero to π transitions as soon as $L \to L_2 - 0$ and the collapses of π states in the $L = L_2 + 0$ region with L increase. Finally in the interval $10.32 \lesssim L/\xi_N \lesssim 11.5$ there are only two transitions of $I_C(d_F)$ and at

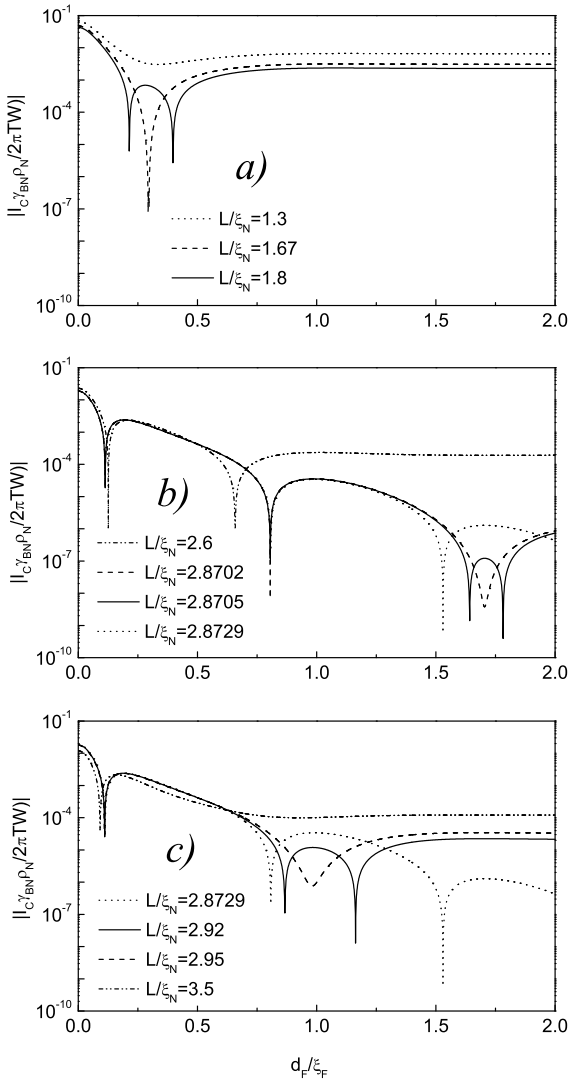

Figure 5.11. Normalized absolute value of critical current versus the thickness of F film d_F/ξ_F for $\gamma = 0.03, \gamma_B = 0.01$, $\xi_N/\xi_F = 10, d_N/\xi_N = 0.05$, $h = 10$, $\gamma_{BN}/\gamma_{BF} = 1$, $T = 0.5T_C$ for several distances between the superconducting electrodes $L/\xi_N = 1.3, 1.67, 1.8, 2.6, 2.8702, 2.8705, 2.8729, 2.95, 2.95, 3.5$.

$d_F/\xi_F \gtrsim 0.012$ there is only zero state of the critical current.

5.4 Conclusion

In this Chapter Josephson effect in S-FN-S structures under condition of relatively large suppression parameters γ_{BN} and γ_{BF} at SN and SF interfaces was discussed. General expression for the critical current of these structures, applicable for arbitrary values of suppression parameters at FN interface and in the practically important case of relatively thin normal film and arbitrary thickness of a ferromagnetic layer were derived. It is shown

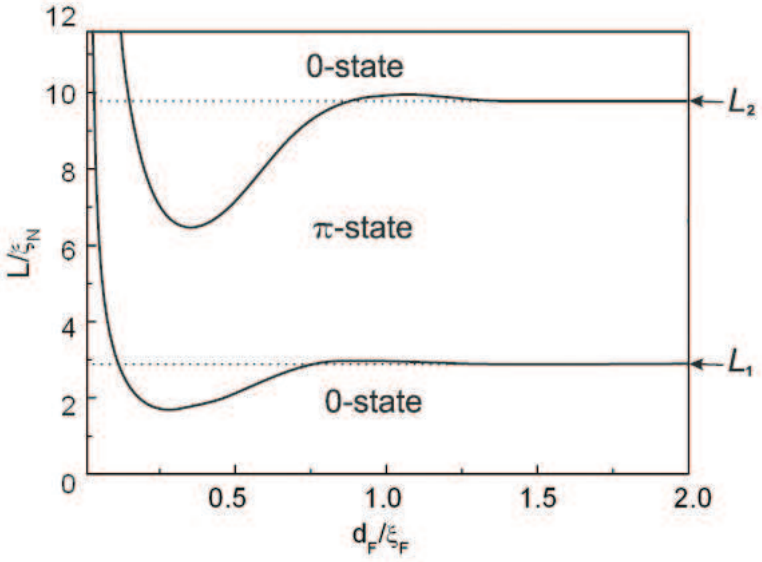

Figure 5.12. (L, d_F) phase diagram for S-FN-S junction at $\gamma = 0.03, \gamma_B = 0.01$, $\xi_N/\xi_F = 10, d_N/\xi_N = 0.05$, $h = 10$, $\gamma_{BN}/\gamma_{BF} = 1, T = 0.5T_C$.

that the critical current of the junction, I_C, exhibits damped oscillations as a function of a distance L between S electrodes. It was demonstrated that for typical values of exchange energy $h \approx 30$ and in the limit of thin F and N layers ($(d_F \lesssim 0.1\xi_F$ and $d_N \lesssim \xi_N)$ the results obtained for the critical current cross over to the previously derived in [8]. It is qualitatively clear that the considerations performed in [9]- [10] for more sophisticated S-FNF-S Josephson junctions are also valid in this parameter range. Further increase of d_N results in increase of both period of $I_C(L)$ oscillations and its decay length. The 0-π transition point shifts to larger L, so that the properties of the structure continuously transform into those of S-N-S devices.

Increase of d_F is accompanied by more complicated processes. The period of I_C oscillations and the decay length have minima as a function of d_F. The maximum value of d_F at which these minima can be achieved for typical values of h is $d_F/\xi_F \lesssim 0.6$.

In the practically interesting range of F layer thickness $d_F \gtrsim \xi_F$ the dependence of $I_C(L)$ is qualitatively the same as previously found in [8]. There is continuous transition from zero to π state with increase of L. Noticeable exceptions are narrow intervals of L located in the vicinity of $L = L_n$, where L_n is the distance at which $I_C(L_n, d_F) = 0$ for $d_F \gg \xi_F$ (see insert in Fig.5.10 and Fig.5.11). In these intervals the position of the point at which $I_C = 0$ exhibits damping oscillations as a function of d_F and number of transitions

from 0 to π states in $I_C(L, d_F)$ increases under $L \to L_n$. Outside these intervals sign and value of I_C are independent on d_F for $d_F \gtrsim \xi_F$. This fact is very important for possible applications of S-FN-S Josephson junctions and S-FNF-S spin valve Josephson devices.

These calculations have shown that to fabricate the proposed S-FNF-S structures it is favorable to have the thickness of the N film in the range $d_N \approx 0.1 \div 0.2\xi_N$. For typical decay length high-conductivity metals, ξ_N, of the order of 100 nm this restriction results in $d_N \approx 10 \div 20$ nm. This range of d_N thicknesses is ordinary used in fabricating SNS Josephson devices. In our particular case this interval of thicknesses provides the required coupling strength between the polarized electron subsystems in the two F films, and simultaneously such d_N range is sufficient to support superconducting correlations induced into from the S electrodes.

From the data presented in Fig.6 it also follows that the smaller is the suppression parameter γ_B at the FN interface, the smaller is the decay length of I_C and the period of its oscillations. Typical values of specific boundary resistance at a sharp metal interface [19], $R_B\mathcal{A} \approx 10^{-11}$ Ωcm^2, and typical values of $\rho_F\xi_F$ product are close to each other resulting in $\gamma_B \lesssim 1$. Increase of γ_B does not strongly influence the decay length, which tends to ξ_N when γ_B goes to infinity. Contrary to that, the period of I_C oscillations depends stronger on γ_B. It goes to infinity in the limit of large γ_B thus preventing the experimental observation of 0 to π transition. Therefore we may conclude that the smaller is suppression parameter γ_B the stronger is the interaction of polarized electrons in the N film of S-FNF-S junctions and the better are the conditions for realization of effects predicted in [8]- [10].

It is also necessary to note that in these calculations we have chosen the suppression parameter γ equal to 0.03 or 0.1. For small γ_B, this suppression parameter has to be small in order to prevent strong suppression of superconductivity induced into N film due to the proximity with the F films. For $\gamma \lesssim 0.1$ the superconducting correlations in the F films are supported due to the proximity effect and the back influence of F films on superconductivity in the N part of FNF trilayer is small. The conclusion about smallness of γ comes also from inequality (5.15). For $d_N/\xi_N \approx 0.1, d_F/\xi_F \approx 1, h \approx 30$ and $\gamma_B \to 0$ the rough estimate from inequality (5.15) gives $\gamma << 2$.

The restriction $\gamma \lesssim 0.1$ is not too strong since for typical values of $\rho_N\xi_N$ and $\rho_F\xi_F$ products their ratio just provides the necessary small values for the γ parameter.

Finally,t his analysis shows that for practically interesting interval of F layer thickness $d_F \gtrsim \xi_F$ the parameters of S-FNF-S spin valve devices are very robust to variations

of d_F if the distance between superconductors is not very close to the critical points L_n, at which the $I_C = 0$.

5.5 Appendix

5.5.1 Solution of linearized Usadel equations

It is convenient to write the general solution of the boundary value problem (5.1)-(6.8) in the form

$$\Phi_N(x,y) = \Phi_N(y) + \sum_{n=-\infty}^{\infty} A_n(x)\cos\frac{\pi n(y-L)}{L}, \tag{5.19}$$

$$\Phi_F(x,y) = \Phi_F(y) + \sum_{n=-\infty}^{\infty} B_n(x)\cos\frac{\pi n(y-L)}{L}, \tag{5.20}$$

where $\Phi_N(y)$ and $\Phi_F(y)$ are asymptotic solutions of Eq.(5.1),(6.32) at the distance far from FN interface

$$\Phi_N(y) = \frac{G_0\Delta}{\sqrt{\Omega}\gamma_{BN}}\left(\frac{\cos\frac{\varphi}{2}\cosh\frac{L-2y}{2\xi_{N\Omega}}}{\sinh\frac{L}{2\xi_{N\Omega}}} - \frac{i\sin\frac{\varphi}{2}\sinh\frac{L-2y}{2\xi_{N\Omega}}}{\cosh\frac{L}{2\xi_{N}\Omega}}\right),$$

$$\Phi_F(y) = \frac{\sqrt{\widetilde{\Omega}}G_0\Delta}{\Omega\gamma_{BF}}\left(\frac{\cos\frac{\varphi}{2}\cosh\frac{L-2y}{2\xi_{F\Omega}}}{\sinh\frac{L}{2\xi_{F\Omega}}} - \frac{i\sin\frac{\varphi}{2}\sinh\frac{L-2y}{2\xi_{F\Omega}}}{\cosh\frac{L}{2\xi_{F\Omega}}}\right), \qquad \text{where } \xi_{N\Omega} = \xi_N/\sqrt{\Omega},\ \xi_{F\Omega} = \xi_F/\sqrt{\widetilde{\Omega}},$$

while functions $A_n(x)$ and $B_n(x)$ satisfy the following boundary problem

$$\xi_N^2\frac{\partial^2}{\partial x^2}A_n(x) - u_n^2 A_n(x) = 0, \tag{5.21}$$

$$\xi_F^2\frac{\partial^2}{\partial x^2}B_n(x) - v_n^2 B_n(x) = 0, \tag{5.22}$$

$$\frac{\gamma_B}{\gamma}\xi_N\frac{\widetilde{\Omega}}{\Omega}\frac{\partial}{\partial x}A_n(0) - \frac{\widetilde{\Omega}}{\Omega}A_n(0) + B_n(0) = R_n, \tag{5.23}$$

$$\gamma_B\xi_F\frac{\partial}{\partial x}B_n(0) + B_n(0) - \frac{\widetilde{\Omega}}{\Omega}A_n(0) = R_n, \tag{5.24}$$

$$R_n = \frac{\widetilde{\Omega}}{\Omega}\frac{G_0\Delta}{L}\kappa_n\left(e^{\frac{i\varphi}{2}} + (-1)^n e^{\frac{-i\varphi}{2}}\right), \tag{5.25}$$

$$\frac{\partial}{\partial x}A_n(d_N) = 0, \qquad \frac{\partial}{\partial x}B_n(-d_F) = 0. \tag{5.26}$$

Here $\Omega = |\omega|/\pi T_C$, $\widetilde{\Omega} = \widetilde{\omega}/\pi T_C$ and

$$\kappa_n = \frac{1}{\gamma_{BN}}\frac{\xi_N}{u_n^2} - \frac{1}{\gamma_{BF}}\frac{\xi_F}{v_n^2}, \tag{5.27}$$

$$u_n = \sqrt{\left(\frac{\pi n\xi_N}{L}\right)^2 + \Omega}, \quad v_n = \sqrt{\left(\frac{\pi n\xi_F}{L}\right)^2 + \widetilde{\Omega}}. \tag{5.28}$$

Solution of (5.21)-(5.26) has the form

$$A_n(x) = -\frac{R_n\gamma v_n\Omega\cosh\left\{\frac{x-d_N}{\xi_N}u_n\right\}}{\widetilde{\Omega}\delta_n\sinh\frac{u_nd_N}{\xi_N}}, \tag{5.29}$$

$$B_n(x) = \frac{R_nu_n\cosh\left\{\frac{x+d_F}{\xi_F}v_n\right\}}{\delta_n\sinh\frac{v_nd_F}{\xi_F}}, \tag{5.30}$$

where δ_n is defined as:

$$\delta_n = \gamma_Bv_nu_n + u_n\coth\frac{v_nd_F}{\xi_F} + \gamma v_n\coth\frac{u_nd_N}{\xi_N} \tag{5.31}$$

5.5.2 Calculation of supercurrent across S-FN-S junction.

To calculate the supercurrent across the S-FN-S junction we substitute of the expressions (5.19)-(5.20), (5.29)-(5.31) into formula for the general formula for supercurrent

$$\begin{aligned} I_S(x,y) &= \frac{-i\pi TW}{e\rho_F}\sum_{\omega=-\infty}^{\infty}\frac{1}{\widetilde{\omega}^2}\int_{-d_f}^{0}\left[\Phi^*_{-\omega,F}\frac{\partial}{\partial y}\Phi_{\omega,F}\right] - \\ &\quad -\frac{i\pi TW}{e\rho_N}\sum_{\omega=-\infty}^{\infty}\frac{1}{\omega^2}\int_{0}^{d_n}\left[\Phi^*_{-\omega,N}\frac{\partial}{\partial y}\Phi_{\omega,N}\right]. \end{aligned}$$

The calculations gives $I_S = I_C\sin\varphi$, where

$$\begin{aligned} I_C &= \frac{\Delta^2\pi TW\gamma}{e\rho_N}\sum_{\omega=-\infty}^{\infty}\frac{G_0^2}{\omega^2}\left[\sum_{j=1}^{6}k_jS_j + \right. \\ &\quad \left. + \frac{d_F}{\sqrt{\widetilde{\Omega}}\xi_N\gamma_{BF}^2\sinh\frac{L}{\xi_{F\Omega}}} + \frac{d_N/\gamma}{\sqrt{\Omega}\xi_N\gamma_{BN}^2\sinh\frac{L}{\xi_{N\Omega}}}\right] \end{aligned} \tag{5.32}$$

and W is a width of junction in the direction perpendicular to axes 0y and 0x. The last two items in (5.32) determine the critical current of the structures with ether ferromagnetic (SFS) or normal (SNS) interlayers [4], [15]- [18]. By S_j we define the ordinary and double

sums:

$$
\begin{aligned}
S_1 &= \sum_{n=-\infty}^{\infty} \frac{n\kappa_n u_n \sin\frac{\pi n}{2}}{v_n \delta_n}, S_2 = \sum_{n=-\infty}^{\infty} \frac{n\kappa_n v_n \sin\frac{\pi n}{2}}{u_n \delta_n}, \\
S_3 &= \sum_{n=-\infty}^{\infty} \frac{\kappa_n u_n \cos\frac{\pi n}{2}}{v_n \delta_n}, S_4 = \sum_{n=-\infty}^{\infty} \frac{\kappa_n v_n \cos\frac{\pi n}{2}}{u_n \delta_n}, \\
S_5 &= \sum_{n,m=-\infty}^{\infty} \frac{C_{nm} u_n u_m}{\sinh\frac{v_n d_F}{\xi_F} \sinh\frac{v_m d_F}{\xi_F}} I_v, \\
S_6 &= \sum_{n,m=-\infty}^{\infty} \frac{C_{nm} v_n v_m}{\sinh\frac{u_m d_N}{\xi_N} \sinh\frac{u_n d_N}{\xi_N}} I_u, \\
I_v &= \frac{\sinh\frac{(v_n+v_m)d_F}{\xi_F}}{v_n+v_m} + \frac{\sinh\frac{(v_n-v_m)d_F}{\xi_F}}{v_n-v_m}, \\
I_u &= \frac{\sinh\frac{(u_n+u_m)d_N}{\xi_N}}{u_n+u_m} + \frac{\sinh\frac{(u_n-u_m)d_N}{\xi_N}}{u_n-u_m}, \\
C_{nm} &= \frac{n \sin\frac{\pi n}{2} \cos\frac{\pi m}{2} \kappa_m \kappa_n}{\delta_m \delta_n},
\end{aligned}
\tag{5.33}
$$

and coefficients k_j are

$$
\begin{aligned}
k_1 &= \frac{\sqrt{\widetilde{\Omega}}\xi_{F\Omega}^2 \pi}{\gamma_{BF} L^2 \sinh\frac{L}{2\xi_{F\Omega}}}, k_2 = \frac{-\sqrt{\Omega}\xi_{N\Omega}^2 \pi}{\gamma_{BN} L^2 \sinh\frac{L}{2\xi_{N\Omega}}}, \\
k_3 &= \frac{\sqrt{\Omega}\xi_{N\Omega}^2 \pi}{\gamma_{BN} L^2 \sinh\frac{L}{2\xi_{N\Omega}}}, k_4 = \frac{-\xi_N}{\gamma_{BN} L \cosh\frac{L}{2\xi_N\Omega}}, \\
k_5 &= \frac{\pi \xi_N \xi_F^2}{L^3},\ k_6 = \gamma \frac{\pi \xi_N^3}{L^3}.
\end{aligned}
\tag{5.34}
$$

Expressions (6.14)-(5.34) are the main mathematical result of this work and are the subject of more detailed analysis given below. They give the general expression for the critical current of S-FN-S Josephson structure.

5.5.3 Critical current of S-FN-S junction.

To calculate the sums (5.33) we may use the procedure known from the theory of functions of complex variables

$$
\sum_{n=-\infty}^{\infty} f(n) \sin(\pi n/2) = \frac{\pi}{2} \sum_k \frac{res(f(z_k))}{\cos(\pi/2 z_k)}, \tag{5.35}
$$

$$
\sum_{n=-\infty}^{\infty} f(n) \cos(\pi n/2) = -\frac{\pi}{2} \sum_k \frac{res(f(z_k))}{\sin(\pi/2 z_k)}, \tag{5.36}
$$

where $res(f(z_k))$ is residue of function $f(z)$ at the critical point z_k. From (5.33) it follows that there are critical points $z_u = \pm iL\sqrt{\Omega}/(\xi_N \pi)$ and $z_v = \pm iL\sqrt{\widetilde{\Omega}}/(\xi_F \pi)$, which are the

roots of equations $u(z) = 0$, and $v(z) = 0$, respectively. In addition there is also an infinite number of z_k, which are the roots of equation:

$$\delta(z) = 0. \tag{5.37}$$

Applying the procedure (5.35)-(5.36) to calculation of (5.33) it is possible to show that the last two terms in expression for I_C (5.32) are exactly compensated by the parts of these sums, which are calculated from the residue at critical points $z = z_u$ and $z = z_v$. Therefore critical current (5.32) can be expressed as the sum of terms resulting from the application of the rule (5.35)-(5.36) to (5.33) at $z = z_k$.

Our analysis have shown that the value part of z_k consists of a root having the lowest real part, $z = z_{min}$, and the two systems of roots. In the first system, $z_{k,N}$, there is an item in the real part of $z_{k,N}$, which at large k increase with the number k of the root as $k\xi_N/d_N$, while in the second, $z_{k,F}$, this increase is proportional to $k\xi_F/d_F$. Below we will restrict ourselves to the consideration of the limit at which z_{min} makes the major contribution to the junction critical current, i.e. $|z_{min}| << |z_k|$. It can be shown that the lowest value among the roots of $z_{k,F}$ group is achieved at the limit of large d_F and is bounded by $\sqrt{\widetilde{\Omega}}L/(\pi\xi_F)$. The lowest value of second group of the roots, $z_{k,N}$, is bounded by $\sqrt{\xi_N^2/d_N^2 - \Omega}(L/(\pi\xi_N))$, the value at which $z_{k,N}$ are approached to in the limit of small γ. Thus under the condition

$$|z_{min}| << \quad |\sqrt{\widetilde{\Omega}}L/(\pi\xi_F)|, \tag{5.38}$$

$$|z_{min}| << \quad |\sqrt{\xi_N^2/d_N^2 - \Omega}(L/(\pi\xi_N))| \tag{5.39}$$

we can rewrite equation (5.37) in the form

$$u^2 = -\frac{\xi_N}{d_N}\frac{\gamma\sqrt{\widetilde{\Omega}}}{\gamma_B\sqrt{\widetilde{\Omega}} + \coth\left\{\frac{d_F}{\xi_F}\sqrt{\widetilde{\Omega}}\right\}} \tag{5.40}$$

and for z_{min} finally get

$$z_{min} = i\frac{L}{\pi\xi_N}\sqrt{\frac{\gamma\sqrt{\widetilde{\Omega}}}{\gamma_B\sqrt{\widetilde{\Omega}} + \coth\left\{\frac{d_F}{\xi_F}\sqrt{\widetilde{\Omega}}\right\}}\frac{\xi_N}{d_N} + \Omega}. \tag{5.41}$$

Note, that the imaginary parts of the roots of both groups ($z_{k,F}$, $z_{k,N}$) do not exceed their real parts. It means that inequality (5.39) guarantees the smallness of $\mathrm{Re}\, z_{min}$ compared to $\mathrm{Re}(z_{k,F}, z_{k,N})$.

Assuming further that the total contribution to I_C from the all the residues at critical points $z_{k\geq 1}$ is small compared to that at $z = z_{min}$

$$\left|\mathrm{Re}\,\frac{1}{z_{min}\sinh\pi z_{min}}\right| >> \Sigma_F + \Sigma_N, \tag{5.42}$$

$$\Sigma_{F(N)} = \left|\mathrm{Re}\sum_k \frac{1}{z_{k,F(N)}\sinh\pi z_{k,F(N)}}\right| \tag{5.43}$$

we arrive at the following expression for I_C:

$$\begin{aligned} I_C &= \frac{4\pi T}{e}\frac{W}{\gamma_{BN}^2\rho_N}\gamma\,\mathrm{Re}\sum_{\omega>0}^{\infty}\frac{G_0^2\Delta^2k^2\,(S_F+S_N)}{D^2\omega^2q\xi_N\sinh(qL)}, \\ S_F &= \frac{\xi_F^2}{\xi_N^2}\left[1+\frac{2vd_F}{\xi_F}\sinh^{-1}\frac{2vd_F}{\xi_F}\right]\frac{u^2}{v}\coth\frac{vd_F}{\xi_F}, \\ S_N &= \gamma\left[1+\frac{2ud_N}{\xi_N}\sinh^{-1}\frac{2ud_N}{\xi_N}\right]\frac{v^2}{u}\coth\frac{ud_N}{\xi_N}, \end{aligned} \tag{5.44}$$

where $u = \sqrt{\Omega - q^2\xi_N^2}$, $v = \sqrt{\widetilde{\Omega} - q^2\xi_F^2}$, and characteristic inverse coherence length q is given by

$$q = \frac{1}{\xi_N}\sqrt{\frac{\xi_N}{d_N}\frac{\gamma\sqrt{\widetilde{\Omega}}}{\gamma_B\sqrt{\widetilde{\Omega}}+\coth\left\{\frac{d_F}{\xi_F}\sqrt{\widetilde{\Omega}}\right\}}+\Omega}. \tag{5.45}$$

The coefficients k and D in (5.44) have the form

$$k = \frac{1}{u^2} - \frac{\gamma_{BN}}{\gamma_{BF}}\frac{\xi_F}{\xi_N}\frac{1}{v^2},$$

$$\begin{aligned} D = &\left(\frac{d_N}{\xi_N}+\gamma\frac{\xi_F^2}{\xi_N^2}\frac{d_F}{\xi_F}\right)\coth\frac{ud_N}{\xi_N}\coth\frac{vd_F}{\xi_F} + \\ + &\left(\gamma_B v\frac{d_N}{\xi_N}+\frac{\xi_F^2}{\xi_N^2}\frac{\gamma}{v}\right)\coth\frac{ud_N}{\xi_N} + \\ &+\left(\gamma_B u\frac{d_F}{\xi_F}\frac{\xi_F^2}{\xi_N^2}+\frac{1}{u}\right)\coth\frac{vd_F}{\xi_F} \\ + &\frac{v}{u}\left(\gamma_B+\gamma\frac{d_N}{\xi_N}\right)+\frac{\xi_F^2}{\xi_N^2}\frac{u}{v}\left(\gamma_B+\frac{d_F}{\xi_F}\right). \end{aligned} \tag{5.46}$$

From (5.39) and (5.41) it follows that the approximation (5.45) for q is valid if

$$\frac{\xi_F^2}{\eta h\xi_N^2} << \frac{d_N}{\xi_N} << \eta, \tag{5.47}$$

where

$$\eta = \begin{cases} \frac{1}{\gamma}\sqrt{\gamma_B^2+\gamma_B\sqrt{2h^{-1}}+h^{-1}}, \\ fracd_F\xi_F >> 1/\sqrt{h}, \\ \frac{1}{\gamma}\sqrt{\gamma_B^2+2\gamma_B\frac{\xi_F}{d_F}\frac{\Omega}{h^2}+\frac{\xi_F^2}{d_F^2h^2}},\ \frac{d_F}{\xi_F} << 1/\sqrt{h}. \end{cases} \tag{5.48}$$

where $h = H/\pi T_C \operatorname{sgn}\omega$. To get (5.47) we additionally restricted ourselves by considering the most interesting from practical point of view situation when

$$h >> T/T_C, \quad \xi_F << \xi_N. \tag{5.49}$$

It follows from inequalities (5.47) and (5.48) that the range of validity of expression (5.41) is the larger, the smaller is the parameter γ and thickness of F film d_F or the larger is γ_B. At $\gamma = 0$ or $\gamma_B \to \infty$ rigid boundary conditions take place at NF interface and expression (5.41) is valid for arbitrary thickness of the normal film.

From (5.42)-(5.43) it follows that in the limit of thin F and N films, $d_F/\xi_F << 1/\sqrt{h}$ and $d_N/\xi_N << 1/\sqrt{\Omega}$, the result (5.44)-(5.46) is valid if the conditions (5.47) are fulfilled.

The inequality (5.42) provides also the restriction on the thickness d_F and d_N of F and N films. Physically, it comes from the fact that with d_F (d_N) increase the full supercurrent flowing across F (N) film is enlarged proportionally to d_F (d_N). Therefore the smallness of this current component compared to contribution to I_C, which is accumulated in vicinity of FN interface, results in

$$d_F \operatorname{Re}(q) << \exp\left\{\frac{L}{\xi_F}\sqrt{h}\right\}. \tag{5.50}$$

$$d_N \operatorname{Re}(q) << \exp\left\{L\left(\frac{\sqrt{\Omega}}{\xi_N} - q\right)\right\}. \tag{5.51}$$

Finally we should take into account that the form of the boundary conditions (6.2) is valid for relatively large γ_{BN} thus providing additional restriction for application of (5.44), which sets the limit on the distance between superconducting electrodes

$$L >> \operatorname{Re}\left(\frac{1}{q}\operatorname{arctanh}\frac{1}{\gamma_{BN} q \xi_N}\right). \tag{5.52}$$

From (5.45), (5.49), (5.52) it follows that inequality (5.50) is always fulfilled for experimentally reasonable thickness of F layer and does not apply a serious restriction on the use of (5.44).

Taking into account the inequality (5.47) we can further simplify the expression for the critical current (5.44) and transform it into the formula

$$I_C = \frac{2\pi T}{e}\frac{d_N}{\xi_N}\frac{W}{\gamma_{BN}^2 \rho_N} \operatorname{Re}\sum_{\omega>0}^{\infty} \frac{G_0^2 \Delta^2}{\omega^2 q \xi_N \sinh(qL)}, \tag{5.53}$$

in which the dependence of $I_C(d_F)$ enters only via functional dependence $q(d_F)$ determined by (5.45). It is important to note that to use expression (5.53) it is enough to be in the range of parameters, which guarantees the implementation of (5.47).

Bibliography

[1] S. M. Frolov, M. J. A. Stoutimore, T. A. Crane, D. J. Van Harlingen, V. A. Oboznov, V. V. Ryazanov, A. Ruosi, C. Granata, M. Russo, Nature Physics, **4**, 32 (2008).

[2] V.I.Zdravkov, A.S.Sidorenko et al, Phys. Rev. Lett, **97**, 057004 (2006).

[3] A.S.Sidorenko, V.Zdravkov et al, Jorn. Phys. Conf. Ser., **150**, 052242 (2009).

[4] F. S. Bergeret, A. F. Volkov, and K. B. Efetov, Rev. Mod. Phys. **77**, 1321 (2005).

[5] A. F. Volkov, Ya. V. Fominov, and K. B. Efetov, Phys. Rev. B **72**, 184504 (2005); Ya. V. Fominov, A. F. Volkov, and K. B. Efetov, Phys. Rev. B **75**, 104509 (2005).

[6] T. Champel, T. Lofwander, and M. Eschrig, Phys. Rev. Lett. **100**, 077003 (2008).

[7] M. Houzet and A. I. Buzdin, Phys. Rev. B **74**, 214507 (2006).

[8] B. Crouzy, S. Tollis, D. A. Ivanov, Phys. Rev. B **76**, 134502 (2007).

[9] T. Yu. Karminskaya and M. Yu. Kupriyanov, Pis'ma Zh. Eksp. Teor. Fiz. **85**, 343 (2007) [JETP Lett. **85**, 286 (2007)].

[10] T. Yu. Karminskaya and M. Yu. Kupriyanov, Pis'ma Zh. Eksp. Teor. Fiz. **85**, 343 (2007) [JETP Lett. **86**, 61 (2007)].

[11] T. Yu. Karminskaya, M. Yu. Kupriyanov, and A. A. Golubov, Pis'ma Zh.Eksp. Teor. Fiz. **87,** 657 (2008) [JETP Lett., **87**, 570 (2008)].

[12] Ya. V. Fominov, A. A. Golubov, and M. Yu. Kupriyanov, Pis'ma Zh. Eksp. Teor. Fiz. **77**, 609 (2003) [JETP Lett. **77**, 510 (2003)].

[13] G. Nowak, H. Zabel et al, Phys. Rev. B **78**, 134520 (2008).

[14] M. Yu. Kuprianov and V. F. Lukichev, Zh. Eksp. Teor. Fiz. **94**, 139 (1988) [Sov. Phys. JETP **67**, 1163 (1988)].

[15] L. Usadel, Phys. Rev. Lett. **25**, 507 (1970).

[16] K. K. Likharev, Rev. Mod. Phys. **51**, 101 (1979).

[17] A. A. Golubov, M. Yu. Kupriyanov, and E. Il'ichev, Rev. Mod. Phys. **76**, 411 (2004).

[18] A. I. Buzdin, Rev. Mod. Phys. **77**, 935 (2005).

[19] J. Bass and W. P Pratt Jr, J. Phys.: Condens. Matter **19**, 183201 (2007).

Chapter 6

Josephson effect in superconductor/ferromagnet structures with different geometries

Introduction

Among the most appealing recent experimental results are: the first observation of double suppression of superconductivity in Nb/Cu_xNi_{1-x} bilayers ($x = 0.59$), which provides evidence for a multiple reentrant superconducting state [4]; the demonstration of existence of a long-range proximity effect predicted in [3] in Nb-Cu/PdNi/Cu/CoReCo/Cu/PdNi/Cu-Nb Josephson junctions, where the direction of magnetization vector in antiferromagnetically oriented CoReCo block does not coincide with that of PdNi films, thus creating a weak link region with artificially rotated magnetization vector [5]; the first observation [6] of strong critical temperature suppression in S-FNF structures under a small off-orientation of magnetization vectors in initially antiferromagnetically ordered FNF block, which is a sequent of generation of long-range triplet component providing a strong connection of NF part of the multilayer to the S film [12]; visualization of supercurrent spatial distribution in SIFS devices with various arrangements of 0 and π segments [7].

Despite of noticeable achievement in understanding of the physical background of superconducting spin valves, in which either critical temperature T_C or critical current I_C is controlled by mutual off-orientation of magnetization vectors $\mathbf{M}_{1,2}$ of individual F films located inside of a spin valve, they are still far from practical realization. Among the reasons are relatively large values of exchange energies H in F films resulting in very fast decay of superconducting correlations into a ferromagnet [13], [14], as well as the problems in supply of off-orientation of $\mathbf{M}_{1,2}$ in Josephson spin valves.

Recently [8] - [11] it has been shown that both problems can be effectively solved in novel types of S-FN-S and S-FNF-S Josephson junctions. In these structures the weak link region consists of FN or FNF multilayer which separates the superconducting banks, while a supercurrent flows in the direction parallel to FN interfaces and is injected across

the end-walls of FN or FNF structure. There are two kinds of proximity effects in these junctions. The first one is the penetration of superconductivity into normal metal from superconducting electrodes. The second one is the suppression of the induced superconductivity due to interaction between N and F layers. It is obvious that for nontransparent NF interfaces the S-FNF-S junction should have the same characteristics as that of SNS devices and the decay length of superconducting correlations into the complex weak link region should coincide with that for the normal metal, ξ_N, if the distance between superconducting electrodes L are larger than the scale ξ_{F1} of superconductivity decay into F films. In [8]- [11] it was also shown that switching on interaction between N and F metals results in generation of a set of decay lengths. Moreover, it was demonstrated that it is possible to find the conditions under which at least one among these lengths has both real and imaginary parts of the order of ξ_N. In S-FNF-S Josephson devices there is no limitation on thickness of N film and it can be made thin enough to realize an effective control upon the junction parameters by changing the mutual orientation of magnetization vectors of ferromagnetic films [10].

The choice of junction geometry considered in [8]- [11] was based on existing concept [15], [16], that in such ramp type configuration the critical current I_C is larger than in overlap geometry, when S electrodes are located on the top of weak link multilayer. In this paper Chapter this statement is reconsidered andit is demonstrated that it valid only for the fully transparent interfaces between S electrodes and a weak link region. Three different geometries of Josephson junctions: (1) SN-NF-NS devices which consist of two SN complex electrodes connected by NF weak region; (2) SNF-N-FNS structures, in which N film connects two SNF complex electrodes and (3) SNF-NF-FNS junctions with S electrodes located on the top of FN bilayer are studied. Critical currents of these Josephson structures in the framework of linearized Usadel equations for arbitrary length of complex electrodes will be discussed and then it will be compared with the results for the above three cases and those obtained in [8] - [11] in order to determine the geometry which provides the largest magnitude of the critical current. Also in this Chapter it will be demonstrated that 0-π transition in the considered structures can be driven not only by variation of distance L between S electrodes, as predicted by known models, but also by changing the length d of the SNF overlap region.

6.1 New geometry of SFNS junctions

Consider multilayered structures presented in Fig.1 and Fig.2. They consist of superconducting electrodes with the length d deposited on the top either a single N film or on NF bilayer. The bilayer consists of ferromagnetic (F) and normal metal (N) films having a thickness d_F, and d_N respectively (see Fig.6.2). The junctions shown in Fig.6.1b and Fig.6.2d are the structures having ramp type geometry intensively studied previously (see [1] - [3], [15] and [8] - [11]). The width of layers in the direction perpendicular to the current flow is equal to W and the distance between electrodes is L. For simplicity it is suggested below that the parameters γ_{BN} and γ_{BF} which characterize the transparency of NS and FS interfaces are large enough to neglect the suppression of superconductivity in S part of the proximity system.

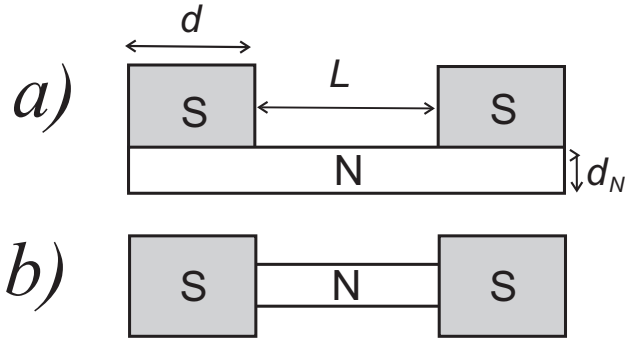

Figure 6.1. a) $SN-N-NS$ junction, b) the SNS junction.

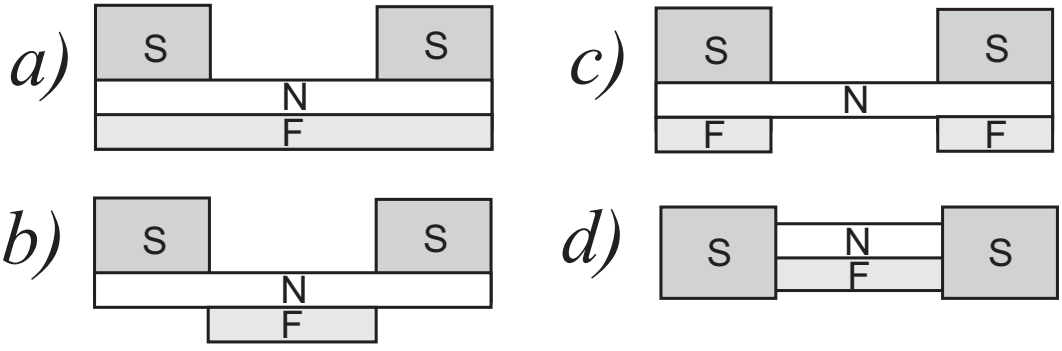

Figure 6.2. a) $SNF-NF-FNS$ junction, b) the $SN-NF-NS$ junction, c) the $SNF-N-FNS$ junction, d) the $S-NF-S$ junction.

Under the above conditions for dirty limit the problem of calculation of the critical current in the structures reduces to solution of the set of linearized Usadel equations [1]

- [3], [17]

$$\xi_N^2\left\{\frac{\partial^2}{\partial x^2}+\frac{\partial^2}{\partial y^2}\right\}\Phi_N-\Omega\Phi_N=0,$$
$$\xi_F^2\left\{\frac{\partial^2}{\partial x^2}+\frac{\partial^2}{\partial y^2}\right\}\Phi_F-\tilde{\Omega}\Phi_F=0, \tag{6.1}$$

where $\Omega=|\omega|/\pi T_c, \widetilde{\Omega}=(|\omega|+iHsign(\omega))/\pi T_c$, $\xi_{N,F}^2=(D_{N,F}/2\pi T_c)$, $D_{N,F}$, are diffusion coefficients, $\omega=\pi T(2n+1)$ are Matsubara frequencies, H, is exchange integral of ferromagnetic material. The x and y axis have been chosen in the directions perpendicular and parallel to the plane of N film and put the origin in the middle of structure at FN interface (Fig.6.2a,b,d) or at the lower free interface of N film (Fig.6.1, Fig.6.2c).

Equations (6.1) must be supplemented by the boundary conditions [18]. For the structures presented in Fig.6.1b, Fig.6.2d they have the form

$$\gamma_{BN}\xi_N\frac{\partial}{\partial y}\Phi_N=\pm G_0\Delta\exp\left\{\pm i\frac{\varphi}{2}\right\},\ y=\pm L/2,$$
$$\gamma_{BF}\xi_F\frac{\partial}{\partial y}\Phi_F=\pm G_0\Delta\exp\left\{\pm i\frac{\varphi}{2}\right\},\ y=\pm L/2, \tag{6.2}$$

while for the junctions presented in Fig.6.1a and Fig.6.2a,b,c they can be written as

$$\gamma_{BN}\xi_N\frac{\partial}{\partial x}\Phi_N=G_0\Delta\exp\left\{\pm i\frac{\varphi}{2}\right\},\ x=d_N. \tag{6.3}$$

At SF interfaces (see Fig.6.2d) we also have

$$\gamma_{BF}\xi_F\frac{\partial}{\partial y}\Phi_F=\pm\frac{\widetilde{\Omega}}{\Omega}G_0\Delta\exp\left\{\pm i\frac{\varphi}{2}\right\},\ y=\pm L/2. \tag{6.4}$$

Here L is the distance between superconducting electrodes, $G_0=\omega/\sqrt{\omega^2+\Delta^2}$, Δ is the modulus of the order parameter of superconducting electrodes.

At the FN interface located at $(x=0)$ the boundary conditions have the form [18]

$$\frac{\xi_N}{\Omega}\frac{\partial}{\partial x}\Phi_N=\gamma\frac{\xi_F}{\widetilde{\Omega}}\frac{\partial}{\partial x}\Phi_F, \tag{6.5}$$
$$\gamma_B\xi_F\frac{\partial}{\partial x}\Phi_F+\Phi_F=\frac{\widetilde{\Omega}}{\Omega}\Phi_N, \tag{6.6}$$

where $\gamma_B=R_{B3}\mathcal{A}_{B3}/\rho_F\xi_F,\quad \gamma=\rho_N\xi_N/\rho_F\xi_F$, R_{B3} and $\mathcal{A}_{B3}$ are the resistance and area of the NF interface.

The boundary conditions at free interfaces come from the demand of an absence a current across them and reduce to equality to zero of appropriate derivatives, e.g. for the junction presented in Fig.6.2d they look as

$$\frac{\partial}{\partial x}\Phi_N = 0,\ x=d_N, \tag{6.7}$$
$$\frac{\partial}{\partial x}\Phi_F = 0,\ x=-d_F. \tag{6.8}$$

The formulated above boundary problems can be reduce from two-demensional to one-dimensional in the limit of small thicknesses of N and F films

$$d_N \ll \xi_N, \quad d_F \ll \xi_F. \tag{6.9}$$

This procedure have been described in detail in [8] - [10], and the range of its validity has been examined in [11]. Below we will apply the developed in [8] - [10] approach to the junctions presented in Fig.6.1, Fig.6.2 mostly being concentrated on the discussion of the obtained results. The details of calculations are summarized in Appendix.

6.2 Critical current of SN-N-NS Josephson junction

The expressions for the critical currents, I_C^{SNS}, $I_C^{SN-N-NS}$, of SNS junction shown in Fig.6.1 are well known in the considered model [1]. They have the form

$$I_C^{SNS} = K\frac{d_N}{\xi_N}\sum_{n=0}^{\infty}\frac{\Gamma}{q\sinh(qL)}, \tag{6.10}$$

$$I_C^{SN-N-NS} = \frac{K}{\xi_N d_N}\sum_{n=0}^{\infty}\frac{\Gamma\sinh^2(qd)}{q^3\sinh(q(L+2d))}, \tag{6.11}$$

where coefficient $K = (2\pi TW)/(R_{BN}\mathcal{A}_{BN}\gamma_{BN}e)$, $q = \xi_N^{-1}\sqrt{\Omega}$ is inverse decay length and $\Gamma = \Delta^2/(\omega^2+\Delta^2)$.

As it is shown in Appendices **A-C** expression (6.11) is also followed from the more general formula for critical current of SNF-NF-SNF devices shown in Fig.6.2a in the limit of small thickness of F film ($d_F \to 0$).

The ratio of these two critical currents, $I_C^{SN-N-NS}/I_C^{SNS}$, is visualized in Fig.6.3 as a function of thickness of normal layer, d_N, for several lengths of complex electrode $d/\xi_N = 0.5, 1, 10$. It is clearly seen that there are intervals of parameters under which critical current of SN-N-NS junction can essentially exceed of I_C^{SNS}. The physics of this effect is evident.

In the considered limit of small SN interfaces transparency for ramp type geometry (Fig.6.1a) under condition $L >> 1/q$ the magnitude of induced into N metal Φ_N functions at SN interfaces is close to

$$\Phi_N(d_N) = \frac{G_0\Delta}{\gamma_{BN}\xi_N q}, \quad \gamma_{BN}\xi_N q >> 1, \tag{6.12}$$

while in the case of overlap geometry (Fig.6.1b) for $d_N << 1/q$ magnitude of Φ_N functions induced into N metal is in the first approximation on d_N/ξ_N independent on coordinate x

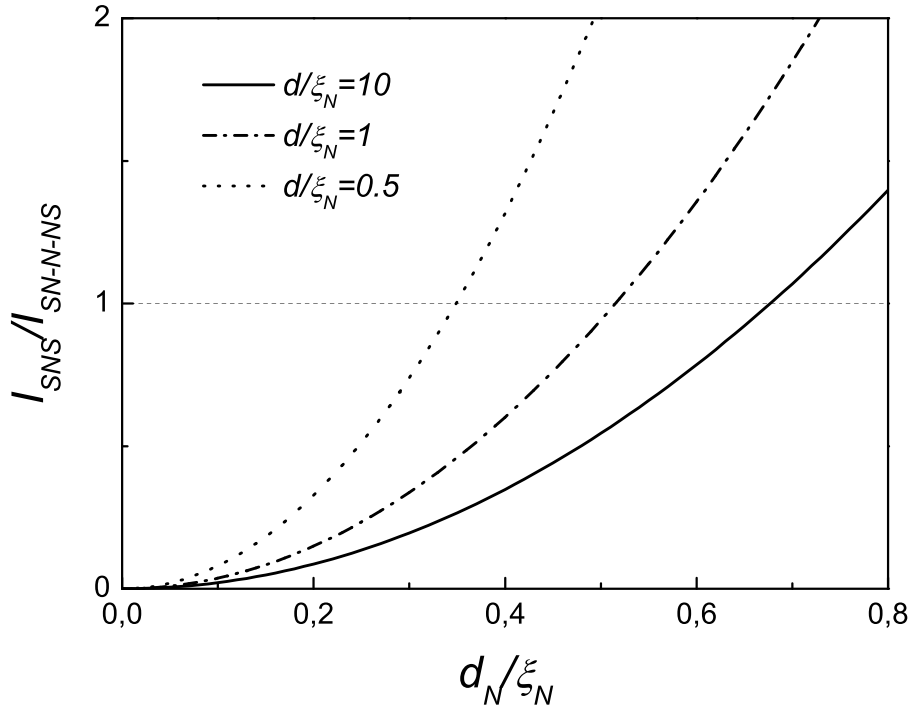

Figure 6.3. $I_C^{SN-N-NS}/I_C^{SNS}$ versus thickness of N film d_N/ξ_N for $d/\xi_N = 0.5, 1, 10, L/\xi_N = 2$, $T/T_C = 0.5$.

and is equal to

$$\Phi_N(d_N) = \frac{G_0\Delta}{\gamma_{BN}\xi_N q^2 d_N}, \quad \gamma_{BN}\xi_N q^2 d_N >> 1. \tag{6.13}$$

From (6.12), (6.13) it immediately follows that the large factor γ_{BN} in (6.13) can be renormalized by a small ratio of d_N/ξ_N thus leading to effective increase of superconductivity at the interface between the N film and SN composite electrode compare to the strength of superconducting correlations at SN boundary of SNS ramp type devices.

6.3 Critical current of devices with F film in weal link region

To calculate the critical current of the junctions shown in Fig.6.2 under conditions (6.9) one have to solve the boundary problem (6.1) - (6.7) and substitute the obtained solution into general formula for supercurrent:

$$\begin{aligned} I_S &= \frac{-i\pi TW}{e\rho_F}\sum_{\omega=-\infty}^{\infty}\frac{1}{\widetilde{\omega}^2}\int_{-d_F}^{0}\left[\Phi^*_{-\omega,F}\frac{\partial}{\partial y}\Phi_{\omega,F}\right] - \\ &\quad -\frac{i\pi TW}{e\rho_N}\sum_{\omega=-\infty}^{\infty}\frac{1}{\omega^2}\int_{0}^{d_N}\left[\Phi^*_{-\omega,N}\frac{\partial}{\partial y}\Phi_{\omega,N}\right]. \end{aligned} \tag{6.14}$$

The details of this procedure are allocated in Appendix.

It is shown there that in the practically interesting limit of strong N film

$$\zeta_N >> \zeta_F, \quad \xi_N >> \xi_F. \tag{6.15}$$

the critical current of SNF-NF-FNS (Fig.6.2a), SN-NF-NS (Fig. 6.2b) and SNF-N-FNS (Fig. 6.2c) structures

$$I_C^{SNF-NF-FNS} = \frac{K}{\xi_N d_N} \mathrm{Re} \sum_{n=0}^{\infty} \frac{\Gamma U q_1 \sinh^2(q_1 d)}{\sinh(q_1(L+2d))}, \tag{6.16}$$

$$I_C^{SN-NF-NS} = \frac{K}{\xi_N d_N} \mathrm{Re} \sum_{n=0}^{\infty} \frac{\Gamma q_1}{q^4 (Q_{q,q_1} + P_{q,q_1})}, \tag{6.17}$$

$$I_C^{SNF-N-FNS} = \frac{K}{\xi_N d_N} \mathrm{Re} \sum_{n=0}^{\infty} \frac{\Gamma U q}{Q_{q_1,q} + P_{q_1,q}} \tag{6.18}$$

can be expressed by formulas (6.16), (6.17) and (6.18), respectively. Here functions $Q(\alpha, \beta)$, $P(\alpha, \beta)$, and U are defined as

$$Q_{a,b} = \frac{2 \coth(ad) \cosh(bL)\, b}{a}, \tag{6.19}$$

$$P_{a,b} = \sinh(bL) \left(1 + \frac{b^2 \coth^2(ad)}{a^2}\right), \tag{6.20}$$

$$U = \left(\frac{v^2 \zeta_F^2 \zeta_N^2}{1 - v^2 u^2 \zeta_F^2 \zeta_N^2}\right)^2, \tag{6.21}$$

where q_1 is fundamental wave vector of the problem:

$$q_1^2 = \frac{1}{2}[u^2 + v^2 - \sqrt{(u^2 - v^2)^2 + 4\zeta_F^{-2}\zeta_N^{-2}}], \tag{6.22}$$

while u and v

$$u^2 = \left(\frac{1}{\zeta_N^2} + \frac{\Omega}{\xi_N^2}\right), \quad v^2 = \left(\frac{1}{\zeta_F^2} + \frac{\Omega}{\xi_F^2} + i\frac{h}{\xi_F^2}\right), \tag{6.23}$$

are partial wave vectors. The parameters ζ_F and ζ_N are the coupling constants $\zeta_F^2 = \gamma_B d_F \xi_F$, $\zeta_N^2 = \gamma_B d_N \xi_N / \gamma$, which describe the mutual influence of N and F films on superconducting correlations in the junction.

Strictly speaking the formulas (6.16), (6.17), (6.18) are valid in the limit of thin N and F films (6.9). However making use of the formalism developed in [11] it is possible to prove that all of them can be also valid for arbitrary thickness of F film if one simply use in (6.16), (6.17), (6.18) the more general expression for fundamental wave vector q_1, namely

$$q_1 = \frac{1}{\xi_N} \sqrt{\frac{\xi_N}{d_N} \frac{\gamma \sqrt{\widetilde{\Omega}}}{\gamma_B \sqrt{\widetilde{\Omega}} + \coth\left\{\frac{d_F}{\xi_F}\sqrt{\widetilde{\Omega}}\right\}} + \Omega}. \tag{6.24}$$

Expressions (6.16), (6.17), (6.18) can be simplified in several practically interesting cases.

In the limit of large d ($d >> 1/q, 1/q_1$) both $\coth(qd) \to 1$ and $\coth(q_1 d) \to 1$. As a result for SN-NF-NS and SNF-N-NFS junctions one may use the same formulas (6.17), (6.18) with more simple forms of functions $Q(\alpha, \beta)$ and $P(\alpha, \beta)$

$$Q_{a,b} = \frac{2\cosh(bL)\, b}{a}, \tag{6.25}$$

$$P_{a,b} = \sinh(bL)\left(1 + \frac{b^2}{a^2}\right), \tag{6.26}$$

while for SNF-NF-FNS junction

$$I_C^{SNF-NF-FNS} = \frac{1}{2}\frac{K}{\xi_N d_N}\,\mathrm{Re}\sum_{n=0}^{\infty}\Gamma U q_1 \exp(-q_1 L). \tag{6.27}$$

In the limit of large distance L between S electrodes, $L >> 1/q, 1/q_1$ the main contribution to the sums in (6.16), (6.17), (6.18) comes from the first item and for the critical current of SNF-NF-FNS, SN-NF-NS and SNF-N-NFS one can get, respectively:

$$I_C^{SNF-NF-FNS} = \frac{2K}{\xi_N d_N}\,\mathrm{Re}\sum_{n=0}^{\infty}\frac{\Gamma U q_1 \exp(-q_1 L)}{(1+\coth(qd))^2} \tag{6.28}$$

$$I_C^{SN-NF-NS} = \frac{2K}{\xi_N d_N}\,\mathrm{Re}\sum_{n=0}^{\infty}\frac{\Gamma q_1 \exp(-q_1 L)}{q^2\,(q + q_1\coth(qd))^2}, \tag{6.29}$$

$$I_C^{SNF-N-FNS} = \frac{2K}{\xi_N d_N}\,\mathrm{Re}\sum_{n=0}^{\infty}\frac{\Gamma U q q_1^2 \exp(-qL)}{(q_1 + q\coth(q_1 d))^2}. \tag{6.30}$$

Below the obtained results (6.16), (6.17), (6.18) will be compared with the the value of the critical current calculated in [8] for ramp type SFNS junction

$$I_C^{SFNS} = K\frac{d_N}{\xi_N}\,\mathrm{Re}\sum_{n=0}^{\infty}\Gamma\frac{(1 - \frac{1}{q_1^2 - v^2}\frac{\gamma_{BN}}{\gamma_{BF}}\frac{\xi_N}{\xi_F\zeta_N^2})^2}{q_1\sinh(q_1 L)}. \tag{6.31}$$

It is necessary to mention that in the limit of decoupled F and N films ($\gamma_B \to \infty$) expressions for the critical currents (6.16, 6.17, 6.18) reduce to the formula for SN-N-NS devices (6.11), while the critical current of SFNS ramp type structure (6.31) transforms to that (6.10) valid for SNS junctions.

Fig.6.4-Fig.6.9 show the phase diagrams for critical current, which in (L/ξ_N,d/ξ_N) plane gives the information about the sign of I_c. In the areas marked in Fig.6.4-Fig. 6.9 by 0 and π the critical current is positive (0-state) and negative (π-state), correspondingly, while the lines give the point curves at which $I_c = 0$. The position of these curves in (L/ξ_N,d/ξ_N) plane also depends on relative thickness (d_F/ξ_F and d_N/ξ_N) of both F and N films.

The phase diagrams for SNF-N-FNS structures are given in Fig.6.4 and Fig.6.5. In this geometry there is the only N film in the region between SNF multilayers. The inverse coherence length $q = \xi_N^{-1}\sqrt{\Omega}$ in N film is real, therefore there are no oscillations of critical current in the structure.

The calculations show that in this case there can be only one curve on the (L/ξ_N, d/ξ_N) plane, at which $I_c = 0$ for fixed other parameters. The existence of only one point curve for SNF-N-FNS structure can be understood from the following argumentations. Contrary to well studied SFS junctions the coherence length in the part of weak link region of SNF-N-FNS devices located between SNF electrodes is real, thus preventing the oscillations of function Φ_N in that region of the N film. The oscillations of condensate function exist only in the NF part of weak link located under the S electrodes. Obviously, under these circumstances the sign of I_c must be only controlled by value of condensate function at the boundary between the SNF electrodes and the N film connecting them. This value of condensate function determines two complex coefficients, A_1, and, A_2, (see (6.58) and (6.59)). In combination with nonoscillatory decay of $\Phi_N$function into the N film from the SNF electrodes these coefficients provide only two choices for the sign of I_c and only one curve at which $I_c = 0$. This is in contrust to SFS devices with F film in between of S - electrodes. In the latter case the sign of I_c depends also on relation between the geometrical size of a junction and the imaginary part of the coherence length (the period of oscillations of the order parameter). It is combination of these two factors that provides the opportunity to have multiple changes of I_c sign and infinite number of curves at (L/ξ_N,d/ξ_N) plane at which $I_c = 0$.

Therefore in the considered SNF-N-FNS structures there is only one of these two factors and only one opportunity for I_c to change its sign, which can be realized or not depending on the parameters of the structure.

The position of the transition curve calculated for fixed ratio $d_N/\xi_N = 0.1$ and several values of $d_F/\xi_F = 0.04, 0.1, 0.2$ is show in Fig.6.4. The location of the curve depends on d_F by nonmonotonic way. At $d_F = 0$ there is only 0-state in the structure. With the increase of d_F, the curve first shifts to the left bottom corner of the phase diagram, then it turns back and at some critical value of d_F it tends to infinity, thus providing only 0-state in the structure with further d_F increase. Such nonmonotonic behavior is due to nonmonotonic behavior of q_1 from (6.24).

Figure 6.5 shows (L/ξ_N,d/ξ_N) phase diagram calculated for fixed ratio $d_F/\xi_F = 0.1$

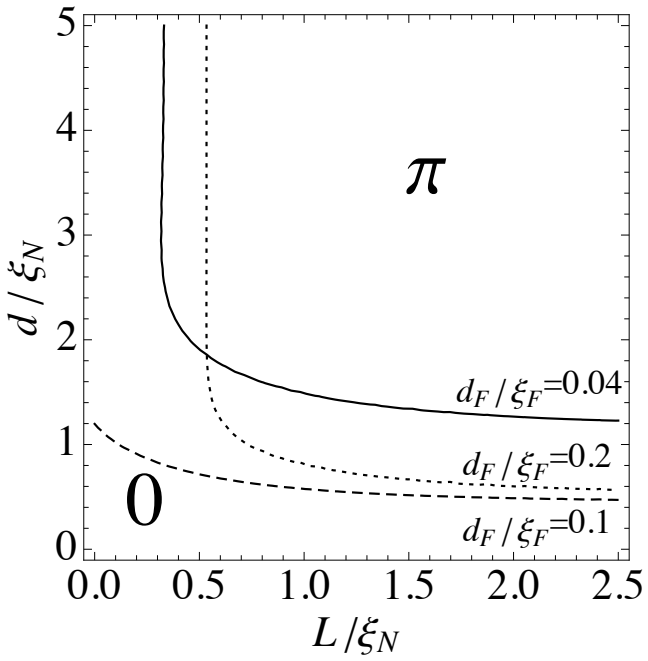

Figure 6.4. (L/ξ_N,d/ξ_N) phase diagram for SNF-N-FNS structure for $d_F/\xi_F = 0.04, 0.1, 0.2$ (solid, dashed, dotted lines) at $\gamma = 0.1$, $\gamma_B = 0.1$, $d_N/\xi_N = 0.1$, $\xi_N/\xi_F = 10$, $T/T_C = 0.5$, $H/\pi T_C = 30$.

and several values of $d_N/\xi_N = 0.05, 0.1, 0.2$. It is seen that with d_N increase the point curves at which $I_c = 0$ shifts in the direction to the right corner of diagram providing the increase of area for 0 state. This fact can be understood if one takes into account that under fixed d_F the lager is N layer thickness the smaller is the influence of the F layer on the junction properties. It is obvious that at $d_N \gtrsim \xi_N$ the critical current of SNF-N-FNS junction will tends to that of SN-N-NS since the current will flow in the areas located closer to S electrodes thus decreasing the probability to have SNF-N-FNS structure in the π state. Also it is important to mention that at some fixed parameters only 0-state or π-state can be realized for any L, and at some fixed parameters only 0-state can be realized for any d.

The phase diagrams for SN-FN-NS structures are given in Fig.6.6 and Fig.6.7. Figure 6.6 presents the data calculated under fixed value of $d_N/\xi_N = 0.1$ for a set of ratio $d_F/\xi_F = 0.08, 0.1, 0.2$, while Fig.6.7 gives diagram obtained under fixed value of $d_F/\xi_F = 0.1$ for a set of parameters $d_N/\xi_N = 0.08, 0.1, 0.15$. In this geometry there is the only N film in the complex SN electrodes. The inverse coherence length q in N film is real value. Consequently both 0 and π-states in SN-FN-NS junctions can be realized due oscillatory behavior of superconducting correlations in NF region inside the weak link area, which connects SN electrodes. So there are infinite number of point curves. The point curves at which $I_c = 0$ looks like practically vertical lines thus demonstrating weak influence of overlap distance d

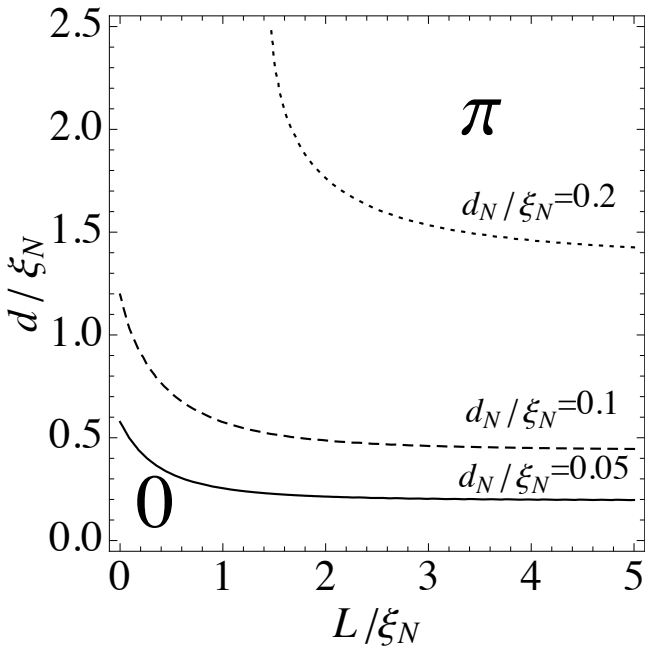

Figure 6.5. (L/ξ_N,d/ξ_N) phase diagram for SNF-N-FNS structure for $d_N/\xi_N = 0.05, 0.1, 0.2$ (solid, dashed, dotted lines) at $\gamma = 0.1$, $\gamma_B = 0.1$, $d_F/\xi_F = 0.1$, $\xi_N/\xi_F = 10$, $T/T_C = 0.5$, $H/\pi T_C = 30$.

on alternation of 0 and π states in the junction.

Finally, Fig. 6.8, Fig. 6.9 give (L/ξ_N,d/ξ_N) phase diagrams for SNF-FN-FNS junctions. In these structures coherence lengths are complex both under superconductor in complex SNF electrodes and in NF part of weak link region. The appearance of 0 or π state in this case depends also on matching these oscillations at SNF/NF boundary. As a result the point curves at which $I_c = 0$ are not as vertical as them one can see in Fig. 6.6, Fig. 6.7 thus demonstrating their strong dependence on both lengths L/ξ_N and d, and the $0-\pi$ transition with d increase is not so sensetiv to L variations as for SN-FN-NS structure.

Fig. 6.10 shows dependence of absolute value of normalized critical currents of SNF-NF-FNS, SNF-N-FNS, SN-NF-NS and SFNS junctions as a function of L/ξ_N for infinite length of SN interface d. It is seen that at given magnitude of L/ξ_N critical current of SN-N-NS junction, $I_C^{SN-N-NS}$, has the maximum value among all others. This fact is obvious since in this structure there is no additional suppression of superconductivity provided by the F film. If we compare the value of I_C far from the 0 - π transition points for all other considered structures, then we may have $I_C^{SN-FN-NS} > I_C^{SNF-N-FNS} > I_C^{SNF-FN-FNS} > I_C^{S-FN-S}$. This sequence of values are due to consecutive increase of suppression of superconductivity provided by F film.

In SN-FN-NS junctions in the considered region of parameters the superconducting correlations are suppressed by F film only in weak link region, thus providing the large

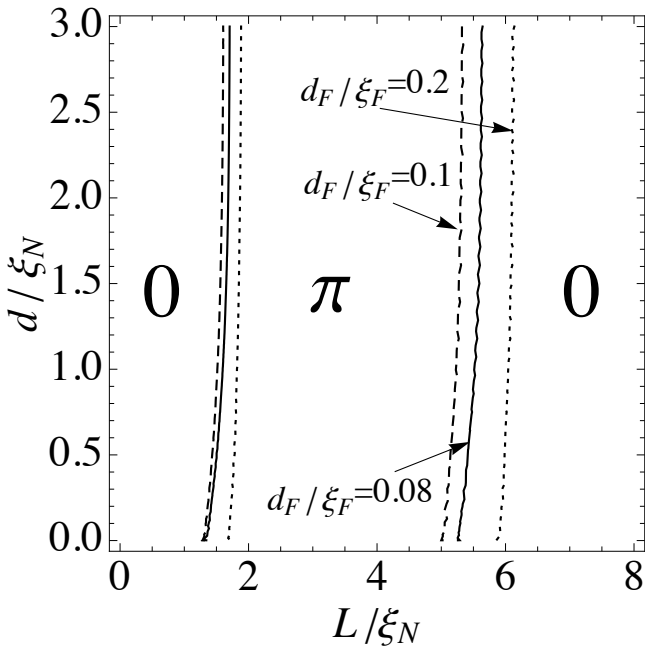

Figure 6.6. (L/ξ_N,d/ξ_N) phase diagram for SN-FN-NS structure for $d_F/\xi_F = 0.08, 0.1, 0.2$ (solid, dashed, dotted lines) at $\gamma = 0.1$, $\gamma_B = 0.1$, $d_N/\xi_N = 0.1$, $\xi_N/\xi_F = 10$, $T/T_C = 0.5$, $H/\pi T_C = 30$.

value of I_C. In SNF-N-FNS junctions the critical current is smaller than in SN-FN-NS devices due to suppression of superconductivity in SNF part of the structure. Due to it the decay of superconducting correlations into N part of weak link starts from the values, which are smaller than in SN-FN-NS devices.In SNF-FN-FNS devices there is suppression of superconductivity in all parts of structure by F film. Finally in SNFS ramp type structures the critical current has the smallest value. In SN-N-NS and SNF-N-FNS junctions I_C decays with L without oscillations. However as it follows from the phase diagram presented in Fig. 6.4, under the chosen set of parameters the SNF-N-FNS structure is the π state, so that its critical current is negative, while SN-N-NS is always in 0-state.

The decay length in NF part of SN-FN-NS, SNF-FN-FNS and SNFS devices is complex providing damping oscillations of I_C as a function of L. The period of these oscillations and their decay length are the same for all the junctions and controlled by bulk properties of NF part of weak link. The initial conditions for these oscillations at SN/NF, SNF/FN and S/NF interfaces are different resulting in shift of the oscillations along L axis.

Figure 6.11 shows the amplitude of critical current of SNF-FN-FNS, SN-FN-NS, SNF-N-FNS structures versus the length of SN interface in complex electrodes calculated under fixed ratio of $L/\xi_N = 2$.

From the presented curves it follows that critical currents have a tendency to increase with d as $\tanh^2(d/\xi_N)$, while at large d they arrive at independent on d values.

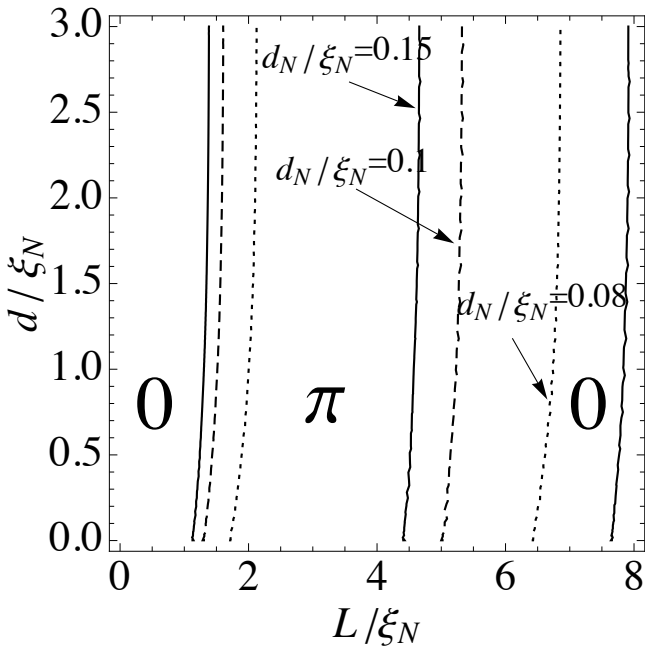

Figure 6.7. (L/ξ_N,d/ξ_N) phase diagram for SN-FN-NS structure for $d_N/\xi_N = 0.08, 0.1, 0.15$ (solid, dashed, dotted lines) at $\gamma = 0.1$, $\gamma_B = 0.1$, $d_F/\xi_F = 0.1$, $\xi_N/\xi_F = 10$, $T/T_C = 0.5$, $H/\pi T_C = 30$.

The continuous support of superconductivity from the S electrodes along all the SN interfaces results in considerable difference between $I_C(L)$ and $I_C(d)$ dependencies. The last may have only one sign change of I_C as a function of d.

It is also necessary to note that maximum of I_C in $I_C(d)$ dependence maybe not necessarily achieved in the limit of $d \to \infty$. For instance, at $d_N/\xi_N = 0.2$ and $d/\xi_N = 0.5$ (see Fig. 6.11c) the magnitude of I_C is fifty times larger compared to the value, which is reached at $d \to \infty$. This strong enhancement may be important for practical applications of these structures.

6.4 Conclusion

In this Chapter three types of SFNS Josephson junctions with different geometries of electrodes (S electrodes are on the top of N film) and weak links are considered. Analytical expressions for critical currents of these structures were derived. These expressions are valid in the limit of thin normal and ferromagnetic films, hence one can use expressions for critical currents with more accurate formula for inverse coherence length (6.24) for films with arbitrary thickness.

The ramp type junctions are not absolutely favorable both from technological and applicable points of view, critical current I_C of SN-NF-NS, SNF-NF-NFS or SNF-N-NFS

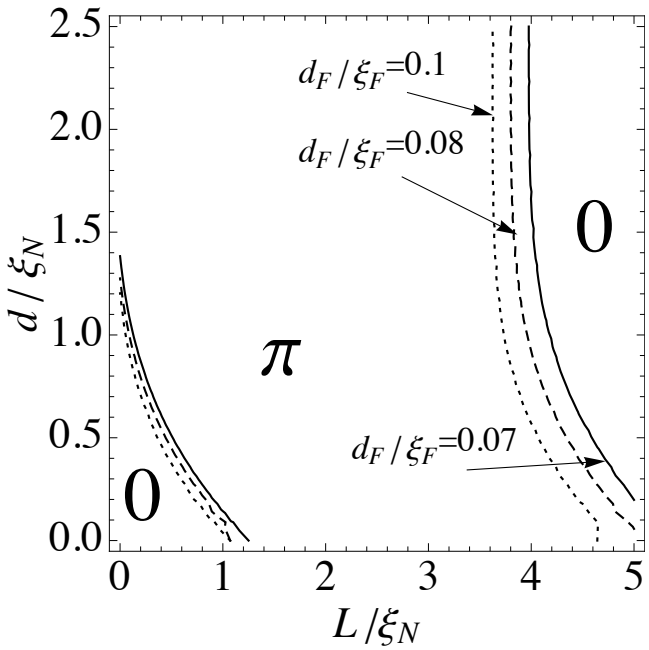

Figure 6.8. $(L/\xi_N, d/\xi_N)$ phase diagram for SNF-FN-FNS structure for $d_F/\xi_F = 0.07, 0.08, 0.1$ (solid, dashed, dotted lines) at $\gamma = 0.1$, $\gamma_B = 0.1$, $d_N/\xi_N = 0.1$, $\xi_N/\xi_F = 10$, $T/T_C = 0.5$, $H/\pi T_C = 30$.

junctions can be even large compared to that in the ramp type structures under the same suppression parameters at NS interface and distance between S electrodes. The largest value of critical current can be achieved in SN-NF-NS junction in which there are no additional suppression from F film under S electrode.

In such structures $0-\pi$ transition takes place not only under increase of the distance between the superconducting electrodes, but also as a result of the length change of the area of Cooper pair injection under the S electrodes. Hence there is single transition compared to multiple transitions with the increase of L. In SNF-N-FNS structures, in which coherence length of weak link is not complex, the critical current can change sign as a function of distance between superconducting electrodes.

In ramp type devices the weak link area is determined by geometrical factors, namely by the distance L between superconducting electrodes. Under conditions, which minimizes suppression of superconductivity in the S electrodes, the initial values of anomalous Green's function at SN and SF interfaces are strongly fixed by the boundary conditions and transition from 0 to π states in $I_C(L)$ dependence is a result of interplay between the complex value of decay length into NF bilayer and its geometrical size L.

In the structures presented in Fig.6.2 a,b,c under the same quality of SN interfaces, the area of the weak link may not coincide with the distance between superconducting banks since suppression of superconductivity induced into NF bilayer can occur due to

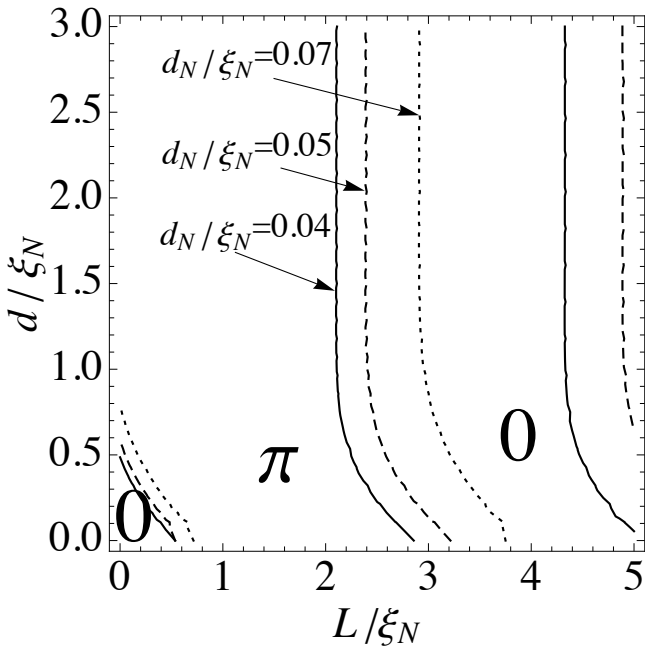

Figure 6.9. $(L/\xi_N, d/\xi_N)$ phase diagram for SNF-FN-FNS structure for $d_N/\xi_N = 0.04, 0.05, 0.07$ (solid, dashed, dotted lines) at $\gamma = 0.1$, $\gamma_B = 0.1$, $d_F/\xi_F = 0.1$, $\xi_N/\xi_F = 10$, $T/T_C = 0.5$, $H/\pi T_C = 30$.

proximity effect between this bilayer and the part of weak link which is not covered by a superconductor. It means that the boundary conditions at SNF/NF interfaces are soft and do not fix the initial conditions for $I_C(L)$ dependence thus providing additional degree of freedom responsible for 0 to π transition in the considered structures. This feature is most clearly revealed in SNF-N-FNS junctions. In these devices the decay length in the part of N film located between SNF electrodes is a real quantity, which prevents the oscillations of function Φ_N in that region of the N film. However, 0 to π transition may take place in these structures under a change of their transport parameters despite of the absence of oscillations of function Φ_N in the area between SNF electrodes. It is worth to mention that in the last case there is a possibility for only a single 0 to π transition. From practical point of view it means that making use of SNF-N-FNS geometry provides an opportunity to fabricate a junction definitely in the π state keeping simultaneously large value of its critical current.

The second important conclusion of this consideration is demonstrated in Fig. 6.10 . One can see that the absolute values of the critical current of the considered devices exceed those in SNFS ramp-type junctions. This difference comes from the fact that in ramp-type configuration superconducting correlations are induced directly into the interelectrode coupling area through the cross section of N and F films. In the considered limit of small SN interface transparency this results in small values of superconducting correlations (on

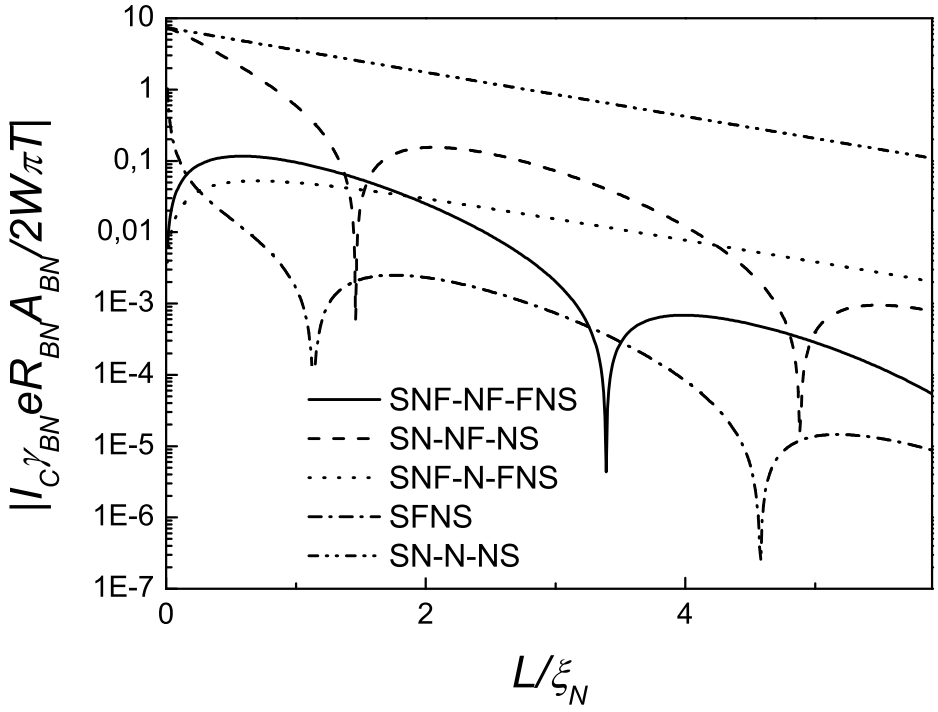

Figure 6.10. I_C for SN-N-NS, SFNS, SNF-N-FNS, SN-FN-NS, SNF-FN-FNS structures versus L/ξ_N calculated for $\xi_N/\xi_F = 10$, $T/T_C = 0.5$, $H/\pi T_C = 30$, $d_N/\xi_N = 0.1$, $d_F/\xi_F = 0.1$.

the order of Δ/γ_{BN}) induced in the vicinity of S/N interface. Contrary to that, in the overlap geometry the superconducting correlations induced into the area located under S electrode can be large enough, on the order of $\Delta/(\gamma_{BN}d_N/\xi_N)$ if d_N is considerably smaller than ξ_N.

6.5 Appendix

6.5.1 Calculation of supercurrent for SNF-NF-FNS junction.

To calculate critical current of SNF-NF-FNS Josephson junction in the framework of formulated model it is enough to solve linearized Usedel equations for condensate functions of normal (Φ_N) and ferromagnetic (Φ_F) films in weak link region, as well as for condensate functions in N films under left (Φ_{N1}) and right (Φ_{N2}) superconducting electrodes. These equations have the form

$$\begin{aligned} \xi_N^2 \left\{ \frac{\partial^2}{\partial x^2} + \frac{\partial^2}{\partial y^2} \right\} \Phi_{N,N1,N2} - \Omega \Phi_{N,N1,N2} &= 0, \\ \xi_F^2 \left\{ \frac{\partial^2}{\partial x^2} + \frac{\partial^2}{\partial y^2} \right\} \Phi_{F,F1,F2} - \tilde{\Omega} \Phi_{F,F1,F2} &= 0. \end{aligned} \tag{6.32}$$

They should be supplemented by the boundary conditions on SN interfaces at $x = d_N$

$$\gamma_{BN}\xi_N \frac{\partial}{\partial x}\Phi_{N1,N2} = G_0 \Delta \exp^{\mp i\varphi/2}, \tag{6.33}$$

where sign minus (plus) should be chosen for left (right) S electrode. At FN interface located at $x = 0$ the boundary conditions have the form:

$$\frac{\xi_N}{\Omega}\frac{\partial}{\partial x}\Phi_{N,N1,N2} = \gamma \frac{\xi_F}{\widetilde{\Omega}}\frac{\partial}{\partial x}\Phi_{F,F1,F2}, \tag{6.34}$$

$$\gamma_B \xi_F \frac{\partial}{\partial x}\Phi_{F,F1,F2} + \Phi_{F1} = \frac{\widetilde{\Omega}}{\Omega}\Phi_{N,N1,N2}, \tag{6.35}$$

while at free interfaces

$$\frac{\partial}{\partial y}\Phi_{N1,N2} = 0, \quad y = \mp(L/2 + d) \tag{6.36}$$

$$\frac{\partial}{\partial y}\Phi_{F1,F2} = 0, \quad y = \mp(L/2 + d)$$

$$\frac{\partial}{\partial x}\Phi_{F,F1,F2} = 0, \quad x = -d_F \tag{6.37}$$

$$\frac{\partial}{\partial x}\Phi_{N} = 0, \quad x = d_N \tag{6.38}$$

they follow from the demand of preventing a current flow across them. Finally at the interfaces between complex electrodes and weak link region (at $y = \mp L/2$) all the functions and their first derivatives should be continuos:

$$\frac{\partial}{\partial y}\Phi_{N1,N2} = \frac{\partial}{\partial y}\Phi_{N}, \tag{6.39}$$

$$\Phi_{N1,N2} = \Phi_{N}, \tag{6.40}$$

$$\frac{\partial}{\partial y}\Phi_{F1,F2} = \frac{\partial}{\partial y}\Phi_{F}, \tag{6.41}$$

$$\Phi_{F1,F2} = \Phi_{F}. \tag{6.42}$$

In the considered limit of thin F and N films

$$d_N \ll \xi_N, \quad d_F \ll \xi_F,$$

the two-dimensional boundary problem (6.32) - (6.42) can be reduced to a one-dimensional one. To do so we suppose that in the main approximation condensate functions do not depend on the coordinate x,

$$\Phi_{N,N1,N2} = A_{N,N1,N2}(y), \ \Phi_{F,F1,F2} = B_{F,F1,F2}(y), \tag{6.43}$$

and that their derivatives with respect to x can be expressed as follows:

$$\frac{\partial \Phi_{N,N1,N2}}{\partial x} = \left\{ \frac{\Omega}{\xi_N^2} A_{N,N1,N2} - \frac{\partial^2 A_{N,N1,N2}}{\partial y^2} \right\} (x - d_N),$$

$$\frac{\partial \Phi_{F,F1,F2}}{\partial x} = \left\{ \frac{\widetilde{\Omega}}{\xi_F^2} B_{F,F1,F2} - \frac{\partial^2 B_{F,F1,F2}}{\partial y^2} \right\} (x + d_F). \tag{6.44}$$

After substitution of (6.43) and (6.44) into the boundary conditions (6.34), (6.35) we arrive at one-dimensional differential equations in respect to functions $A_{N,N1,N2}(y)$ and $B_{F,F1,F2}(y)$. Solution of thus obtained one-dimensional boundary problem for the weak link region can be expressed in the form:

$$A_N = A_1 \cosh(q_1 y) + A_2 \sinh(q_1 y) +$$
$$+ \frac{\beta}{\zeta_N^2} \frac{\Omega}{\widetilde{\Omega}} (B_1 \cosh(q_2 y) + B_2 \sinh(q_2 y)) \tag{6.45}$$
$$B_F = B_1 \cosh(q_2 y) + B_2 \sinh(q_2 y) -$$
$$- \frac{\beta}{\zeta_F^2} \frac{\widetilde{\Omega}}{\Omega} (A_1 \cosh(q_1 y) + A_2 \sinh(q_1 y)) \tag{6.46}$$

where fundamental wave vectors of the problem:

$$q_{1,2}^2 = \frac{1}{2}[u^2 + v^2 \mp \sqrt{(u^2 - v^2)^2 + 4\zeta_F^{-2}\zeta_N^{-2}}], \tag{6.47}$$

$$u^2 = \left(\frac{1}{\zeta_N^2} + \frac{\Omega}{\xi_N^2} \right), \quad v^2 = \left(\frac{1}{\zeta_F^2} + \frac{\widetilde{\Omega}}{\xi_F^2} \right), \tag{6.48}$$

and $\zeta_F^2 = \gamma_B d_F \xi_F$, $\quad \zeta_N^2 = \gamma_B d_N \xi_N / \gamma$, $\beta = (q_1^2 - v^2)^{-1}$.

The appropriate solutions for F and N films located under S electrodes are

$$A_{N1,N2} = A_{11,12} \cosh(q_1 y) + A_{12,22} \sinh(q_1 y) +$$
$$+ \frac{\beta}{\zeta_N^2} \frac{\Omega}{\widetilde{\Omega}} (B_{11,12} \cosh(q_2 y) + B_{12,22} \sinh(q_2 y)) - N e^{\mp i\varphi/2} \tag{6.49}$$
$$B_{F1,F2} = B_{11,12} \cosh(q_2 y) + B_{12,22} \sinh(q_2 y) -$$
$$- \frac{\beta}{\zeta_F^2} \frac{\widetilde{\Omega}}{\Omega} (A_{11,12} \cosh(q_1 y) + A_{12,22} \sinh(q_1 y)) - F e^{\mp i\varphi/2} \tag{6.50}$$

The integration coefficients in (6.45), (6.46), (6.49), and (6.50) can be found by substituting these expressions into the boundary conditions. This procedure leads to

$$A_1 = \frac{\cos(\varphi/2) \sinh(q_1 d)}{\sinh(q_1(L/2 + d))} \frac{F\beta\zeta_N^{-2} - N}{\nu + 1}, \tag{6.51}$$
$$A_2 = \frac{i \sin(\varphi/2) \sinh(q_1 d)}{\cosh(q_1(L/2 + d))} \frac{F\beta\zeta_N^{-2} - N}{\nu + 1},$$
$$B_1 = -\frac{\cos(\varphi/2) \sinh(q_2 d)}{\sinh(q_2(L/2 + d))} \frac{N\beta\zeta_F^{-2} + F}{\nu + 1},$$
$$B_2 = -\frac{i \sin(\varphi/2) \sinh(q_2 d)}{\cosh(q_2(L/2 + d))} \frac{N\beta\zeta_F^{-2} + F}{\nu + 1},$$

where

$$N = \frac{1}{\xi_N d_N}\frac{2v^2\zeta_N^2\zeta_F^2}{1-4v^2u^2\zeta_N^2\zeta_F^2}\frac{G_0\Delta}{\gamma_{BN}},$$
$$F = \frac{\widetilde{\Omega}}{\Omega}\frac{1}{\xi_N d_N}\frac{\zeta_N^2}{1-4v^2u^2\zeta_N^2\zeta_F^2}\frac{G_0\Delta,}{\gamma_{BN}},$$

and $\nu = \beta^2\zeta_N^{-2}\zeta_F^{-2}$.

By substituting of the solution (6.45), (6.46), (6.51) into general formula for supercurrent (6.14) we obtain the expression for supercurrent in the SNF-NF-FNS structure:

$$I_S = (I_{C1} + I_{C2})\sin(\varphi), \tag{6.52}$$

where

$$I_{C2} = \frac{K\zeta_F^2\zeta_N^2}{\xi_N d_N}\,\mathrm{Re}\sum_{\omega=0}^{\infty}\frac{q_2\Gamma\left(1+v^2\beta\right)^2(\nu+1)^{-1}\sinh(q_2 d)^2}{(1-v^2u^2\zeta_F^2\zeta_N^2)^2\sinh(q_2(L+2d))},$$

$$I_{C1} = \frac{K}{\xi_N d_N}\,\mathrm{Re}\sum_{\omega=0}^{\infty}\frac{q_1\Gamma\left(v^2\zeta_F^2\zeta_N^2-\beta\right)^2(\nu+1)^{-1}\sinh(q_1 d)^2}{(1-v^2u^2\zeta_F^2\zeta_N^2)^2\sinh(q_1(L+2d))},$$

and $\Gamma = \Delta^2/(\Omega^2+\Delta^2)$.

In the limit $\zeta_N >> \zeta_F, \quad \xi_N >> \xi_F$, the part of the full critical current,I_{C2}, is small, so that the magnetidute of I_C of SNF-NF-FNS structure is reduced to

$$I_C^{SNF-NF-FNS} = \frac{K}{\xi_N d_N}\sum_{\omega=0}^{\infty}\mathrm{Re}\,\frac{\Gamma U q_1\sinh(q_1 d)^2}{\sinh(q_1(L+2d))}.$$

6.5.2 Calculation of supercurrent for SNF-N-FNS junction.

To calculate supercurrent across SNF-N-FNS junction we should sligtly change the procedure discribed in Appedix A by taking into account the appearance of additional three interfaces in the structure. Since the current can not flow across them instead of (6.42) we should use

$$\frac{\partial}{\partial y}\Phi_{F1,F2} = 0,\ y = \mp L/2,\ -d_F \le z \le 0, \tag{6.53}$$
$$\frac{\partial}{\partial x}\Phi_N = 0,\ x = 0,\ -\frac{L}{2} \le y \le \frac{L}{2}. \tag{6.54}$$

In the limit of thin F and N films $d_N \ll \xi_N$, $d_F \ll \xi_F$, the of solution of Usadel equations in the N film of weak link has more simple form compare to (6.45):

$$A_N = A_1\cosh(qy) + A_2\sinh(qy), \tag{6.55}$$

while in FN bilayer under S electrodes it closes to that of (6.49), and (6.50)

$$A_{N1,N2} = A_{11,12}\cosh(q_1 y) + A_{12,22}\sinh(q_1 y) +$$
$$+\frac{\beta}{\zeta_N^2}\frac{\Omega}{\widetilde{\Omega}}\left(B_{11,12}\cosh(q_2 y) + B_{12,22}\sinh(q_2 y)\right) - Ne^{\mp i\varphi/2}, \tag{6.56}$$
$$B_{F1,F2} = B_{11,12}\cosh(q_2 y) + B_{12,22}\sinh(q_2 y) -$$
$$-\frac{\beta}{\zeta_F^2}\frac{\widetilde{\Omega}}{\Omega}\left(A_{11,12}\cosh(q_1 y) + A_{12,22}\sinh(q_1 y)\right) - Fe^{\mp i\varphi/2}. \tag{6.57}$$

The integration constants in (6.55), (6.56), (6.57) can be found from the boundary conditions. In particular for A_1 and A_2 one can get

$$A_1 = \frac{-N\cos\{\varphi/2\}}{\left(Q_{q_1,\frac{q}{2}} + \nu Q_{q_2,\frac{q}{2}}\right)/(\nu+1)\tanh\frac{qL}{2} + \cosh\frac{qL}{2}}, \tag{6.58}$$

$$A_2 = \frac{-iN\sin\{\varphi/2\}}{\left(Q_{q_1,\frac{q}{2}} + \nu Q_{q_2,\frac{q}{2}}\right)/(\nu+1) + \sinh\frac{qL}{2}}. \tag{6.59}$$

Substitution of (6.55), (6.58), (6.59) into general formula for supercurrent:

$$I_S = -\frac{i\pi TW}{e\rho_N}\sum_{n=-\infty}^{\infty}\frac{1}{\omega^2}\int_0^{d_N}\left[\Phi^*_{-\omega,N}\frac{\partial}{\partial y}\Phi_{\omega,N}\right]$$

in the limit $\zeta_N >> \zeta_F$, $\xi_N >> \xi_F$ leads to

$$I_C^{SNF-N-FNS} = \frac{K}{\xi_N d_N}\,\mathrm{Re}\sum_{n=0}^{\infty}\frac{\Gamma U q}{Q_{q_1,q} + P_{q_1,q}}, \tag{6.60}$$

where functions $Q_{q_1,q}$ and $P_{q_1,q}$ are determined by Eq. (6.19) and (6.20), respectively.

6.5.3 Calculation of supercurrent for SN-NF-NS junction.

To calculate of supercurrent across SN-FN-NS junction we should change the procedure discribed in Appedix A by taking into account the abcence of F film in complex SN electrode. To do this the boundary conditions (6.42) in appropriate regions should be replaced by

$$\frac{\partial}{\partial y}\Phi_F = 0,\ y = \mp L/2, . - d_F \le x \le 0, \tag{6.61}$$
$$\frac{\partial}{\partial x}\Phi_{N1,N2} = 0,\ x = 0, .\frac{L}{2} \le |y| \le \frac{L}{2} + d \tag{6.62}$$

In the limit of thin F and N films $d_N \ll \xi_N$, $\quad d_F \ll \xi_F$, solution of the boundary problem in the weal link can be found in the form

$$A_N = A_1\cosh(q_1 y) + A_2\sinh(q_1 y) +$$

$$+\frac{\beta}{\zeta_N^2}\frac{\Omega}{\widetilde{\Omega}}\left(B_1\cosh\left(q_2y\right)+B_2\sinh\left(q_2y\right)\right), \tag{6.63}$$

$$B_F=B_1\cosh\left(q_2y\right)+B_2\sinh\left(q_2y\right)-$$

$$-\frac{\beta}{\zeta_F^2}\frac{\widetilde{\Omega}}{\Omega}\left(A_1\cosh\left(q_1y\right)+A_2\sinh\left(q_1y\right)\right), \tag{6.64}$$

while for it in the N films located under S electrodes they are

$$A_{N1,N2}=A_{11,12}\cosh(q_1y)+A_{12,22}\sinh(q_1y)-Ne^{\mp i\varphi/2}. \tag{6.65}$$

Integration constants A_1, A_2, B_1, B_2 in (6.63) - (6.65) can be found from the boundary conditions resulting in

$$A_1=\frac{\cos\left\{\varphi/2\right\}q^{-2}G_0\Delta/(\xi_N d_N\gamma_{BN})}{\cosh\frac{q_1L}{2}+\left(\nu Q_{\frac{q_2}{2},\frac{q_1}{2}}/2+Q_{q,\frac{q_1}{2}}\left(\nu+1\right)\right)\tanh\frac{q_1L}{2}},$$

$$A_2=\frac{i\sin\left\{\varphi/2\right\}q^{-2}G_0\Delta/(\xi_N d_N\gamma_{BN})}{\sinh\frac{q_1L}{2}+\nu\tanh^2\left(\frac{q_2L}{2}\right)Q_{\frac{q_2}{2},\frac{q_1}{2}}/2+Q_{q,\frac{q_1}{2}}\left(\nu+1\right)}, \tag{6.66}$$

$$B_1=A_1\frac{1}{\zeta_F^2}\beta\frac{\widetilde{\omega}}{|\omega|}\frac{q_1\sinh\left(q_1L/2\right)}{q_2\sinh\left(q_2L/2\right)}, \tag{6.67}$$

$$B_2=A_2\frac{1}{\zeta_F^2}\beta\frac{\widetilde{\omega}}{|\omega|}\frac{q_1\cosh\left(q_1L/2\right)}{q_2\cosh\left(q_2L/2\right)}. \tag{6.68}$$

Substituting this result into general formula for supercurrent (6.14) in the limit $\zeta_N >> \zeta_F, \xi_N >> \xi_F$ we arrived at the following formula for critical current of the SN-FN-NS junction

$$I_C^{SN-NF-NS}=\frac{K}{\xi_N d_N}\,\mathrm{Re}\sum_{n=0}^{\infty}\frac{\Gamma q_1}{q^4(Q_{q,q_1}+P_{q,q_1})}.$$

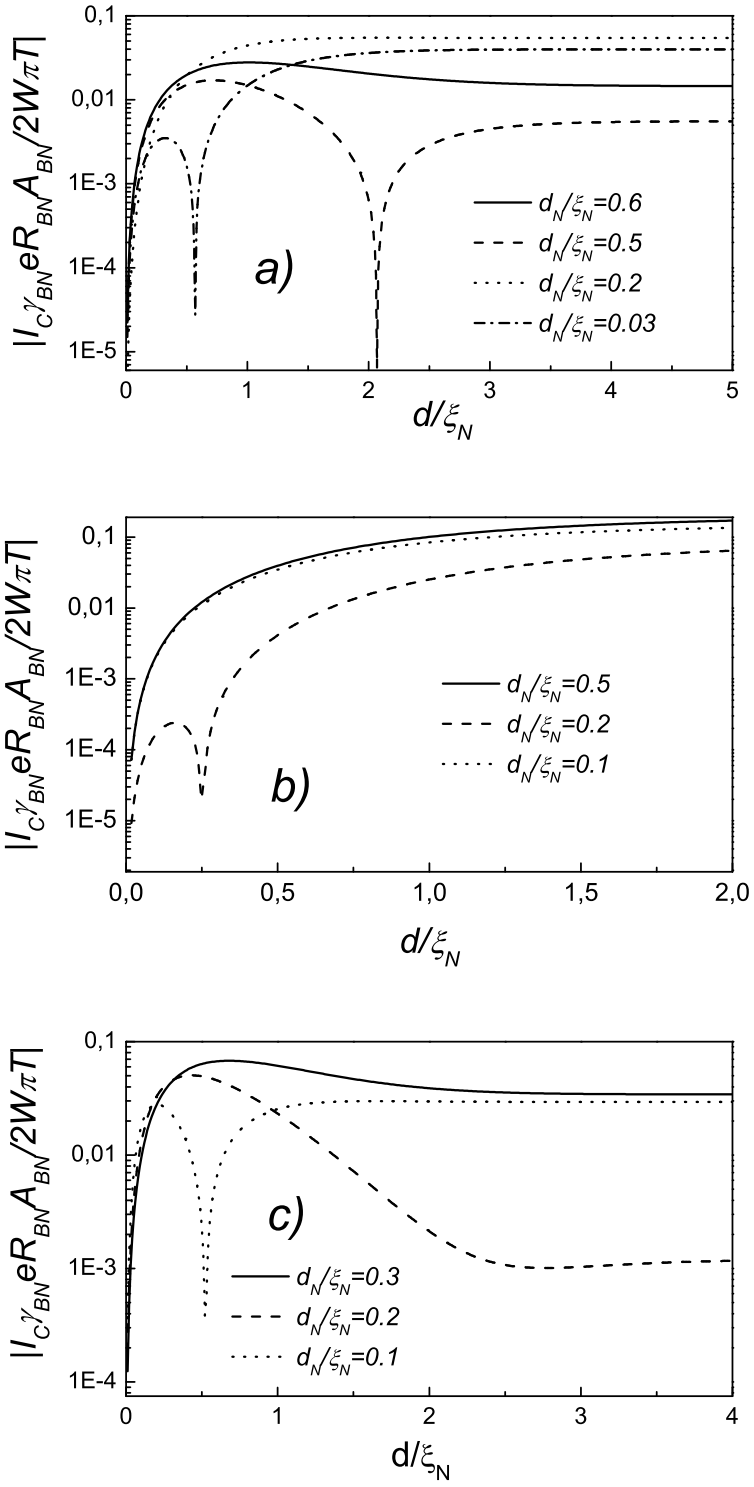

Figure 6.11. I_C for a) SNF-FN-FNS, b) SN-FN-NS, c) SNF-N-FNS structures versus d/ξ_N calculated at $\xi_N/\xi_F = 10$, $T/T_C = 0.5$, $H/\pi T_C = 30$, $d_F/\xi_F = 0.1$, $L/\xi_N = 2$.

Bibliography

[1] A. A. Golubov, M. Yu. Kupriyanov, and E. Il'ichev, Rev. Mod. Phys. **76**, 411 (2004).

[2] F. S. Bergeret, A. F. Volkov, K. B. Efetov, Rev. Mod. Phys. **77**, 1321 (2005).

[3] A. I. Buzdin, Rev. Mod. Phys. **77**, 935 (2005).

[4] A.S.Sidorenko, V.I.Zdravkov, J.Kehrle, R.Morari, G.Obermeier, S.Gsell, M.Schreck, C.Muller, M.Yu.Kupriyanov, V.V.Ryazanov, S.Horn, L.R.Tagirov, and R.Tidecks, Pis'ma Zh.Eksp. Teor. Fiz. **90,** 149 (2009) [JETP Lett., **90**, 139 (2009)].

[5] T. S. Khaire, M. A. Khasawneh, W. P. Pratt, Jr., N. O. Birge, "Observation of spin-triplet superconductivity in Co-based Josephson Junctions" cond.mat.supercond arXiv: 0912.0205v1.

[6] G. Nowak, H. Zabel, and K. Westerholt et al., Phys. Rev. B **78** 134520 (2008).

[7] C. Gurlich, S. Scharinger, M. Weides, H. Kohlstedt, R.G. Mints, E. Goldobin, D. Koelle, and R. Kleiner, "Visualizing supercurrents in ferromagnetic Josephson junctions with various arrangements of 0 and π segments", cond.mat.super-cond arXiv: 0911.4831v1.

[8] T. Yu. Karminskaya and M. Yu. Kupriyanov, Pis'ma Zh. Eksp. Teor. Fiz. **85**, 343 (2007) [JETP Lett. **85**, 286 (2007)].

[9] T. Yu. Karminskaya and M. Yu. Kupriyanov, Pis'ma Zh. Eksp. Teor. Fiz. **85**, 343 (2007) [JETP Lett. **86**, 61 (2007)].

[10] T. Yu. Karminskaya, M. Yu. Kupriyanov, and A. A. Golubov, Pis'ma Zh.Eksp. Teor. Fiz. **87,** 657 (2008) [JETP Lett., **87**, 570 (2008)].

[11] T. Yu. Karminskaya, M. Yu. Kupriyanov, and A. A. Golubov, Phys. Rev. B **79,** 214509 (2009).

[12] M. Yu. Kupriyanov, R. G. Deminov, Ya. V. Fominov, A. A. Golubov, T. Yu. Karminskaya, and L. R. Tagirov, "Spin valve effects in superconductor/ferromagnetic devices", I.F. Schegolev memorial conference "Low-Dimensional Metallic and Superconducting Systems", Chernogolovka, Moscow region, October 11-16, p. 33, (2009).

[13] F. Born, M. Siegel, E. K. Hollmann, H. Braak, A. A. Golubov, D. Yu. Gusakova, and M. Yu. Kupriyanov, Phys. Rev. B. **74**, 140501 (2006).

[14] J. W. A. Robinson, S. Piano, G. Burnell, C. Bell, and M. G. Blamire, Phys. Rev. Lett. **97**, 177003 (2006).

[15] K. K. Likharev, Rev. Mod. Phys. **51**, 101 (1979).

[16] A. A. Golubov, M. Yu. Kupriyanov, V. F. Lukichev, Mikroelektronika, **12** 342 (1983) [Soviet-Microelectronics, **12** 180 (1983)].

[17] L. Usadel, Phys. Rev. Lett. **25**, 507 (1970).

[18] M. Yu. Kuprianov and V. F. Lukichev, Zh. Eksp. Teor. Fiz. **94**, 139 (1988) [Sov. Phys. JETP **67**, 1163 (1988)].

Summary

The main goal of this thesis is to present theoretical study of physical foundations for creation of fundamentally new devices for nanoelectronics, spintronics and superconducting electronics. Superconducting spintronics is a rapidly developing area of modern nanoelectronics. Significant interest is due to new fundamental effects in structures containing ferromagnetic and superconducting layers, as well as the possibility of utilizing these effects for the spin valves. There are serious restrictions on the operating parameters of known prototypes of superconducting spin valves, in which control of the critical current and critical temperature is possible. As a consequence, there is a need to improve their performance by exploring new design solutions based on the characteristic features of the proximity effect in S / F heterostructures. Another class of spin switches uses the idea of changing the critical current in SFS Josephson junctions by creating conditions for the generation of triplet order parameter components which are odd functions of the electronic energy. Research on the triplet superconducting correlations that arise in multilayered structures containing superconducting, normal, and ferromagnetic layers is very timely for creation of a new class of effective spin-valves.

In Chapters 2 and 3, on the basis of the microscopic theory of superconductivity, analysis of processes in Josephson nanostructures which area multilayered structures consisting of alternating layers of normal (N) and ferromagnetic (F) metals, was performed. Considerable interest in such Josephson structures is due to the fact that they are important for the creation of a new type of spin valves and so-called π- junctions with a negative value of the critical current I_C. Currently fabricated structures with F layers have typical scale of decay of the critical current and period of oscillations in the range of few nanometers. This fact considerably complicates the practical use of such structures. In Chapters 2 and 3 a solution to this problem is offered. This solution allows to increase characteristic dimensions by almost two orders of magnitude. It also shows that both the magnitude and sign of the critical current can be controlled by changing the mutual orientation of the magnetization vectors of individual F films of FNF multilayer structures in Josephson junctions. This work transforms the problem of interplay of ferromagnetism and superconductivity from a

purely fundamental to practical area.

In Chapter 4, FNF structures with the magnetization of ferromagnets, oriented at an arbitrary angle relative to each other, were investigated. In such structures the triplet component of the spectrum of the superconducting correlations arises. In Chapter 4, the fact is proven that the triplet component in S-(FNF)-S junctions leads to the emergence of a new type of π - contact. This π - contact arises from the superposition of two contributions to the critical current which do not oscillate with junction length. The presence of such π - contact can be used as an experimental confirmation of the existence of the triplet component. It was also found that the effective control of magnitude and sign of the critical current of S-(FNF)-S spin valves can be achieved at small angles of rotation of the magnetizations from the antiferromagnetic configuration, which is more energetically favorable than the complete remagnetization of the structure.

In Chapters 2-4, results were obtained for limiting case when N and F films are thin in comparison with their coherence lengths. In an experimental situation, this condition is easily achieved for a normal metal. However, its realization for the ferromagnetic layers presents certain difficulties. It is for this reason, in Chapter 5, the effect of finite thickness of the ferromagnetic films and normal S-FN-S transition in the critical current was analyzed. It is shown that for an arbitrary film thickness, the critical current oscillates as a function of the distance between superconducting electrodes, hence the damping length and oscillation period depend strongly on the thickness of the films. Thus, for arbitrary thickness of the films the results obtained in the thin film limit are also qualitatively applicable. If the thickness of F is larger than the coherence length, then the damping length and the oscillation period do not depend on the thickness of the F film. For thickness of a ferromagnet much larger than its coherence length, one can define critical distances L_n when I_C changes sign. It is shown that for thickness of ferromagnet comparable to the coherence length, strong variations of I_C occur as a function of thickness of the F film if the distance between superconducting electrodes L is close to L_n. These results are important from a practical point of view, because one can create junctions with parameters that do not depend on the spread of geometric and transport parameters of structures, the inherent in any technological process.

A second major technological constraint on the fabrication of the S-FN-S and S-FNF-S structures proposed in Chapters 2-3 was that they are ramp type junctions. In practice it is much more convenient to work with structures that have only parallel boundaries between

layers. To address this shortcoming, junctions in which the S electrodes are placed on top of the FN structure were studied in Chapter 6. Three different geometries were considered:

- SN-NF-NS structure, which consists of two SN electrodes connected by an NF weak region.

- SNF-N-FNS structure, in which a N film connects SNF multilayer electrodes.

- SNF-NF-FNS structure, in which the S electrodes are located on top of the FN structure.

In Chapter 6, the critical current of SFNS Josephson structures was calculated and the advantages of such geometry were analyzed. The amplitude of the critical current for an SN-FN-NS-type structure reaches the highest value compared with the other geometries because of the lack of additional suppression of superconductivity under the electrodes from the ferromagnetic film. The effect of finite area in SN interface of SFNS junctions with their electrodes located on top of the FN structure, on the realization of states with negative and positive critical current sign was studied. It was shown that, besides multiple 0-π transitions in ramp type structures which are triggered by the variation of the distance between the electrodes, a single 0-π transition is realized in the new geometry when the length of the SN boundary increases. This 0-π transition exists even in SFN-N-FNS structures with non-ferromagnetic weak link region.

Samenvatting (Summary in Dutch)

Het hoofddoel van dit proefschrift is onderzoek en ontwikkeling van de fysische grondslagen van fundamenteel nieuwe devices voor de nanoelektronica, spintronica en supergeleidende elektronica. De supergeleidende spintronica is een zich snel ontwikkelend gebied van de moderne nanoelektronica. Zowel de aanwezigheid van nieuwe fundamentele effecten in structuren die ferromagnetische en supergeleidende structuren bevatten, als de toepassing van deze effecten zijn van significant belang. De gebruiksparameters van bekende prototypes van supergeleidende spin valves, waarmee de kritische stroom en kritische temperatuur ingesteld kunnen worden, zijn erg beperkt. Daarom is het noodzakelijk om hun functionaliteit te verbeteren door nieuwe ontwerpoplossingen te onderzoeken die gebaseerd zijn op karakteristieke eigenschappen van het proximity-effect in S/F heterostructuren. Een andere klasse van spinschakelaars maakt gebruik van de mogelijkheid de kritische stroom te veranderen door voorwarden te scheppen waarbij tripletparen voorkomen. Deze tripletparen hebben de eigenschap dat de orde-parameter een oneven functie van de Matsubara frequentie is. Onderzoek aan deze triplet paren, die voorkomen in meerlagenstructuren die supergeleidende normaal geleidende en ferromagnetische lagen bevatten, ondersteunt de ontwikkeling van deze klasse van spin valves.

In hoofdstukken 2 en 3 wordt een analyse gemaakt van de processen in Josephson nanostructuren die bestaan uit afwisselende lagen van normale (N) en ferromagnetische (F) metalen op basis van de microscopische theorie van de supergeleiding. Deze structuren zijn van belang voor de ontwikkeling van een nieuw type spin valves en zogenoemde π-juncties: Josephson juncties met een negatieve waarde van de kritische stroom I_C. In de huidige structuren is de afhankelijkheid tussen deze kritische stroom en de afstand tussen de supergeleidende elektrodes S een gedempte oscillatie. De karakteristieke lengtes van de demping en de oscillaties zijn van de orde van enige nanometers, wat de bruikbaarheid van zulke structuren aanzienlijk beperkt. In hoofdstukken 2 en 3 wordt een oplossing voor dit probleem geboden waarbij bijna tweemaal grotere karakteristieke afmetingen bereikt worden. Ook wordt aangetoond dat zowel de grootte als het teken van de kritische stroom ingesteld kunnen worden door de relatieve oriëntatie van de magnetisatievectoren in de

afzonderlijke F lagen van FNF meerlagige Josephson juncties. Door dit werk krijgt het fundamentele probleem van de interactie tussen ferromagnetisme en supergeleiding praktische relevantie.

In hoofdstuk 4 worden FNF structuren met een willekeurige hoek tussen de magnetisatie vectoren van de ferromagnetische lagen onderzocht. In zulke structuren wordt de triplet component zichtbaar in het spectrum van supergeleidende correlaties. In hoofdstuk 4 wordt bewezen dat het meenemen van de tripletcomponent leidt tot een nieuw type π-junctie. Deze junctie wordt gekenmerkt door de superpositie van twee niet oscillerende bijdragen aan de kritische stroom. Het bestaan van zulke π-juncties kan gebruikt worden als experimentele bevestiging van het bestaan van de tripletcomponent. Ook wordt gevonden dat een effectieve regelbaarheid van grootte en teken van de kritische stroom in S-(FNF)-S spin valves bereikt kan worden door kleine draaihoeken ten opzichte van de antiferromagnetische configuratie. Dit is energetisch gunstiger dan de volledige hermagnetisatie van de structuur.

De resultaten in hoofdstukken 2 tot en met 4 zijn verkregen voor de limiet waar de lagen dunner zijn dan de coherentielengte in zowel het normale metaal als de ferromagneet. In het experimentele geval wordt deze limiet gemakkelijk bereikt voor normale metalen. Voor de ferromagnetische lagen is dit echter problematisch. Daarom wordt in hoofdstuk 5 het effect van een eindige dikte geanalyseerd. Hierbij wordt aangetoond dat de oscillerende afhankelijkheid van de kritische stroom en de afstand tussen de supergeleidende elektrodes behouden blijft. De periode van de oscillaties en de karakteristieke lengte van de demping is daarbij sterk afhankelijk van de laagdikte. Het kwalitatieve gedrag van dikke films onderscheidt zich dus niet van de resultaten berekend in de dunnefilm limiet. Als de dikte van de ferromagneet vergelijkbaar is met (of groter is dan) de coherentielengte dan hangen de periodes van de oscillatie en de karakteristieke lengte van de demping niet langer af van de laagdikte. Ook erg belangrijk is het feit dat rond de kritische afstand tussen de supergeleidende elektrodes (de afstand waarbij de stroom voor oneindig dikke ferromagnetische lagen gelijk is aan nul) het teken en de grootte van de kritische stroom sterk afhankelijk zijn van de dikte van de ferromagneet. Buiten deze kleine kritische gebieden hangen de grootte en het teken van de kritische stroom af van de laagdikte. Deze resultaten zijn vanuit praktisch oogpunt belangrijk, omdat dit het mogelijk maakt juncties te fabriceren waarbij de eigenschappen van deze juncties niet sterk beïnvloed worden door de onvermijdelijke spreiding in de geometrie en transporteigenschappen van de structuren die inherent zijn aan ieder

technisch proces.

De tweede belangrijke technische randvoorwaarde aan de in hoofdstukken 2 tot en met 3 beschreven S-FN-S en S-FNF-S structuren is de noodzaak tot zijdelingse contacten door middel van juncties van het ramp-type. Vanuit technisch oogpunt is het veel eenvoudiger om te werken met structuren waarbij alle overgangen tussen de verschillende lagen parallel lopen. Om aan dit problem tegemoet te komen, zijn in hoofdstuk 6 structuren bestudeerd waarbij de juncties bovenop de FN-structuren zijn geplaatst. De volgende drie geometrieën worden behandeld:

-SN-NF-NS structuur bestaande uit twee SN elektrodes verbonden door een zwak NF gebied.

-SNF-N-FNS structuur, waarbij de N-laag twee meerlagen-elektrodes verbindt.

-SNF-NF-FNS structuur, waarbij de S-elektroden zich bovenop de FN-structuur bevindt.

In hoofdstuk 6 wordt de kritische stroom van SFNS-Josephson structuren berekend. Hierbij worden de voordelen van de experimenteel makkelijker realiseerbare structuren waarbij de S elektrodes bovenop de FN structuur geplaatst worden ten opzichte van de ramp-type SFNS juncties gerealiseerd. De amplitude van de kritische stroom bereikt de hoogste waarde voor de SN-FN-NS-type structuur in vergelijking met de andere geometrieën. Dit is omdat de supergeleiding niet extra wordt onderdrukt door de ferromagnetische laag onder de elektrodes. Het effect van de eindige oppervlakte van de SN-overgang van SFNS-juncties waarbij de elektrodes bovenop de FN-structuur geplaatst worden op het voorkomen van toestanden met positieve en negatieve kritische stroom is bestudeerd. Er is bewezen dat, in tegenstelling tot de meerdere $0-\pi$ overgangen met toenemende afstand tussen de elektrodes voor de structuren van het ramp-type, er bij structuren met de nieuwe geometrie slechts één $0-\pi$ overgang optreedt met toenemende lengte van de SN-overgang. Deze $0-\pi$ overgang kan zelfs optreden in SFN-N-FNS structuren met een zwakke binding in een niet ferromagnetisch gebied.

List of publications

1. T. Yu. Karminskaya and M. Yu. Kupriyanov, Pis'ma Zh. Eksp. Teor. Fiz. **85**, 343 (2007) [JETP Lett. **85**, 286 (2007)].

2. T. Yu. Karminskaya and M. Yu. Kupriyanov, Pis'ma Zh. Eksp. Teor. Fiz. **85**, 343 (2007) [JETP Lett. **86**, 61 (2007)].

3. T. Yu. Karminskaya, M. Yu. Kupriyanov, and A. A. Golubov, Pis'ma Zh.Eksp. Teor. Fiz. **87,** 657 (2008) [JETP Lett. **87**, 570 (2008)].

4 T. Yu. Karminskaya, M. Yu. Kupriyanov, and A. A. Golubov, Phys. Rev. B **79,** 214509 (2009).

5. Ya. V. Fominov, A. A. Golubov, T. Yu. Karminskaya, M. Yu. Kupriyanov, R. G. Deminov, L. R. Tagirov, Pis'ma Zh. Eksp. Teor. Fiz. **91**, 329 (2010) [JETP Lett. **91**, 308 (2010)].

6. T. Yu. Karminskaya, A. A. Golubov, M. Yu. Kupriyanov, and A. S. Sidorenko, Phys. Rev. B **81**, 214518, (2010).

Acknowledgments

I would like to thank my promotor, Horst Rogalla, for providing me the opportunity to carry out this research as a joint project between Moscow State University and University of Twente.

I'm really grateful to Alexander Golubov and Mikhail Kupriyanov for comprehensive support and help in work.

I also want to thank Valery Ryazanov, Vitaly Bolginov, Lenar Tagirov, Anatoly Sidorenko, Jan Aarts and Yakov Fominov for fruitful discussions of obtained results.